

INFLUENCE OF ADDITIVES ON THE MAGNETIC AND ELECTRICAL
PROPERTIES OF IRON-EXCESS Mn-Zn FERRITES

BY



MD. MANJURUL HAQUE

SUBMITTED IN PARTIAL FULFILMENT
OF THE REQUIRMENTS FOR
THE DEGREE OF M.Phil



DEPARTMENT OF PHYSICS
BANGLADESH UNIVERSITY OF ENGINEERING AND TECHNOLOGY

DHAKA-1000

May, 2000

BANGLADESH UNIVERSITY OF ENGINEERING AND TECHNOLOGY
DHAKA
DEPARTMENT OF PHYSICS

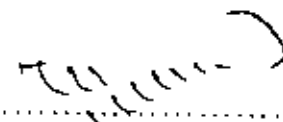
Certification of Thesis
A Thesis on

“THE INFLUENCE OF ADDITIVES ON THE MAGNETIC AND ELECTRICAL
PROPERTIES OF IRON-EXCESS Mn-Zn FERRITES”
BY
MD. MANJURUL HAQUE

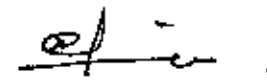
has been accepted as satisfactory in partial fulfilment for the degree of
Master of Philosophy in Physics and certifying that the student has
demonstrated a satisfactory knowledge of the field covered by this thesis
in an oral examination held on 28 May, 2000.

Board of Examiners


1. Dr. Mominul Huq
Professor,
Department of Physics,
BUET, Dhaka.


.....
Supervisor & Chairman

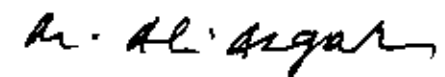
2. Dr. A. K. M. Abdul Hakim
Principal Engineer,
Magnetic Material Division,
AECD, Dhaka.


.....
Co-supervisor & member

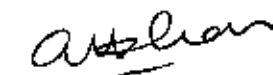
3. Head
Department of Physics
BUET, Dhaka.


.....
Member

4. Dr. M. Ali Asgar
Professor,
Department of Physics,
BUET, Dhaka.

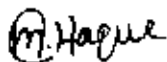

.....
Member

5. Dr. Amir Hussain Khan
Professor,
Department of Physics,
Jahangirnagar University
Savar, Dhaka.


.....
Member (External)

CERTIFICATE

This is to certify that the author is solely responsible for the work reported in this thesis and this work has not been submitted to any University or elsewhere for the award of any degree or diploma.



Candidate

(Md. Manjurul Haque)

Roll No. 9414022F

Session : 1993-94-95



Supervisor

(Dr. Mominul Haque)

Professor

Department of Physics

BUET, Dhaka-1000.

▼

Report on the thesis entitled "Influence of additives on the magnetic and electrical properties of iron-excess Mn-Zn ferrites" submitted by Md. Manjurul Haque for the degree of M. Phil. in Physics.

The student Md. Manjurul Haque from the Dept of Physics, BUET, has been associated with me for his M. Phil thesis work. During the course of his thesis work he prepared two series of Mn-Zn ferrite samples of non-stoichiometric compositions under different sintering conditions.

Studies have been made on the effect of temperature, holding time and cooling rate during the sintering processes on the initial permeability and loss factor of the prepared samples. For the study of intrinsic magnetic properties like magnetic moment and Curie temperature measurements have been made on magnetization as a function of field. Phase characterization of the samples have been done by X-ray diffraction. Microstructure study has also been performed to have information on grain size distribution.

The results have established that the appropriate sintering condition, temperature, time and cooling rate are vital parameters to prepare high frequency Mn-Zn ferrites as core materials with reasonable permeability and minimum magnetic loss. In this study, the influences of additives on Mn-Zn ferrite polycrystals were investigated in a manner as the magnetic properties of polycrystalline ferrites had been improved by some additives.

The results have been well presented in the thesis with reasonable discussion and interpretation. The studies provide useful information and addition to the processing of quality Mn-Zn ferrites of non-stoichiometric composition.

During the period of his research work Md. Manjurul Haque was hard working, active and perform all the experiments with utmost sincerity. In my opinion M.Phil. degree should be awarded to Mr. Md. Manjurul Haque.



(Dr. A. K. M. Abdul Hakim)
Co-supervisor & member
Examination Committee
Principal Engineer
Bangladesh Atomic Energy Commission

Acknowledgment

I am greatly indebted to so many of my teachers, members of our group and other individuals that to acknowledge them all it would need a much larger space than is available here. hence, I am sure to do injustice to many of my friends and well wishers.

First of all, I like to offer my grateful thanks and indebtedness to my supervisor Prof. M. Mominul Haq, Department of Physics, BUET, Dhaka for his indispensable guidance, keen interest and constant encouragement through the progress of this research work.

I would also like to express my gratitude to my co-supervisor Dr. A. K. M. Abdul Hakim, Principal Engineer, magnetic Material division, AECD, Dhaka for his sincere help and enthusiastic guidance.

I am grateful to Prof. Md. Abu Hasan Bhuiyan, Head, Department of Physics, BUET, Dhaka. I am thankful to Prof. M. Ali Asgar, Prof. Gias Uddin Ahmad, Prof. Tafazzal Hossain of the same department for their kind cooperation and inspiration during the work. I want to thank Dr. Jibon Podder, Associate Professor, Dr. Feroj Alam Khan Associate Professor, Department of Physics, BUET and Dr. S. S. Sikder for their valuable suggestions throughout the work. my gratitude is also to Mr. M. A. Mazid, Mr. Amanullah Chowdhury and Mr M.A. Bari of Magnetic Material Division of AECD for allowing me to use their facilities.

My special thanks are to my friends A. T. M Kaosar Janil, Syed Jamal Ahmad and Md. Abu Taher who relentlessly reminded me what I can and what I can not. Thanks to Salim, Shuvo, Farid Bhai, Shyamal, Tahid Bhai, Israil, Rajjak, Allauddin, Farahi, Shipu for their help and care.

I owe deep sense of gratitude to Perveen Apa and Kalam Bhai of Magnetic Material Division, AECD, Dhaka for rendering their helping hands in my sample preparation.

Thanks to my wife, Rupa and to others of my family for being so patient, caring and keeping my spirit up. Without them I could not have done this

I also want to thank the authority of BUET for giving me the opportunity of research. Thanks to Department of MME, BUET, Dhaka for allowing me to use their facilities for taking microphotograph of the samples.

Thank you all.

Md. Manjurul Haque

Abstract

Iron-excess Mn-Zn ferrite samples with and without additives are prepared by ceramic method and are subjected to different sintering conditions. The additives, used in this work are V_2O_5 , TiO_2 and CoO in the composition $Mn_{0.51}Zn_{0.44}Fe_{2.05}O_4$ and CuO substitutes in the sample $Mn_{0.7-x}Cu_xZn_{0.22}Fe_{2.08}O_4$. For characterization and determination of lattice parameters, X-ray diffraction is carried out. Curie temperature measurements, magnetization measurements, permeability measurements and microstructure study are performed for the understanding of the magnetic properties of the prepared samples as modified by compositional change, additives and heat treatment.

X-ray diffraction results indicate that samples are in good crystalline form. From Curie temperature measurements, a decreasing trend in the Curie temperature is observed for the substitution of Cu^{2+} for Mn^{2+} . The Curie temperature is found to be very sensitive for the additives like V_2O_5 , TiO_2 and CoO . The magnetization measurements reveal that crystal site preference can significantly affect the saturation magnetization, M_s . The saturation magnetization increases for $x=0.03$ in $Mn_{0.7-x}Cu_xZn_{0.22}Fe_{2.08}O_4$ and then decreases for further increase of Cu^{2+} content. Saturation magnetization significantly increases by the addition of CoO in $Mn_{0.51}Zn_{0.44}Fe_{2.05}O_4$. But it decreases for the addition of TiO_2 and V_2O_5 and the effect is drastic for V_2O_5 doped sample than for TiO_2 ones. The microstructure study shows that grain size increases with sintering temperature. The quenched samples have smaller grain size and almost uniform in size.

From permeability spectra, it is noticed that sintering condition and additives substantially affect the permeability values. Quenched samples are found to possess higher permeability. From 10 KHz to 1 MHz, for all the samples the permeability is found to remain almost frequency independent. The loss factors and quality factors are also calculated and this study revealed that sintering condition is a determining factor for high quality Mn-Zn ferrites. It has been found that the sample $Mn_{0.7-x}Cu_xZn_{0.22}Fe_{2.08}O_4$ with $x=0.15$ has the best composition for high permeability.

CONTENTS

CHAPTER 1		INTRODUCTION	PAGE NO.
1.1	Introduction		1
1.2	Ferrites and their importance		3
1.3	Advantages of ferrite research in Bangladesh		6
1.4	Review of others work		7
1.5	Present work		15
CHAPTER 2		THEORETICAL BACKGROUND	
2.1	Theory of Ferrimagnetism		19
2.2	Ferrites		26
2.3	Different types of ferrites		26
2.4	Crystal structures of Spinel ferrite		28
CHAPTER 3		SPECIMEN PREPARATION	
3.1	Methodology of ferrite preparation		32
3.2	Method of preparation		33
CHAPTER 4		EXPERIMENTAL	
4.1	The X- ray diffraction		40
4.2	Curie Temperature measurement		41
4.3	Magnetization measurement		44
4.4	Permeability measurement		55
4.5	Microstructure study		63

CHAPTER 5 RESULTS AND DISCUSSIONS

5.1	The XRD analysis	65
5.2	The results of Curie temperature measurements	71
5.3	The results of Magnetization measurements	77
5.4	The Microstructure study	86
5.5	The results of Permeability measurements	98

CHAPTER 6 CONCLUSIONS

6.1	Conclusions	146
6.2	Further suggestions	147

APPENDIX		148
-----------------	--	-----

CHAPTER-1

INTRODUCTION



1.1 INTRODUCTION

Ferrites constitute a special branch of ferrimagnetics. Ferrites are double oxide of iron and another metal. They have two unequal sublattices and are ordered anti-parallel to each other. Each sublattice exhibits spontaneous magnetization at room temperature, like the normal ferrimagnetics. Because of unequal magnitudes magnetization in the two sublattices the material has resultant magnetization is similar to ferromagnets. Again like ferromagnetics, these ferrites have spontaneously magnetized domains and show the phenomena of magnetic saturation and hysteresis and have a critical temperature T_c called the Curie temperature, above which they become paramagnetic. But what makes these materials more interesting is their very high resistivity. The resistivity of ferrites varies from 10^2 to 10^{10} ohm-cm which is about 15 orders of magnitude higher than that of ferromagnetic iron. This outstanding property of ferrites makes them highly demandable for high frequency applications. This fact was first envisaged by S. Hilpert (1909) [1]. Since then the ferrites have become one of the most attractive materials for high frequency applications. The ferrites were developed into commercially useful materials, chiefly during the years 1933-1945 by Snoek and his associates at the Philips Research Laboratories in Holland.

The Mn-Zn ferrites is the most popular among the ferrites. Mn-Zn ferrites generally have lower losses at high frequency in comparison with Ni-Zn ferrites and metallic magnetic materials. Commonly it is categorized as non-microwave ferrite. The unique properties of non- microwave ferrites are high magnetic permeability and high electrical resistivity. The resultant lower eddy current losses allow their use to higher frequencies than possible with metals. Non-

microwave ferrites which will henceforth be referred to as ferrites are used at frequencies from audio to about 500 MHz. As a soft magnetic materials Mn-Zn ferrites have been proved to be smart candidate of highest rank. The greatest advances for the Mn-Zn ferrites were made in the mid-sixties. The Mn-Zn ferrite has a superior behaviour in respect of temperature dependent properties.

The requisites for modern ferrite are so many in number that only extensive research in this field can meet the huge demand of technology. The demanded characteristics of the soft ferrites under study that make them technologically useful are :

- a) *Excellent magnetic and electrical performance*
- b) *Controllable mechanical dimensions*
- c) *High quality factor*
- d) *Low cost*
- e) *Large number of controllable parameters*

In view of the great interest of Mn-Zn ferrites, both for their technological applications and theoretical understanding of the mechanisms involved, the present work is aimed at finding the effect of additives on the magnetic characteristics like Curie temperature, permeability, loss factor, etc. of the magnetic system. The main objectives has been the search for the best suited composition and preparation parameters for optimum performance of ferrite samples in respect of permeability and frequency response.

In this respect, Mn-Zn ferrites were prepared using non-stoichiometric weight ratio and then subjected to various sintering conditions. There are two series of samples. In one series, Mn-Zn ferrite samples were prepared with and without different additives like V_2O_5 , TiO_2 , and CoO . In other series, Mn-Zn ferrites were prepared with the substitution of Cu^{2+} ions for Mn^{2+} ions.

Chapter-1 of this thesis deals with the importance of ferrites, advantage of ferrite research and gives a glimpse of the present work. Chapter-1 also contains a survey of others work in this field.

The theoretical side is covered in Chapter-2. It deals with the theories of ferrimagnetism and the crystal structure of ferrites.

Chapter-3 contains the methodology of specimen preparation and the detail description of preparation procedure.

Chapter-4 describes the experimental side and the description of different measurements that have been performed on the doped and undoped Mn-Zn ferrites samples.

The results and discussions are given in Chapter-5 and the conclusions drawn from the overall experimental results and discussions are presented in Chapter-6. Some of the experimental data and tables not included in the main text are given in the appendix.

1.2 FERRITES AND THEIR IMPORTANCE

Polycrystalline ferrites are still the optimum magnetic material in high and very high frequency circuits and can not be replaced by any other magnetic elements. These ferrites having high resistivity are used in a wide range of technological applications in radio frequency devices, high quality filters, operating devices and transformer cores [2] because such ferrites are relatively inexpensive and more stable than competing materials. Ferrites have fulfilled various needs of electronics industry because of their many advantages over metallic materials. Ferrites pervade almost every sphere of modern technology. The present day technology owes a lot to the ferrite industry. Ranging from the very ordinary radio sets to the complicated and exhaustive hardwires involved in computers, ferrites have found their way to prove their importance.

The outstanding property of ferrite which first attracted the attention was their high electrical resistivity as compared to that of metals. As a result, at high frequency application eddy current losses are negligible in ferrites compared to metals. Such intrinsic properties make the ferrites indispensable materials in tele-communications and in the electronic industry where frequency in the range of 10^3 to 10^{11} Hz have to be handled.

In the year around 1950, telephone industry was badly in need of a new magnetic material to be used as load coils for their long distance lines and to be used as low loss magnetic materials in band pass filters. Ferrite inductors were smart candidate for that requirements. So, ferrite and telephone technology developed in close cooperation. Six (1952) [3] was the intensive and leading promotor of this development.

One of the principal use of ferrite is in resonance circuit. Ferrite cores are used as inductors. Controlling and minimizing the various loss factors, ferrite cores became the very best inductors having high initial permeability and reduced physical size. Ferrite cores are also important in power transformers, where high saturation induction and low hysteresis losses are of principal importance. The Mn-Zn ferrites on which the present thesis is concerned, presently finding increasing application in Switching Mode Supply for small to medium power level.

High frequency ferrite application can be broadly divided into two categories. Microwave and Non-microwave applications. A Microwave ferrite can be defined as highly resistive magnetic materials used at frequencies between 100 MHz and 500 GHz, the highest microwave frequency now in use. Microwave ferrites are again of two types: Non-reciprocal and Reciprocal devices. The Non-reciprocal devices for which ferrites are almost irreplaceable have greatest number of applications. These devices are essentially isolators or circulators which perform the following functions:

- An isolator is merely a wave guide section in which the incident electromagnetic wave (from input to output) can propagate without attenuation but an electromagnetic wave coming from reverse direction will be highly attenuated.
- An n-port circulator is a device having n ports or inputs and works in a rather complicated manner.

The devices of these type provide easy isolation between different channels of a microwave circuit which is essential in present techniques for radar and radio links.

The second category comprises of reciprocal devices, e.g. electrically controlled phase shifters. On the other hand, the unique properties of non-microwave ferrites are high magnetic permeability and high electrical resistivity. These are the ferrites used at frequencies from audio to about 500 MHz.

The computer technology got a new thrust when it was discovered that some polycrystalline spinel ferrite can have a rectangular hysteresis loop and therefore can be used as computer memory elements. Until 1970 nearly all main frame computer memories consisted of ferrite cores. Around 1968, according to Jacobs (1969) [4] the yearly world production of ferrite cores was about 2×10^{10} cores.

Ferrites also play important role in Particle Accelerators. The operation of these large machines is based on accelerating units consisting of large transformers designed as resonant cavities. High frequency application, low eddy current losses favoured ferrite cores for this application. The alternating gradient

synchrotron in Brookhaven contains 12 such cavities and each unit contains about 500 kg of ferrite (Brockman *et al.*, 1969) [5].

Mn-Zn ferrites are widely used as core materials for coils or transformers in all electronic equipments including information and communication devices. Recently they are used in compact and light weight and high efficiency switching power supplies[ICF-7,p-38]. Magnetically soft Mn-Zn ferrites with spinel structure are the most perspective magnetic materials used in TV sets and videotape recorders[ICF-7,p-60]. Apart from these few examples of specific implementations of ferrites, we recall that the bulk of ferrite is used in telecommunication and consumer application. The main consumer products are TV sets and radio sets in which such parts as the line transformers, deflection coils, tuners and rod antennas contain ferrite materials.

The on going ferrite research is unveiling many mysteries that concern the theoreticians and at the same time revealing many special properties having industrial importance. Perhaps it is not an exaggeration to say that the advent of modern technology thus thrives much on the advancement in ferrite research.

1.3 ADVANTAGES OF FERRITE RESEARCH IN BANGLADESH

Soft ferrites are relatively cheap materials which is within our means and technical ability to develop. There are large number of applications of these soft magnetic materials where high frequency electromagnetic energy use is involved.

At present, imported soft ferrites are being used as high frequency transformer materials, inductors, antennas, recording heads, core in Switched Mode Power Supply (SMPS) etc. Other more sophisticated applications are in magnetic

recording tapes and in computer memory. Research in this field will provide information in choosing appropriate materials for the above uses and ultimately high quality materials with desired characteristics.

At present, Bangladesh is totally dependent upon the imported ferrite cores and other soft magnetic materials. If we can develop a ferrite industry in our country, that may alleviate this problem.

The present thesis reports that the Mn-Zn ferrite samples that are prepared and investigated have high permeability between the frequency range of 0.1 MHz to 5 MHz. The best quality video heads require ferrite cores that can show high permeability in this frequency band. So, these Mn-Zn ferrite samples can be used as video heads. Hence, if we can carry on our research in soft magnetic materials and in ferrites, Bangladesh can easily develop a profitable ferrite industry and can thus strengthen its electronic industry.

1.4 REVIEW OF OTHER WORKS

Ferrites, the double oxides commonly expressed by the general chemical formula $MO.Fe_2O_3$, where M represents divalent metals, first commanded the public attention when S.Hilpert [1] focused on the usefulness of ferrites at high frequency. A systematic investigation was launched by Snoek [6] at Philips Research Laboratory. At the same time Takai [7] at Japan was seriously engaged in the research work on the same materials. Snoek's extensive works on ferrites unveiled many mysteries regarding magnetic properties of ferrites. He was particularly looking for high permeability materials of cubic structure. This particular structure, for symmetry reasons, support low crystalline anisotropy. He found suitable materials in the form of mixed spinels of the type $(MZn) Fe_2O_4$, where M stands for metals like Cu, Mg, Ni or Mn, for which permeability were found to be upto 4000 [8]. Here after starts the story of Mn-

Zn ferrites. Remarkable properties like high permeability, low loss feature, high stability of permeability with temperature and time, high wear resistance, controlled coercive force, low switching coefficient etc. have aptly placed Mn-Zn ferrites as highly demandable ferrites to both researchers and manufacturers. Every year a great deal of papers are being published on various aspects of Mn-Zn ferrites. A large number of scientists and technologists are engaged in research to bring about improvements on the magnetic properties of Mn-Zn ferrites.

The sintering process is considered to be one of the most vital step in ferrite preparation and often plays a dominant role in many magnetic properties. Junzo Tasaki *et al.* [9] studied the effect of sintering atmosphere on permeability of sintered ferrite. They found that high density is one of the factors which contribute to greater permeability, μ . However, μ decreased in an atmosphere without O_2 at high sintering temperature where high density was expected. This decrease in permeability is attributed to the variation of chemical composition caused by volatilization of Zn. At low sintering temperature a high permeability is obtained in an atmosphere without O_2 because densification and stoichiometry plays a principal role in increasing μ . At high sintering temperature the highest μ is obtained in the presence of O_2 because the effect of decrease of Zn content can then be neglected.

Yuzo Shichio *et. al.* worked on vacuum sintered Mn-Zn ferrites [10] and their investigation yielded the following results:

- In vacuum, gas content in a green compact of ferrite is removed and homogeneous grain growth occurs owing to the difference in the temperature ranges of spinel formation and densification so that homogeneous pore free grains can be obtained by sintering in vacuum.
- Grain growth can be promoted by firing the vacuum sintered ferrite in an equilibrium atmosphere. Therefore a high permeability ferrite can be

obtained by this method, rectangular hysteresis ferrites with superior magnetic properties can be obtained also.

- Magnetic properties deteriorate by machining and can be removed by annealing. Vacuum is the best annealing condition for Mn-Zn ferrites

A Mossbauer study of Mn-Zn ferrites performed by C. Michalk [11] also focused on the importance of sintering conditions. He showed that the Mn-Zn formation process goes over an intermediate Zn ferrite phase during the sintering of mixed raw oxides in air. Moreover, at temperature below 600°C a tetragonal phase $ZnMn_2O_4$ was found using MnO_2 as raw materials for Mn component. The Mossbauer study shows that Mn-Zn formation is completed by 800°C instead of 1200°C for sintering in air.

Studying the electromagnetic properties of Mn-Zn ferrites, T. Nakamura[12] suggested that both the sintering density and the average grain size increased with sintering temperature. These changes were responsible for variations in magnetization, initial permeability and electrical resistivity. Both magnetization and electrical resistivity decreases as sintering density increases.

M. J. Tsay reported that [13] the high permeability Mn-Zn ferrites production is very difficult because of the evaporation of Zn at the other surface of sintering cores under a reduced atmosphere, leading to a reduction in initial permeability. A low partial pressure of O_2 and long annealing time usually results in a much serious Zn evaporation. In general the larger the size of Mn-Zn cores, the higher the degree of product homogeneity obtained.

The microstructure study of Mn-Zn ferrites can provide substantial information on various magnetic properties. A. L. Struijts made a detail survey on this matter[14]. Results are presented on theoretical and experimental studies of sintering behaviour of ferrites. Low porosity ferrites can be made when an excess of anion vacancies is present. The sinterability is drastically decreased in ferrites with an excess of cation vacancies. The ferrites also show

exaggerated pore growth, giving rise to a microstructure in which all pores are intragranular.

High quality, high stability Mn-Zn ferrites is one of the principal goal of present trend of research. P. Mossman in his paper [15] emphasise important stages in a mixed oxide process for the production of high stability, low loss Mn-Zn ferrites. The influence of microstructure is discussed with special references to the effects of porosity on disaccommodation and losses. Also tentative mechanism is given which accounts qualitatively for the observed effects. Finally, optimum microstructures are discussed in relation to very low loss materials, having loss factors $\tan\delta/\mu = 2 \times 10^{-6}$ at 100 KHz and disaccommodation factors $DF = 0.2 \times 10^{-6}$.

High permeability attainment is certainly affected by the microstructure of the ferrites. E. Roess shows that [16] the very high permeabilities are restricted to certain temperature ranges and the shapes of permeability versus temperature curves are strongly affected by any inhomogeneity in the ferrite structure.

A. Noordermer, M. T. Johnson et. al. showed [17] that the microstructure and in particular grain size is seen to strongly influence the complex initial permeability of Mn-Zn ferrites with grain size varying between 0.2 and 9 μm . Furthermore, the temperature dependence of permeability reduces with decreasing grain size to the point where little of the intrinsically temperature dependent behaviour remains for the smallest grain sizes

Joseph Pankert et. al. provided a study on the influence of grain boundaries on complex permeability in Mn-Zn ferrites [18]. In that paper, they developed a first principle model for grain boundary. Furthermore, they argued that an increase in the exchange energy is responsible for decrease in permeability and not an increase in demagnetization energy.

S. Yamada and E.Otsuki analyzed the power loss in Mn-Zn ferrites [19]. It is disclosed that the power loss was able to be divided experimentally into the hysteresis loss, the resistivity dependent loss component, and the resistivity independent component by correlating $(P_B - P_h)$ to $1/\rho_p$ at T_{min} . According to the estimated domain size and driving conditions, the residual loss is attributed to the resonance phenomena inside the domain wall due to the high speed rotation of spin inside the domain wall.

Shuichi Ida presented a paper on cation vacancy and ferrite[20]. He argued that since ferrites are bertholide compounds and the ionic radii of O_2 ion is substantially larger than those of iron group cations most of ferrites have non-stoichiometric compositions and crystal lattices contain cation vacancies. Although the densities of vacancies are usually very small i.e. less than 10^4 , they play substantial role in certain aspect of ferrites. In particular, the magnetic relaxation of ferrites at low frequency is seriously related to the cation vacancies.

P.J. Van der Zaag et. al. reported on the relation between grain size and domain size in Mn-Zn studied by Neutron depolarization[21]. This work reports on the domain size determination by means of Neutron depolarization in a series of polycrystalline Mn-Zn ferrites of varying grain size but altered composition. For ferrite sample with grain size between 0.3 to 3 μm , it is found that the domain size is identical to grain size i.e., no magnetic domain walls are present within the grains.

Working on the relation between grain boundary structure and hysteresis losses in Mn-Zn ferrites, M. H. Berger[22] showed in his paper that the influence of post sintering thermochemical conditions on the bulk magnetic properties of Mn-Zn ferrites has been correlated to the electrical behaviour of grain boundaries and to their crystallographic chemistry. It is concluded that in order

to minimize the hysteresis losses, it is imperative to keep the amount of coincidence boundaries small and to maintain a high partial pressure of O_2 during cooling.

Jenica Neaintu et.al. [23] reported in a paper on the influence of additives of Ti^{4+} ions on the properties of Mn-Zn ferrites and found that the magnetic and electrical properties of high permeability ferrites with addition of Ti^{4+} ions improved. Electrical resistivity increases while the loss factor $\tan\delta$ and disaccommodation factor decreases. Structural and magnetic properties of high permeability Mn-Zn ferrites with Ti^{4+} ions confirm that Ti^{4+} make pairs with Fe^{2+} ions and occupy the octahedral sites in the crystalline lattice.

Y. H. Han, J.J. Suh [24] presented a paper on the effect of sintering conditions on the characteristic of Mn-Zn ferrites. The paper reported that the sintering temperature significantly changed the microstructure and effected the power loss behaviour at the frequency range over 100KHz. The best power loss characteristic at 100KHz, 200mT and at 500KHz, 50mT were observed in the samples sintered over $1300^\circ C$ and below $1250^\circ C$ respectively. Those results systematically indicated that the power loss depended on the grain size, electrical resistivity and density of sintered cores.

N. Rezlescu et.al. studied the copper ions influence in Mg-Zn ferrites [25]. in that paper they showed that the incorporation of copper oxide into Mg-Zn ferrite activates the lattice diffusion and makes it possible to reduce the sintering temperature. The properties in these compounds are controlled by the copper content. The optimum copper content was appreciated to be $x=0.3$ which is sufficient to promote sintering at low temperature ($1050^\circ C$) and yield a good density ($4.5 gm/cm^3$).

Several workers have studied the influence on the grain growth and densification in soft ferrites for small additions of various oxides like V_2O_5 ,

SnO_2 and TiO_2 , either singly or in combination with each other [26-27], with a view to manipulating their electrical/magnetic properties. It is already established that defect characteristics like impurity ions in the form of solid solutions, second phase precipitates, and generally exert a drag over the grain boundary during sintering. But a liquid phase, which wets the grains, provides a fast transport medium for the host ions, during sintering.

E. Rezlescu *et. al* [28] have reported on "The influence of additives on the properties of Ni-Zn ferrite used in magnetic heads". The additives were CaO, Na_2O , ZrO_2 , Li_2O , K_2O and Sb_2O_3 . They found that the relative density generally increases with increasing impurity content. The most important increase in the density was obtained by the triple additions of Na_2O -CaO- ZrO_2 and Na_2O -CaO- Li_2O . For these samples the bulk density attains 98% of that given by X-ray. The best properties acceptable for magnetic heads were in fact obtained for these samples. They have also found experimentally that a higher impurity content (0.4-0.5 wt%) does not facilitate the densification of samples, but, on the contrary, it deteriorates the magnetic properties. Concerning the flux density B , this decreases at the beginning with increasing impurity content, has a minimum for 0.1 wt% impurity and then, for 0.2-0.3 wt% impurity, it increases. However, the B values for the samples of Na_2O -CaO- ZrO_2 and Na_2O -CaO- Li_2O are smaller as compared to pure ferrite. As most additives are inclined to decrease the flux density, it is important to select both a certain kind of and a certain amount of additives. Coercivity is also affected by additives. The coercive force increases with increasing additives content up to 0.1 wt% additive and then it decreases; the Li_2O has a little effect on the coercive force H_c . The highest values of H_c were obtained by an addition of ZrO_2 . The value of the coercive force H_c varies between 21.4 A/m for the ferrite without additives and 41.2 A/m for the ferrite with 0.1 wt% ZnO_2 . Also, by a triple addition of Na_2O -CaO- Li_2O a value of 22.4 A/m was obtained which is quite near to that of the sample without additives. The initial magnetic permeability

μ' decreases with increasing impurity content, having a minimum for 0.1 wt% additive and then it increases for 0.2 wt% additive. But, for the Li_2O doped samples, the initial magnetic permeability μ' increases continuously and thus, for these ferrites, the values of permeability can be obtained exceeding those without additives. In addition, the initial magnetic permeability μ' for the sample with triple additive of Na_2O - CaO - Li_2O was higher than that of the ferrite without additives. The frequency dependence of the initial permeability μ' for Na_2O - CaO - Li_2O added ferrite are higher than that of CaO or Na_2O added ferrites or for a ferrite without additives at high frequency. The studied impurities have a little effect on the specific saturation magnetization σ_s . It was observed that for most of the samples, σ_s is a little higher than for the sample without additive, except for the Li_2O additive which gives a slightly smaller value of the specific saturation magnetization σ_s . Also, regarding the Curie temperature T_c , practically, these are not affected by the additives. For all samples with additives, the Curie temperature varies between 428 and 434 K, while for the ferrite without additives T_c is 429K. The dc resistivity, ρ of the sintered ferrites as a function of additives content was measured too. They found that only an addition of Na_2O or CaO increases the ρ values comparatively with the ρ value for the ferrite without additives, other additive had a little effect on the resistivity.

The influence on the grain growth and density of Ni-Zn ferrites in presence of V_2O_5 have been studied by Kulikowski [29], Jain *et al.*[26] and Gasiorek *et al.* [30]. Also M.Amanullah Choudhury, *et al* [31] have studied on "The influence of V_2O_5 on the overall magnetic properties of Ni-Zn ferrites". They have reported that the initial magnetic permeability μ' increases sharply with V_2O_5 content, having a maximum for 0.7 mol% and then it decreases appreciably with further increasing content to 1.4 mol% and 2.1 mol%. The lowest value of coercive force H_c is obtained as per highest density attained at 0.7 mol% agrees with the lowest value of porosity achieved. The remanance and maximum

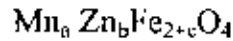
induction B_m also increase with increasing amount of V_2O_5 up to 0.7 mol % and then decrease. There is an appreciable increase in the static initial permeability with increasing amount of V_2O_5 at 0.7 mol %.

From this review work, it is observed that the magnetic properties like permeability, Curie temperature, saturation magnetization etc. are dependent on doping in a very complicated way and there is not straightforward relationship between the nature and the quantity of doping on magnetic characteristics to be understood by any simple theory. These are dependent on several factors like sintering conditions, preparation method, compositions etc. In the present work, it is aimed at determining experimentally the magnetic properties as affected by sintering temperature, compositions and the nature of doping, so that Mn-Zn ferrites with appropriate doping can be obtained in respect of high frequency response with low loss and high permeability.

1.5 PRESENT WORK

Mn-Zn ferro-ferrites are well known as a class of ferrites showing good soft magnetic properties upto frequencies of several MHz. A further attractive property of the Mn-Zn ferro-ferrite system is the possibility to significantly modify the magnetic properties by introducing small amount of dopant ions [32]. It is one of the most extensively used ferrites. The Mn-Zn ferrite has found various uses in the high frequency region. High permeability, low loss feature, high wear resistance, controlled coercive force etc. are the few examples of the remarkable characteristics possessed by the Mn-Zn ferrite. The chemical and magnetic structure of Mn-Zn ferrite are well known. It is ferrimagnetic and possesses a cubic structure

In the present work, our aim is to investigate various magnetic properties exhibited by Mn-Zn ferrite samples with and without dopants having the general chemical formula



where $a+b+c = 1$. The value of a , b and c are chosen in such a way that we can have two distinct series of compositions. Two series are $\text{Mn}_{0.51} \text{Zn}_{0.44} \text{Fe}_{2.05} \text{O}_4$, and $\text{Mn}_{0.7-x} \text{Cu}_x \text{Zn}_{0.22} \text{Fe}_{2.08} \text{O}_4$. In the first series 1 mole % of V_2O_5 , TiO_2 and CoO are doped. In the second series, we used Cu^{2+} ions substitutes for Mn^{2+} .

At first, the X-ray diffraction pattern has been taken to get the information regarding the crystal structure of the samples. The Curie temperature measurements are performed in order to have a closer view on the ferrimagnetic interactions between the magnetic atoms. The magnetization measurements give a general view on magnetic moment arrangements in different crystal sites. The permeability measurements are done in order to find the optimum compositions, the best sintering conditions and microstructure study is also performed to have information on grain size distribution.

The physical properties of ferrites depend sensitively on the chemical composition, preparation conditions, sintering temperature and time, and amount and type of additives [33]. As a result, it is possible to obtain a good soft magnetic material by optimally choosing the additives. The magnetic properties are required to be improved for the ferrite materials. Some improvement of Mn-Zn ferrite single crystals have been undertaken by adjusting chemical compositions, their homogeneities and reducing residual stresses. In this study, the effects of additives on Mn-Zn ferrites single crystals were investigated in a manner as the magnetic properties of polycrystalline ferrites have been improved by some additives. The main theme of this thesis work is to find an optimum composition and a best sintering condition for low loss and uniform high permeability over a large frequency range rather than looking only for theoretical explanations of the complex mechanisms involved in various aspect of Mn-Zn ferrite samples.

REFERENCES

CHAPTER-1

1. S. Hilpert, Ber.Deutsch. Chem. Ges.Bd 2, 42, 2248, 1909.
2. J. Kulikowski, JMMM, 41, 56, 1984.
3. W. Six, Philips Tech, Rev. 13, 301, 1952.
4. I. S. Jacobs, JAP, 40, 917, 1969.
5. F.G. Brockmann, H. Vader Heide and M.W. Rouwerse, Philips Tech R., 30, 323, 1969
6. J.L. Snoek, Physica, 3, 436, 1936.
7. T. Takai, J. Electr Chem. Japan, 5, 411, 1937.
8. J.L. Snoek, New Devel. In ferromagn. Materials (Elesvier, Amsterdam) 1947.
9. J. Tasaki, T. Ito, Intl. Conf. On Ferrite, Japan, 1970.
10. Y. Shichizo, E. Takama, ICF, Japan, 1970.
11. C. Michalk, JMMM, 68(1987) 157.
12. T. Nakamura, Y. Okano, Proc. ICF-7, France, 1996.
13. M.J. Tsay, M.J. Tung, C.J. Chen, Proc. ICF-7, France, 1996.
14. A.L. Struijts, Proc. ICF-1, Japan, 1970.
15. P. Mossman, Proc. ICF-1, Japan, 1970.
16. E. Roess, Proc. ICF-1, Japan, 1970.
17. M.T.Johnson, A.Noordermeer, M.M.E. Severin, W.A.M. Meenwissen, JMMM,116(1992) 169-176.
18. J. Pankert, JMMM, 138(1994) 45-51.
19. S. Yamada, E. Otsuki, J. Appl. Phys., 81(8),(1997)4791-4793
20. S. Ida, Proc. ICF-1, Japan, 1970
21. P.J. van der Zaag, M.T. Johnson, A. Noordenneer, P.T. Por, M. Th. Rekveidt, JMMM, 99 (1991) L1- L6
22. M.H.Berger, J.H. Laval, F. Kools, J. Roelofsoma, Proc ICF-5, India, 1989.

23. Jenica Neamtu, M.I. Toacsen, D.Barb, Proc. ICF-7, France, 1996.
24. Y.H. Han, J.J. Suh, Proc. ICF-7, France. 1996
- 25 N.Rezlescu, E. Rezlescu, P.D. Popa, M.L. Craus, L. Rezlescu, JMMM 182(1998) 199-206.
26. G. C. Jain, B. K. Dass, R. B. Tripathi and Ram Narayan, "Influence of V₂O₅ on the densification and the magnetic properties of Ni-Zn ferrites, JMMM 14 (1979) 80-86.
27. I. Hanke, M. Zengen, Mn-Zn ferrites with combined Sn-Ti substitutions, JMMM 4 (1977) 120-128.
28. E. Rezlescu, N. Rezlescu, C. Pasnicu, M.L. Craus and D.P. Popa, JMMM 117 (1992) 448-454.
29. J. Kulikowski, Sov. Power Metal and Met. Cer. (USA) 12 (1973) 597.
30. S. Gasiorek and J. Kulikowski, JMMM, 26(1982)295.
31. M.A. Choudhury, M.A. Mazid, M.R. Bari, M.A. Hakim, S. Akhter, Nguyen Chau, Dang Le Minh, Bach thann Cong. Proc. of the 2nd Intl. Workshop on Mat. Sci. (IWOMS' 95), Hanai, October 1995
- 32 M.T. Johnson, Proc. ICF-5, 1989, India.
33. M.A. Ahmed, M.E. El Hiti, J. Phys (France) III, 5, 1995, 775.

CHAPTER-2

THEORETICAL BACKGROUND

2.1 THEORY OF FERRIMAGNETISM

The history of the development of theories of Ferrimagnetism is not very ancient one. The substantial importance of magnetic oxides in high frequency application was perceived as early as 1909 by S. Hilpert [1]. He made rigorous investigations on various oxides including some special magnetic ones which are called 'ferrite'. By the year 1915 the crystals structure of ferrite was known. This was independently done by W.H.Bragg [2] in England and S. Nishikawa [3] in Japan. A resourceful study on the chemistry of ferrites was done by Forestier (1928) [4]. In spite of all these endeavours ferrimagnetism had not been marked as a distinct category of magnetism until 1948. L. Neel came up with his revolutionary paper and established ferrimagnetism as a distinct class of magnetism. In practical importance they are second only to ferromagnetics and are superior to them in some applications.

As it is evident from ferromagnetism that, incomplete 3d shells in transition and 4f shells in rare-earth elements result in permanent atomic magnetic moment. When they are all in parallel alignment we get Ferromagnetism. But elements right next to the ferromagnetic transition elements (e.g. iron, cobalt, nickel) such as Chromium, Manganese are not ferromagnetic. It has been found that magnetic moments in these materials alternate from atom to atom as shown in Fig. 2.1(b). Such materials are known to be Anti-ferromagnetic. But Ferrimagnetism is somewhat different from these Ferromagnetism and Antiferromagnetism. It has following features:

1. two or more species of magnetic ions.
2. ordering of all constituent ions.
3. a mixed scheme of ferromagnetic and anti-ferromagnetic spin coupling of magnetic ions, and
4. a net magnetization

These materials are said to possess Ferrimagnetism. The most important ferrimagnetic substances are certain double oxides of iron and other metals. These magnetic substances called *FERRITES* are developed into commercially useful materials chiefly during the years 1933-1945 by Snock [5] and his associates at Philips Research Laboratory in Holland.

Albeit ferrites show some characteristics similar to that of ferromagnetic, there are some marked discrepancies. Unlike the ferrimagnetic, ferrites are ionic compound and hence work as semiconductor, in most of the cases as isolator. That's why Feynman [6] used to call them *ferromagnetic insulator*.

Ferrites have very high resistivity (at least million times that of a metal). This high resistivity ensures their use in high frequency application where eddy current loss minimization is hadly needed. Also, the magnetization curves shown in Fig.-2.2 shows that the reduced magnetization $\sigma_r = \sigma / \sigma_0$ of a typical ferrite decreases rather rapidly with increasing temperature, whereas the value of σ_r / σ_0 for iron remains large until T / T_c exceeds about 0.8 . Furthermore, in the paramagnetic region, the variation of the inverse susceptibility with temperature is decidedly non-linear. This shows that the Curie-Weiss law is not obeyed.

These several facts led Neel to envisage a distinct form of magnetic structure for the ferrites. Crystallographic studies have provided the clue that the cations in a

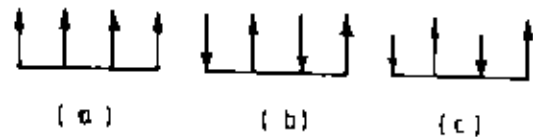


Fig. 2.1: Magnetic arrangements : (a) ferromagnetic
 (b) antiferromagnetic (c) ferrimagnetic

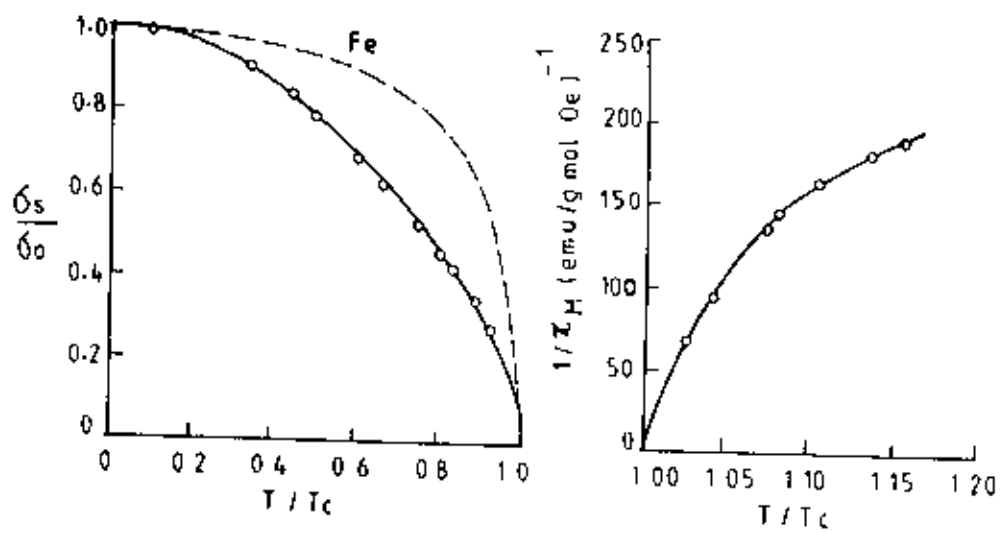


Fig. 2.2: Thermal variation of the magnetic properties of a typical ferrimagnetic ($\text{NiO} \cdot \text{Fe}_2\text{O}_3$) The fractional specific magnetization δ_s / δ_0 in ferrimagnetic region is according to Pauthenet and the reciprocal molecular susceptibility $1 / \chi_M$ in the paramagnetic region is according to Serres (The dashed curve at left applies to metallic iron)

ferrite crystal occupy two crystallographically different kinds of position called *A sites* and *B sites*. Neel made the basic assumption that the exchange interaction between these two sites is negative, meaning that the spin orientation is opposite to each other. This thing also happens in antiferromagnetism. The difference is that, in case of ferrimagnetism magnitudes of the A and B sublattice magnetizations are not equal and a net spontaneous magnetization results.

The exchange interaction acting in ferrites is of a different kind. As pointed out by Neel, the cations are mutually separated by bigger anions (oxygen ions) which practically excludes a direct contact between the cation orbitals, making any direct exchange at least very weak. Instead, we encounter *Super Exchange* i.e. indirect exchange via oxygen p orbitals that may be strong enough to order the magnetic moments. The strength of this interaction depends on the degree of orbital overlap of oxygen p orbital and transition metal d orbital. The interaction decreases as the metal ions move apart and the angle between them decreases from 180° to 90° . In Neel's theory, the interaction are taken as effective inter and intra-sublattice interactions A-A, B-B and A-B. The type of magnetic order depends on their relative strength. The theory of super exchange as given by Anderson (1959, 1963) [7-8] and the semi empirical rules provided by Goodenough (1958) [9] and Kanamori (1959) [10] yield some predictions concerning the sign and strength of this interaction. It is found that A-A interaction is weak compared to B-B interaction. But angle between B-B interaction is 90° thus making it weak compared to A-B interaction where angle is 125° . Thus anti parallel spin alignment takes in two sub lattices. The interaction energy density may be written as

$$U = -2 J S_i \cdot S_j \quad (1)$$

If the exchange integral, J in equation (1) is positive, we achieve ferromagnetism. A negative J may give rise to anti-ferromagnetism or

ferrimagnetism. The mean exchange fields acting on A and B sites may be written as

$$\begin{aligned} B_A &= -\lambda M_A - \mu M_B \\ B_B &= -\mu M_A - \nu M_B \end{aligned} \quad (2)$$

All constants λ , μ , ν are taken to be positive. The minus sign that corresponds to an antiparallel interaction. The interaction energy density is

$$\begin{aligned} U &= -1/2 (B_A \cdot M_A + B_B \cdot M_B) \\ &= 1/2 \lambda M_A^2 + \mu M_A \cdot M_B + 1/2 \nu M_B^2 \end{aligned} \quad (3)$$

This is lower when M_A is anti-parallel to M_B than when M_A is parallel to M_B . The energy of antiparallel alignment should be compared with zero, because a possible solution is $M_A = M_B = 0$. Thus when

$$\mu M_A M_B > 1/2 (\lambda M_A^2 + \nu M_B^2) \quad (4)$$

the ground state will have M_A directed opposite to M_B . Under certain conditions there may be non-collinear spin arrays of still lower energy.

The susceptibility of ferrimagnets is readily formulated if we assign separate Curie constants C_A and C_B to the two sublattices. Neglecting intra sublattice interaction we have ferrimagnets:

<u>Sub lattice A</u>	<u>Sub lattice B</u>
$B_A = -\mu M_B$	$B_B = -\mu M_A$
$M_A T = C_A (B_A - \mu M_B)$	$M_B T = C_B (B_B - \mu M_A)$

(5)

Here B_a is applied field. These equations have a non zero solution for M_A and M_B in zero applied field if

$$\begin{vmatrix} T & \mu C_A \\ \mu C_B & T \end{vmatrix} = 0 \quad (6)$$

from which the ferrimagnetic Curie temperature $T=\theta_f$ is given by

$$\theta_f = \mu (C_A C_B)^{1/2} \quad (7)$$

we solve eqn. (5) for M_A and M_B to obtain the susceptibility at $T > \theta_f$:

$$\chi = \frac{M_A + M_B}{B_a} = \frac{(C_A + C_B)T - 2\mu C_A C_B}{T^2 - \theta_f^2}$$

(8)

This is more complicated than the Curie -Weiss law for ferromagnets at $T > \theta_f$. The plot of $1/\chi$ against T is shown in Fig.2.3. It is to be noted that the reciprocal ferrimagnetic susceptibility shows considerable curvature as the temperature approaches θ_f and becomes infinite at θ_f .

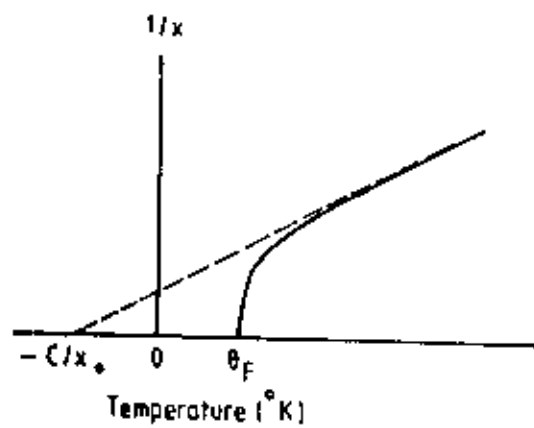


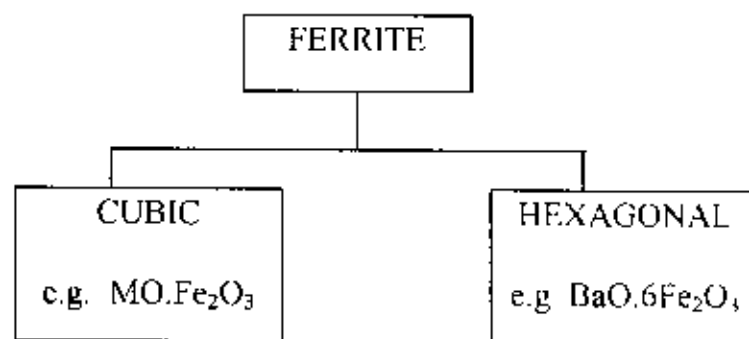
Fig. 2.3: Theoretical variation of the reciprocal susceptibility with temperature for a ferrimagnetic above the Curie point.

2.2 FERRITES

The most important ferrimagnetic substances are certain double oxides of iron and other metal. These magnetic oxides are commonly known as *ferrites*. The general chemical composition can be written as $MeO \cdot Fe_2O_3$, where Me represents a divalent metal ion such as Ni, Mn or Zn. The study of crystallographical experiment on ferrites has proved that they can be taken as direct descendants from 3 natural compounds the spinel, the garnet and the magneto plumbite. The outstanding property of ferrites which makes them suitable for many applications is their high electrical resistivity compared to that of metals. Their specific resistivity ranges from 10^2 to 10^{10} Ω -cm which is upto 15 order of magnitude higher than that of metals like iron. High frequency application thus demands extensive implication of ferrite industry.

2.3 DIFFERENT TYPES OF FERRITE

The magnetic ferrites fall into two groups of different crystal structure as shown below:



CUBIC FERRITES: These have the general formula $MO \cdot Fe_2O_3$ where M is a divalent metal ion like Mn, Ni, Fe, Co, Mg etc. Cobalt ferrite $CoO \cdot Fe_2O_3$ is magnetically hard, but all other cubic ferrites are magnetically soft. These ferrites are said to have *SPINEL* structure and are often called *ferro spinels*

because their crystal structure is closely related to that of mineral spinel $MgO \cdot Al_2O_3$. In case of ferrites the divalent ions replace Mg and trivalent ions replace Al. In all cases the ionic radii of the substituting ion should be between about 0.5 to 1.0 Å [11].

HEXAGONAL FERRITES: These ferrites, essentially employed in microwave frequencies, have hexagonal structure. They have an axis of symmetry, C and a high magnetocrystalline anisotropy. The preparation of hexagonal ferrite is the ceramic technique and is almost same as that of spinels. During the pressing the grains are oriented by a magnetic field in order to align the C-axis of all crystallites in the same direction. As a result, a sample similar to a permanent magnet is produced. When a microwave field is applied to a plane perpendicular to magnetization direction, a gyro-resonance effect is observed. There are two types of this hexagonal ferrites: M-type and W -type.

M-type ferrites are derived from Barium or Strontium ferrites, whose formulae are $BaFe_{12}O_{19}$ and $SrFe_{12}O_{19}$. By partial substitution of Al^{3+} ions (or Ga^{3+} or Cr^{3+}) for Fe^{3+} ions causes the magnetization to increase and magnetocrystalline anisotropy field to increase; where as by substitutions of the groups $Ti^{4+} Me^{2+}$ or $Ge^{4+} Me^{2+}$ (with $Me^{2+} = Co, Ni, Zn$ -----) for Fe^{3+} ions, causes both the magnetization and the anisotropy field to decrease. The combined substitution of both result in better stability of anisotropy field, H_a , with temperature [12]

W-type are derived from barium ferrites whose formula is $Ni_2BaFe_{16}O_{27}$; by partial substitution of Al^{3+} ions for Fe^{3+} ions, causing increment in magnetization and anisotropy field, H_a ; whereas by partial substitution of Co^{2+} for Ni^{2+} causes H_a to decrease keeping magnetization unchanged. These ferrites are used in circulators with resonance frequencies lower than those of M-type [12].

Besides these, there are few other ferrimagnetics of substantial importance. Among them γ - Fe_2O_3 called maghemite and Garnets are worth mentioning. γ - Fe_2O_3 has cubic structure and is formed by oxidizing magnetite. It is unstable and transforms to α - Fe_2O_3 (hematite) on heating above 400°C and γ - Fe_2O_3 is currently the most popular material for magnetic recording tapes.

On the other hand, Garnet, the semi precious stone, is a group of isomorphous minerals with a complex cubic structure. The most common Garnet, Yttrium-iron garnet, the YIG, has important applications at very high frequencies, in microwave region.

2.4 CRYSTAL STRUCTURE OF SPINEL FERRITES

The usual name for cubic ferrites is Spinel ferrite because its crystal structure is similar to the mineral spinel MgAl_2O_4 crystallized in the cubic system. This crystal structure was first determined by Bragg [2] and by Nishikawa [3]. The smallest cell of this spinel lattice having cubic symmetry contains eight molecules or total of $8 \times 7 = 56$ ions. The large oxygen ions (radius about 1.3 \AA) are packed quite close together in a face centered cubic arrangement and the much smaller metal ions (radii ranging from 0.7 to 0.8 \AA) occupy the spaces between them. These spaces are of two types. One is Tetrahedral, called the *A-site* because metal ion is placed at the center of a tetrahedron with oxygen atoms at the corner of the tetrahedron . The other is Octahedral, called the *B-site* because oxygen ions around it occupy the corner of an octahedron as shown in fig.-2.4. The crystallographic environment of

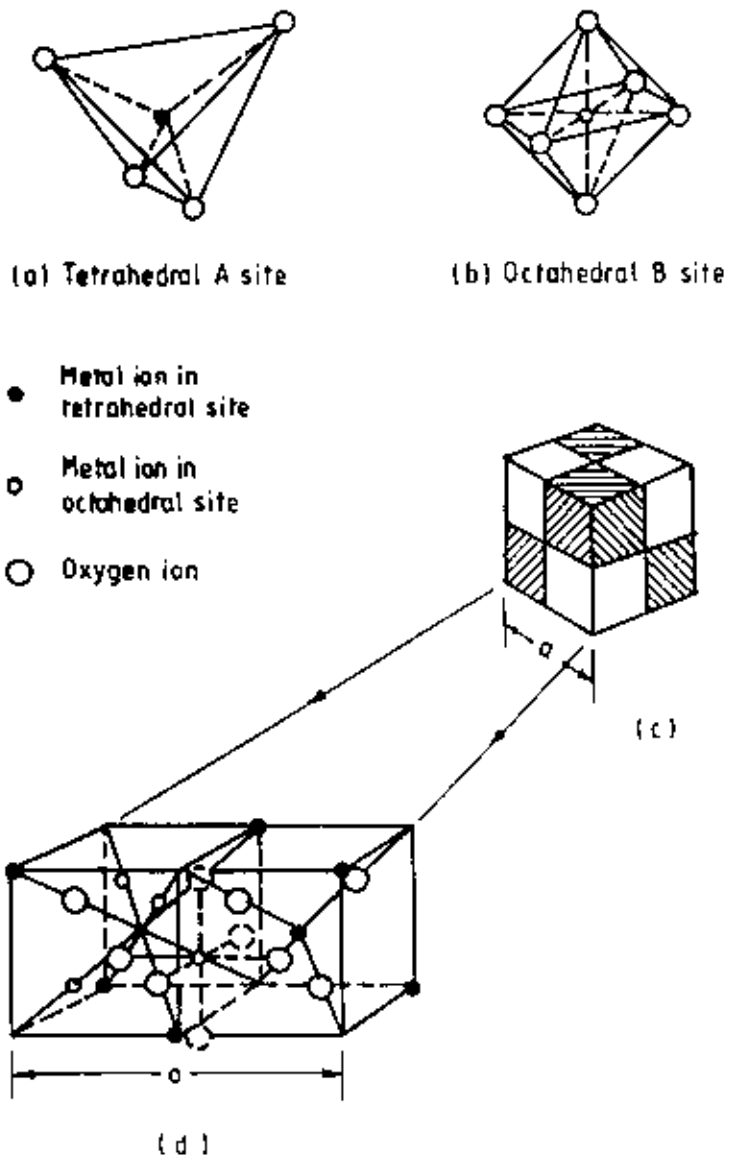
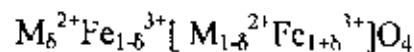


Fig. 2.4: Crystal structure of a cubic ferrite.

A and B sites are therefore distinctly different. In a unit cell there are 64 tetrahedral sites of which 8 are filled and 32 octahedral sites of which 16 are filled. A unit cell contains so many ions that it is better to imagine the unit cell of edge a to be divided into 8 octants each of edge $a/2$ as shown fig. 2.4. The 4 shaded octants have identical contents - so do the other unshaded ones. The octants of two lower left in (c) is shown in (d). As we already know that the general formula for spinel ferrite is $MO.Fe_2O_3$, the distribution of divalent M and trivalent Fe^{3+} ions is very intriguing. It was believed that 8 M ions are in 8 available A sites and the 16 Fe^{3+} ions are in 16 B sites. In many cases, the fact is so, as in mineral spinel, which is therefore known as a *Normal spinel*. Barth and Posnjak [13] have shown, however that this simple assumption is not always right. Employing X-ray diffraction, neutron diffraction technique and from saturation magnetization magnitude at absolute zero it has been found that spinels also occur with 8 M ions in 8 of the 16 B sites and with 16 Fe^{3+} ions uniformly distributed over the remaining sites. These are called *Inverse spinel*.

XRD provided that Zn and Cd-ferrites are normal and other are inverse. Neutron diffraction confirmed this. A completely normal or inverse spinel represents extreme cases. The general cation distribution can be indicated as



where ions on A sites are given in front of square brackets and the B sites ions are within brackets. For a completely random distribution $\delta = 1/3$, for normal spinel $\delta=1$ and for inverse $\delta=0$. The quantity δ is a measure of inversion. In the case of some ferrites δ depends upon the method of preparation.

References

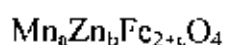
1. S. Hilpert, 1909, Ber. Deutseh. Chem. bes. Bd 2, 42, 2248.
2. W.H. Bragg, 1915, Phil. Mag. 30, 305.
3. S. Nishikawa, 1915, Proc. Tokyo Math. Phys. Soc. 8, 199.
4. H. Forestier, 1928, Ann. de. Chim. 10e ser. 9, 316.
5. J.L. Snoek, 1936, Physica, 3, 463.
6. R.P. Feynman, 1964, Addison-Wesley Pub. Co. Vol.-2, pp-37-12.
7. P.W. Anderson, 1959, Phys. Rev. 115, 2.
8. P.W. Anderson, 1963, Exchange in insulators In: Magnetism. eds , G.T. Rado and H. Suhl (Academic Press, New york, London) Vol. 1, pp-25-86.
9. J.B. Goodenough, 1958, J. Phys. Chem. Solids, 6, 287.
10. J. Kananon, 1959, J. Phys. Chem. Solids, 10, 67.
11. S.W. Gorter, 1954, Philips Res. Rep. 9, 295.
12. J. Nicolas, Microwave Ferrites in: Ferromagnetic Materials. Vol. 2, Edited by E.P. Wohlfarth, North-Holland Pub. Co, 1980.
13. T.F.W. Barth and E. Posnjak, 1932, Z. Kristallor, 82, 325.

CHAPTER-3

SPECIMEN PREPARATION

3.1 METHODOLOGY OF FERRITE PREPARATION

The preparation of polycrystalline ferrites with optimum desired properties is still a complex and difficult task. Knowledge and control of the chemical composition, homogeneity and microstructure are very crucial. The preparation of polycrystalline ferrites with properties optimized has always demanded delicate handling and cautious approach. As the most of the properties needed for ferrite applications are not intrinsic but extrinsic, preparation of samples has to encounter added complexity. The ferrite is not completely defined by its chemistry and crystal structure but also requires knowledge and control of parameters of its microstructure such as density, grain size and porosity and their intra- and intergranular distribution. It is well known that almost all ferrites decomposes at the elevated temperature if we want to melt them under normal conditions. This happens because the oxygen splits off at higher temperature reducing Fe^{3+} to Fe^{2+} . This necessarily implies that ferrite preparation by melting, as in case of metals, is not possible. The normal methods of preparation of ferrites comprise the conventional ceramic method or powder metallurgy, chemical co-precipitation method and sol-gel method. In this thesis work conventional ceramic method has employed for the preparation of Mn-Zn ferrite for its relative simplicity and availability. The powder preparation process and sintering facility available at the Magnetic Material Division, Atomic Energy Centre, Dabka has been utilized for the preparation of samples. Three types of Mn-Zn ferrite polycrystalline samples with and without different dopants with general formula

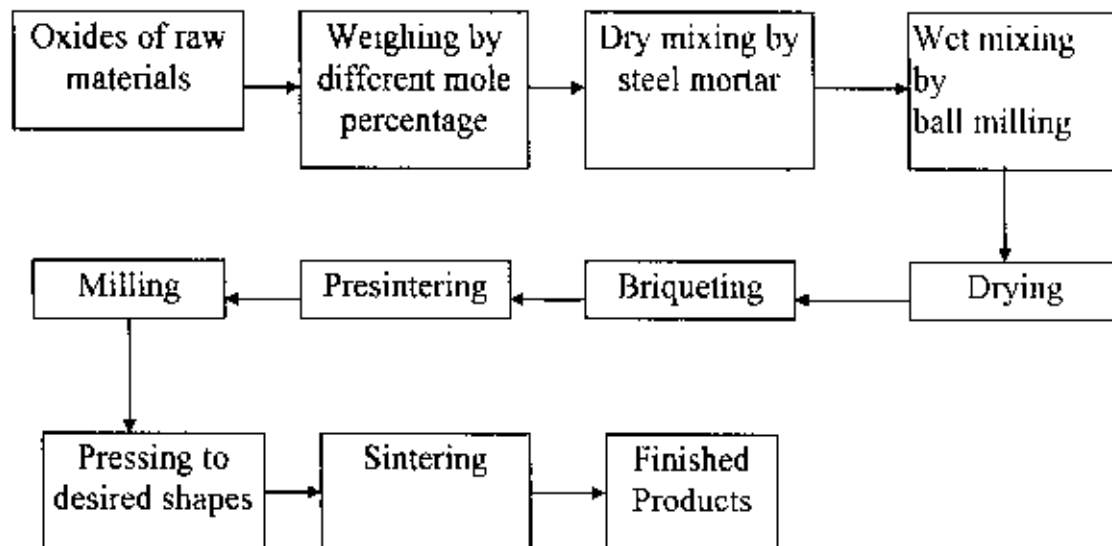


where $a+b+c = 1$, have been prepared by this method. The different samples with varying a, b and c dopant percentage are shown in table-I in Appendix.

The properties of Mn-Zn samples are influenced considerably by sintering temperature and dopants used in this process and is found that a closed correspondence between different samples with and without dopants may be achieved

3.2 METHOD OF PREPARATION

The general preparation procedure of ferrites comprises of following operations as shown in the block diagram below and the detail of which are described subsequently.



As a whole the preparation procedure generally consists of four major steps

1. Preparing a mixture of materials with the cations more or less in the ratio corresponding to that in the final product
2. Prefiring the mixture to form ferrite.
3. Converting the 'raw' ferrite into powder and pressing the powder into the required shape.
4. Sintering to produce a highly densified product.

One thing is to be remembered that, the sintering process is irreversible in terms of microstructure so that constant care must be maintained to keep conditions constant prior to and during sintering.

The following discussion will cover the important features of each step.

1.Preparing a mixture of materials having the right ratio of cations

The extent of work in this step varies greatly, depending on the starting materials. When component oxides are used, the corresponding step involves a mere mixing of the oxides by wet milling. To avoid iron contamination, mixing is done with stainless steel balls in a steel ball milling machine and a fluid such as distilled water is used to prepare the mixture into a slurry.

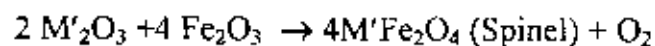
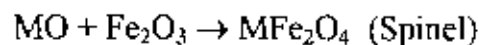
The raw materials for the preparation of the Mn-Zn ferrite were oxides of iron, nickel oxide and zinc oxide. The high purity of raw materials are given in the analytical research grade as supplied by the manufacturer *E.Mark* of Germany. The constituent component in required stoichiometric proportions were weighed first and then were thoroughly mixed using ceramic mortar and pestle. The resultant powder were then ball milled for 6 to 8 hours to produce fine powders of mixed constituents.

2.Prefiring the mixture to form ferrite

The slurry prepared in step 1 is dried, palletized and then transferred to a porcelain crucible for prefiring at temperature between 900°C and 1250°C . This was performed in the furnace named *Gallen Kamp* at AECD. As far as the final composition of the ferrite is concerned step-2 is most crucial because subsequent steps would not change the composition substantially. For this reason, it is important to understand how a ferrite is formed from its component oxides. Few detail studies have reported on formation on Mn-Zn ferrite prepared by conventional mixed oxides ceramic methods [1-8] The solid state

reactions leading to the formation of ferrites actually achieved by counter diffusion. This means that the diffusion involves two or more species of ions which move in opposite direction initially across the interface of two contacting particles of different component oxides. In 1965 Carter, Kooy and Reijnen [9-14] made careful studies of the position of inert markers in diffusions couples and computed that the counter diffusion essentially involves the movement of cations through a more or less rigid lattice of oxygen anions.

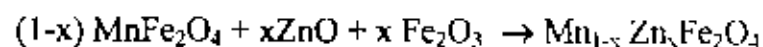
During the prefiring stage, the reaction of Fe_2O_3 with metal oxide (say, MO or M'_2O_3) takes place in the solid state to form spinel according to the reactions [15]:



The MnO creep into Fe_2O_3 as below, to form an intermediate phase $NiFe_2O_3$ at low temperature :



after that Zn ions are introduced by



The mechanism just described for the formation of ferrites justifies the separate prefiring and sintering steps taken in the preparation procedures. The ferrite is formed essentially in step 2 but the 'raw' ferrite thus formed has poor qualities. In order to produce chemically homogeneous and magnetically better material this prefired lump material was crushed. These oxide mixtures were then milled thoroughly for 6-8 hours to obtain homogenous mixture. It is to be mentioned that the grain size can be reduced to $\approx 1\mu$ by normal ball milling.

However, some fraction of the particles in that case may be reduced to even sub micron level.

3. Converting the raw ferrite into powder and pressing the powder

Besides reducing the particle size to $\approx 1\mu$, grinding also eliminates intra particle pores and homogenizes the ferrite by mixing (Int. Symp. React. In Solids, Elsevier, Amsterdam). To promote successful sintering in the next steps, the powder must be well characterized after grinding with respect to such factors as particles size and distribution, particle shape, homogeneity, adsorbed gases, impurities and intraparticle porosity. Iron contamination due to continuous wear of the mill wall and steel balls need to be closely watched and minimized. Now to this ground homogeneous powder polyvinyl alcohol is added as a binder. Pressing the powder into compacts of desired shapes is done either by conventional method in a die-punch assembly or by hydrostatic or isostatic compaction.

We made use of the former one. Pressing a uniformly dense body by this method is difficult owing to the friction gradient of the powder at the walls of the die and between the particles themselves. This problem is somewhat overcome by the addition of external and internal lubricant to the powder such as stearic acid. Mainly, we made two types of samples - cylindrical and toroidal.

Specimens were prepared by a hydraulic press with a pressure of 60 bar. The die was designed and made in the workshop of AECD. This is made of non-magnetic stainless steel.

4. Sintering

This is a heat treatment by which a mass of compacted powder is transformed into a dense object. In this process atomic mobility of the compact is sufficient to permit the decrease of the free energy associated with the grain boundaries. As the final major step in the preparation of ferrite product, sintering must fulfill three requirements : (i) to bond the particles together so as to impart sufficient strength to the product. (ii) to densify the grain compacts by eliminating the pores and (iii) to homogenize the materials by completing the reactions left unfinished in the prefiring step. The theory of heat treatment is based on the principle that when a material has been heated above a certain temperature, it undergoes a structural adjustment or stabilization when cooled to room temperature. In this operation, the cooling rate plays an important role on which the structural modification is mainly based. Sintering of crystalline solids is dealt by Coble and Burke and Zener [16-17] who found the following empirical relationship regarding rate of grain growth:

$$\bar{d} = kt^n$$

where \bar{d} is the mean grain diameter, t is sintering time, n is about 1/3 and k is a temperature dependent parameter. For sintering our samples, we used a programmable furnace NABER (Model-HT 08/16 Germany) at AECD. The temperature of the furnace could be maintained within an accuracy of $\pm 1^\circ\text{C}$. For sintering we followed more or less the following programme. The sample was first heated from temperature of 24°C to 200°C in 30 min. time. Then it was raised upto 600°C in 50 min. after that to 1150°C - 1300°C in 130 - 135 min. time. The highest temperature was kept constant for a period of 2 hour. Then temperature was brought down to 600°C in 120 to 100 min. time. The specification of the sintered samples are shown in table - 1 in Appendix.

References

1. U Konig, Tech. Mitt. Krupp-Forsch. Ber. 32 (1974)75.
2. E. Roess, Ferrites, Proc. Intern. Conf. Japan (1980) 203.
3. G.C. Kuezynski, Ferrites, Proc. Intern. Conf. Japan (1970)87.
4. P.Reijnen, Science of Ceramics, Vol. 3, Ed. G H. Stewart (Academic Press. London, 1967).
5. J. F. Dunean, K. J. D. Mckenzie and D. J. Stewart, The Mossbauer effect, Symp. Faraday Soc. 1 (1967) 103.
6. M. Zaharescu, M. Balasoin, M. Crisan, D. Crisan, T. Tavalala and V. Moser. Rev. Roum. Chim. 29(1984)247.
7. P. Nauber and C. Michalk, Hermsderfer Techn. Mitt. 25 (1985) 2152.
8. A. Chiba and O. Kimura, J. Japan. Soc Powder and Powder Mat. 31 (1984) 75.
9. O. Kimura and A. Chiba, ferrites, Proc. Intern. Conf. San. francisco 1984, preprint.
10. A. L. Struijts, G. W. Rathenan and G H. Weber, Vol 16, No. 5-6, p-141-180, Nov-Dec. (1952).
11. S. Foner, Rev. Sci. Instr 30, (1959) 548.
12. G. W. Rathenan, J. Smit, Al-Stuyts. Z. Phys. 133, No. 1-2, (1952) 250-260.
13. R. E. Carter, J. An. Ceramic Soc. 44, (1961) 116.
14. C. Kooy, 5th Int. Symp. React. In Solids (Elsevier, Amsterdam) p-21 (1965)
15. P. Reijnen, 5th Int. Symp. React. In Solids (Elsevier, Amsterdam) p-562 (1965).
16. P. I. Slick, Ferrites for nNon-microwave Applications, ferromagnetic materials, Vol. 2, Ed. E. P. Wolfarth, 1980, North Holland Pub. Co.
17. H Remy, Lehrbuch der anorg. Chemic (Akad. Verlagsges, Geest & portg K.G. Leipzig) (1973).
18. C. Michalk, JMMM 68 (1987) 157, North Holland, Amsterdam.

- 19 R. L. Coble and J. E. Barkc, 1964, 4th int. Symp. On the Reactivity of Solids, Amsterdam, 1960 (Elsevier, Amsterdam) p-38-51.
20. C. Zener, 1984 [quoted in: C. S.Smith, 1940, Trans. AIME 175, 15].
21. E. Roess, 1971, Proc. Int. Conf. on Ferrites. Kyoto, 1970, eds. Y. Hoshino et. al. (Uni. of Tokyo Press) pp-187-190.
22. y. Schichijo, N. Tsuga, and suzuki, 1961, J. Appl. phys. 35, 1946.

CHAPTER-4

EXPERIMENTAL

4.1 THE X-RAY DIFFRACTION

The X-ray diffraction (XRD) provides substantial information on the crystal structure. XRD is one of the oldest and effective tool for the determination of the atomic arrangement in a crystal.

X-ray are the electromagnetic waves whose wavelength are in the neighborhood of 1 \AA . The wavelength of an X-ray is thus of the same order of magnitude as the lattice constant of crystals, and it is this which makes X-rays so useful in structural analysis of crystals.

Whenever X-rays are incident on a crystal surface, they are reflected from it. The reflection abides by the Bragg's law as given below

$$2d \sin\theta = n\lambda$$

here d is the distance between crystal planes, θ is the incident angle, λ is the wave length of X-ray and n is a positive integer. Bragg's law also suggests that the diffraction is only possible when $\lambda < 2d$.

The crystal structure of our Mn-Zn ferrite samples were identified by taking powder diffraction pattern of the samples with an X-ray diffractometer (Model no.- JDX-8P JEOL CO., Ltd, Tokyo, Japan) available at BUET. Monochromatic CuK_α radiation was used. The XRD patterns spanned an angular deviation of 50° , starting from 25° and ending at 75° . The interplanner distance d was calculated from these 2θ values of the diffraction peaks using

the Bragg's relation. The lattice parameter 'a' was calculated by using the following relation:

$$a = \frac{\lambda}{2 \sin \theta} \sqrt{h^2 + k^2 + l^2}$$

where h, k and l are the indices of the crystal planes. X-ray density ρ_x was also calculated using the lattice parameter. The relation between ρ_x and a is as follows:

$$\rho_x = \frac{8M}{Na^3} \text{ gm/cm}^3$$

where N is the Avogadro's number ($6.02 \times 10^{23} \text{ mol}^{-1}$), M is the molecular weight. The difference between the theoretical density (measured by usual mass and dimensional consideration) and ρ_x gave us the measure of porosity.

4.2 CURIE TEMPERATURE MEASUREMENT

Curie temperature measurement is one of the most important measurements for magnetic materials. Curie temperature provides substantial information on magnetic status of substance in respect of the strength of exchange interaction. So, the determination of Curie temperature accurately is of great importance.

Our experimental set up for Curie temperature measurement is shown in fig. 4.1. We made use of the above experimental facilities available at Magnetic Material Division, AECD. The temperature dependent permeability was measured by using

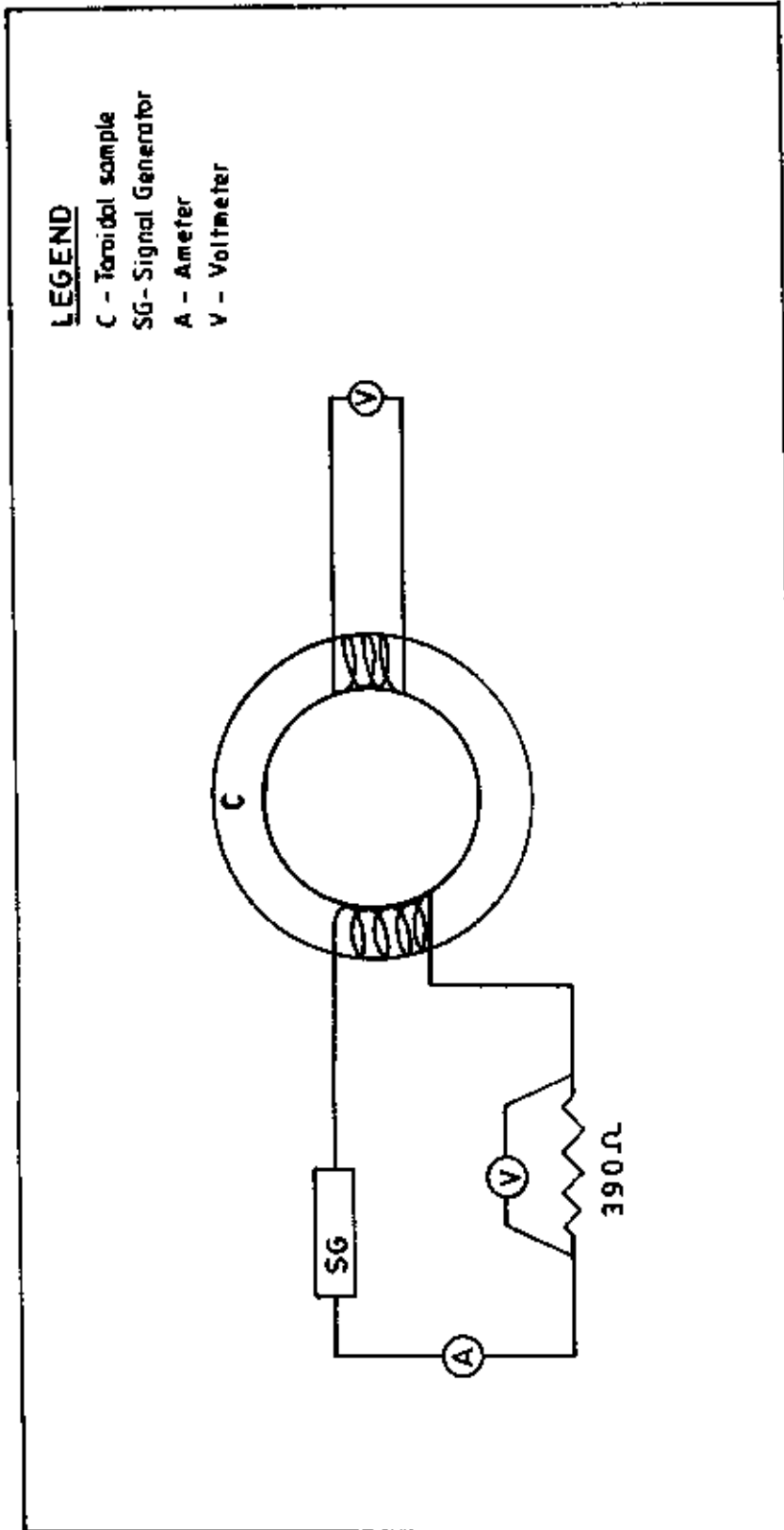


Fig. 4.1: Schematic diagram for the experimental setup for determination of Curie Temperature .

induction method. The specimen formed the core of the coil. By varying temperature, permeability of the substance as a function of temperature was measured. When the magnetic state of the ferrite sample changes from ferrimagnetic to paramagnetic, the permeability falls sharply. From this sharp fall at specific temperature the Curie temperature is determined. This is the basic principle used in our experimental set up.

As shown in the figure, the circuit consists of two parts. The primary part consists of a low frequency generator, a multimeter and a resistance in series. The signal generator generates an alternating signal of frequency 200 KHz. A voltage drop occurs at the resistance of 390 ohm. This voltage drop is measured by the voltmeter. The secondary part of the coil comprises of only voltmeter. The voltage induced in the secondary coil is measured by the voltmeter. The current measured by multimeter gives the field intensity H as given below

$$H = \frac{0.4 n_1 i \sqrt{2}}{\bar{d}} \quad (1)$$

where n_1 is the number of turns in the primary coil, i is the current and \bar{d} is given by

$$\bar{d} = \frac{d_1 + d_2}{2} \quad (2)$$

where d_1 and d_2 are the inner and outer diameter of the toroidal sample. From the current and resistance value we obtain voltage E. This in turn yields magnetic induction B as given below.

$$B = \frac{E \times 10^8}{4 n_2 f s} \quad (3)$$

where n_2 is the number of turns in secondary coil, f is the frequency of the signal and s is given as

$$s = dh \quad (4)$$

where, $d = \frac{d_1 - d_2}{2}$, the thickness of the toroid sample

and h is the height of toroidal sample. Thus using equation (3) and (1) we easily attain the permeability

$$\mu = \frac{B}{H} = \frac{E \cdot \bar{d} \times 10^8}{4f n_1 n_2 \times 0.4 \pi x s i \sqrt{2}} \quad (5)$$

At first we wind two wires in the toroidal sample one as primary and the other as secondary coil. The number of turns in each coil is 10. The sample thus wound is kept inside the little oven with a thermocouple placed at the middle of the sample. The thermocouple measures the temperature inside oven and also of the sample. The sample is kept just in the middle part of the cylindrical oven so that the temperature gradient is minimized. The temperature of the oven is then raised slowly. If the heating rate is very fast then temperature of the sample may not follow the temperature inside the oven and there can be misleading information on the temperature of sample. The thermocouple showing the temperature in that case will be erroneous. Due to the closed winding of wires the sample may not receive the heat at once. So, a slow heating rate was used to eliminate this problem. Also a slow heating ensures accuracy in the determination of Curie temperature. The oven was kept thermally insulated from the surroundings.

4.3 MAGNETIZATION MEASUREMENT

Magnetization is defined as the magnetic moment per unit volume. There are various ways of measuring magnetization of a substance. In the present thesis magnetization has been measured by using a Vibrating Sample Magnetometer (VSM). The measurements have been taken at room temperature for a wide range of magnetic field.

The VSM we used was built up at AECD [1]. A brief description of different sections of the equipment is given below.

The measurement of magnetization is usually performed by measuring the magnetic moment of a specimen and dividing this quantity by the volume or mass of the specimen. The techniques for the measurements of magnetic moment by the direct methods can conveniently be classified into two categories:

(i) The measurement of the force exerted on the magnetic moment of the specimen by an inhomogeneous field and

(ii) The measurement of the emf induced in the suitable coil system by changing relative position of the magnetic moment with respect to the coil system or by varying the magnetic moment.

The technique of VSM used in the present measurement falls into second category. The VSM is a sensitive and versatile equipment for measuring the magnetic moment, magnetization and magnetic susceptibility. The VSM was invented by Van Oosterhout [2] and simultaneously and independently by S.Foner [3-4]. The basic principle of VSM developed by Foner is based on the flux change in a coil when the sample is vibrated near it. The sample, usually a small disc, is cemented to the end of a rod, the other end of which is fixed to a loud speaker cone (as shown in figure 4.2) or to some other kind of mechanical vibrator.

Current through the loud speaker vibrates the rod with the sample at about 80 cycle/ sec and with an amplitude of about 0.1 mm in a direction at right angles to the steady magnetic field. In this steady magnetic field the specimen gets magnetized and behaves as a magnet. Thus the oscillating magnetic field of the sample induces an alternating emf in the detection coils kept cemented on the pole pieces of the electromagnet which generates the steady magnetic field. The vibrating rod also carries a reference specimen, in the form of a small

permanent magnet, near its upper end, the oscillating field of this induces another emf in two reference coils kept near to the reference sample. The voltages from the two sets of coil are compared and the difference is proportional to the magnetic moment of the sample. The procedure makes the measurement insensitive to change in ω , for example vibrating amplitude and frequency. The VSM used in the present work to take the magnetization measurement is of Foner type. The Magnetic Material Division, Atomic Energy Center, Dhaka designed and constructed this Foner type VSM in 1986. The measurement of magnetization for all the samples were taken with the help of this Foner type VSM.

4.3.1 Working Principle of the Magnetometer

A schematic diagram of the VSM used in the present work, including the various mechanical and electronic parts is shown in fig 4.3. The signal generator (SG) feeds a sine wave signal of 80 Hz frequency to the audio amplifier (AA) which in turn drives the speaker (SP). The output of the signal generator is also connected to reference channel input of the lock-in-amplifier (LA) model 124A. The drive-rod assembly (R) tightly coupled to the vibrating paper cone of the speaker vibrates in a vertical direction along its length. The amplitude of vibration may be varied at will by changing the gain of the audio amplifier. A permanent magnet (P) of cylindrical shape is fitted to the drive-rod at its lower end with the help of sample holder (H). Two cylindrical sample coils system (SC) with their axes kept vertically are placed on the opposite sides of the sample and along the line joining the centers of the pole faces (NS) of the electromagnet. They are connected in series opposition and the net output signal is fed into the lock-in-amplifier through a shielded cable. This pair of coils is referred to as the sample coil system. Another pair of coaxial coils (RC) also connected to each other in series opposition is placed symmetrically around the permanent magnet (P). This coil pair is the reference

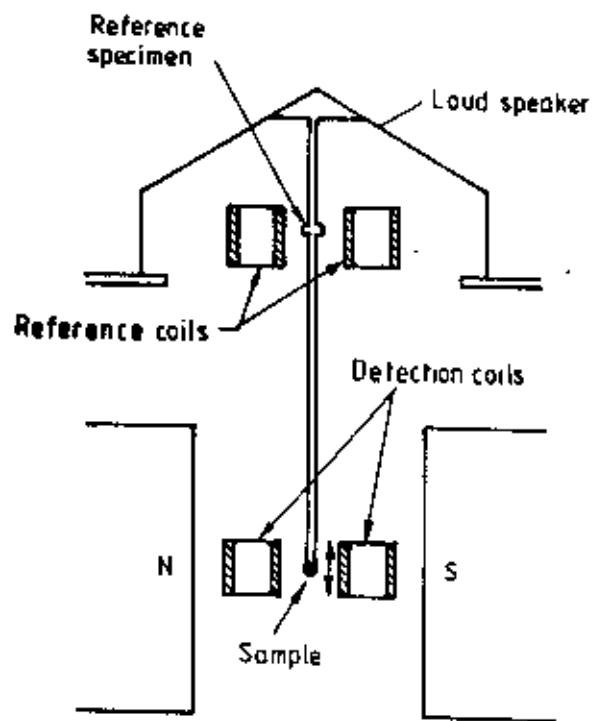


Fig.4.2: Vibrating sample magnetometer (Foner type)

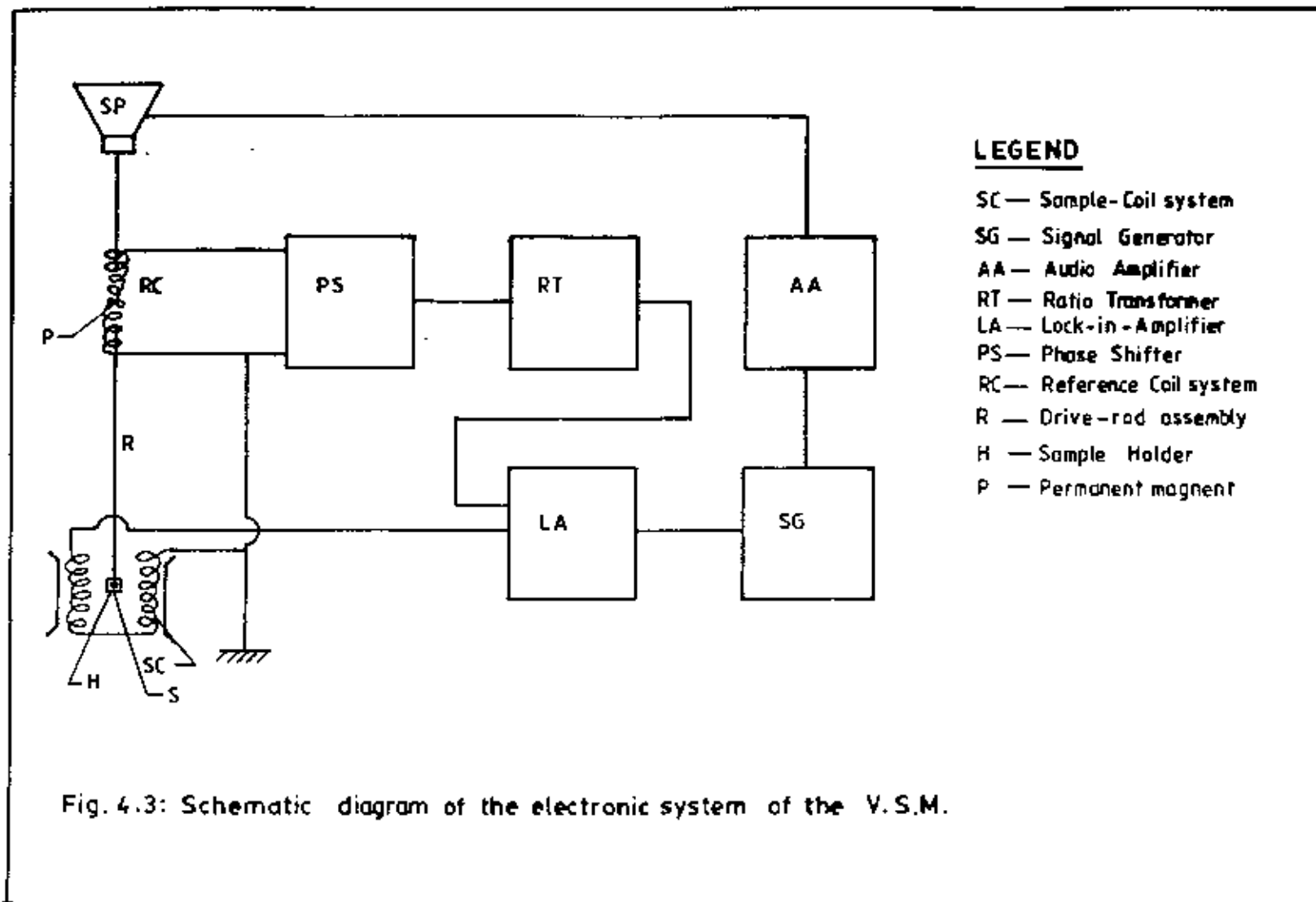


Fig. 4.3: Schematic diagram of the electronic system of the V.S.M.

coil system. As the drive-rod assembly is vibrated with a particular frequency and amplitude, the sample (S) induces a signal of the same frequency in the sample coil system. This signal is proportional to the dipole moment of the sample. As the field in the pole gap is gradually increased by increasing the current through the electromagnet, the sample becomes increasingly magnetized and induces a larger signal in the sample coil system till the sample reaches the state of saturation magnetization. This signal directly goes to one of the inputs of the lock-in-amplifier. Similarly, another signal of the same frequency is induced in the reference coil system due to vibration of the permanent magnet (P). Since the moment of the permanent magnet is fixed, the signal it produces is also of fixed amplitude for a particular frequency and vibration of amplitude. This signal is termed as the reference signal and it is first fed to a unity gain phase-shifter unit.

The phase shifter capable of continuously changing the phase from 0° to 360° , is used to bring the reference signal in phase with the sample signal. From the phase shifter the reference signal passes on to the decade ratio transformer (RD) of a constant input impedance. The output of this transformer then goes to the other input of the lock-in-amplifier. The output to input ratio of the decade transformer can be accurately varied from 10^{-3} to 1. By adjusting the decade transformer the amplitude of its output is made equal to that of the sample signal. The lock-in-amplifier is operated in the differential input mode and is used as a signal detector. When the sample signal and the output signal of the decade transformer are of equal amplitude and are in the same phase, the d.c meter of the lock-in-amplifier gives a null reading. The whole electronic system then correctly measures the ratio of the sample signal and the reference signal have a direct phase and amplitude relationship. As a result the ratio of the sample signal to the reference signal is proportional to the magnetic moment of the sample. The measurement is insensitive to small changes in the amplitude and frequency of vibration and the gain of the amplifier. The accuracy of the equipment depends mainly on the accuracy of the ratio transformer and the gain of the amplifier.

4.3.2 Description of Mechanical Design of the VSM

The various mechanical parts of the magnetometer are shown in detail in the figure 4.4. The base B of the VSM is a circular brass plate of 8 mm thickness and 250 mm diameter. A brass tube T of 25 mm outer diameter and 0.5 mm thickness runs normally through the base such that the axis of the tube and the center of the plate coincide. The tube extends 60 mm upward and 24 mm downward from the base. There is a vacuum port on the lower part of the tube 120 mm below the base. The lower end of the tube T is joined to a brass extension tube L by a threaded coupling and an 'O' ring seal. Another thin tube K made of german silver and 8 mm inner diameter runs through the extension tube L from the coupling point C to about 50 mm below the sample position. Above the base there is a hollow brass cylinder M of 180 mm length and 130 mm inner diameter and having 40 mm wide collars at its both ends. The lower collar seats on an 'O' ring seal which is situated in a circular groove in the base plate. On the upper collar, there rests an aluminium top N with an 'O' ring seal. The brass cylinder M has a side port VP. This is again a brass tube of 41 mm diameter and 43 mm length. The port has a collar at the end away from the cylinder. A perspex vacuum feed through is fitted at its end with 'O' ring seal. This port is connected to the cylinder by soft solder.

Electrical connection from the audio amplifier to the speaker and from the reference coil system to the phase shifter are taken via the perspex feed through. By connecting the vacuum port of the tube T to a vacuum pump the sample environment can be changed.

The speaker (SP) is fitted 25 mm above the tube T with the help of brass stands. The lower ends of stands are screwed to the base plate while the rim of the speaker is screwed on the tops of the stands. The speaker has a circular hole of 10 mm diameter along its axis. An aluminium disc having female threads in

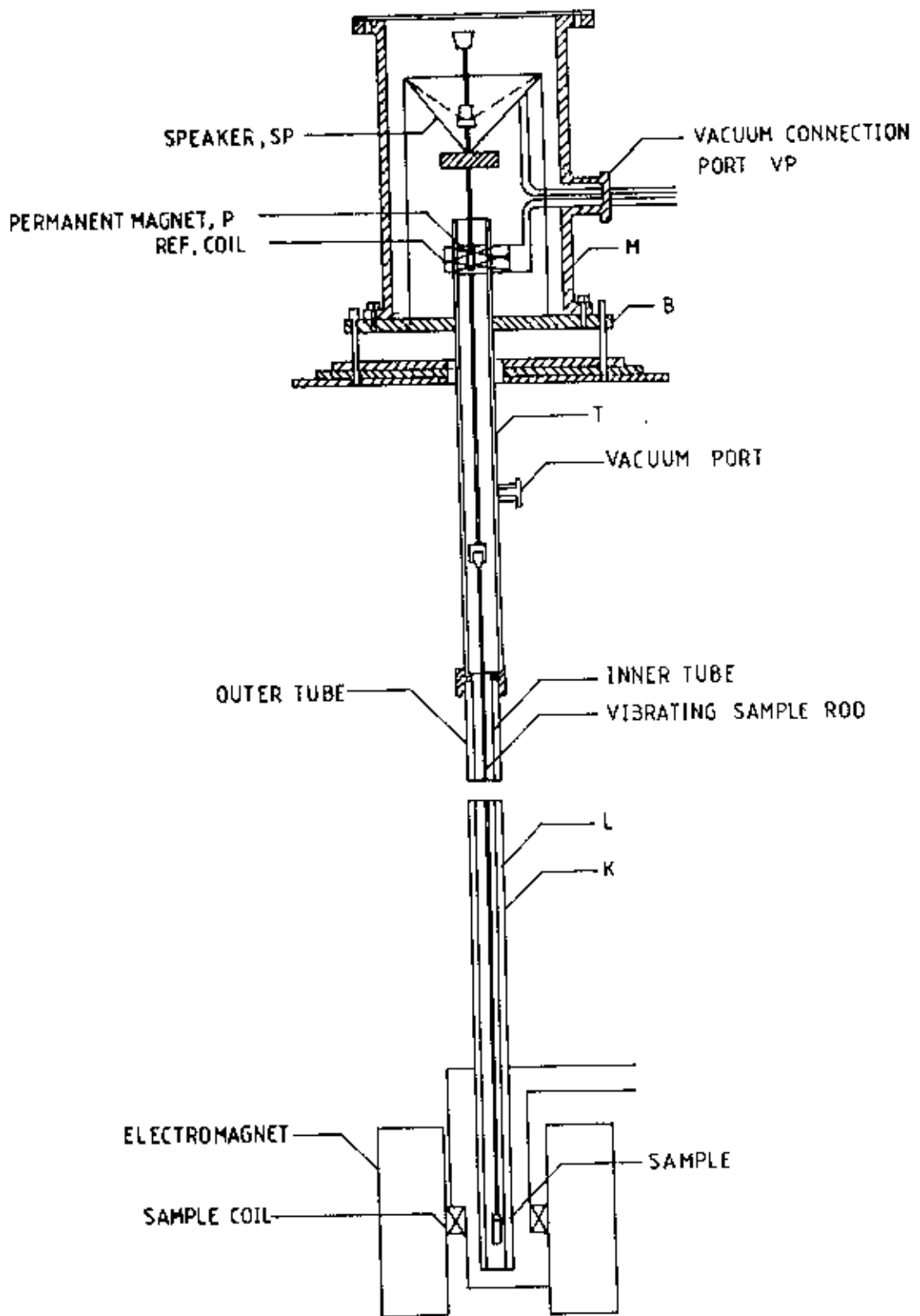


Fig. 4.4: Mechanical Construction of the VSM.

it is fitted to the proper cone with araldite. The aluminium connector having male threads on it and attached to the drive rod assembly fits in the aluminium disc and thus the driver rod assembly is coupled to the speaker. The drive rod assembly consists of two detachable parts which are joined together by means of aluminium threaded connectors. Each part is thin Pyrex glass tubing of 4 mm diameter. The upper part has a small permanent magnet (P) situated 100 mm below the aluminium connector attached to it. At the lower end of the drive assembly a perspex sample holder having quite thin wall can be fitted tightly with the sample in it. A few perspex spacers are also attached to the drive rod throughout its length. The spacers guide the vibration of the sample only in the vertical direction and stops side wise or motion. The total length of the drive rod assembly is 920 mm.

The base plate of the VSM rests on three leveling screws above a brass frame which in turn rests on an iron angle bridge. The bridge is rigidly fitted to the sidewall of the room. The brass frame is provided with arrangements with the help of which it can be moved in two perpendicular directions in the horizontal plane. The levelling screws are used to make the drive rod vertical and to put the sample at the center of the pole-gap between the sample coils. The sample can also be moved up and down by the leveling screws.

4.3.3 Calibration of the VSM

There are usually two methods of calibration of a vibrating sample magnetometer:

1. By using a standard sample and
2. By using a coil of small size whose moment can be calculated for d.c current through it .

The VSM has been calibrated by using a 0.112590 gm spherical sample of Nickel of 99.99 % purity. The sample was made spherical with the help of a sample shaping device. It was then annealed in helium atmosphere at about 900°C . The sample saturation magnetic moment has been calculated using the available standard data. The ratio-transformer reading is obtained by actual measurements and thus from the equation 4.3 the value of the calibration constant K is obtained. The accuracy of this calibration, however, depends on the reliability of the standard Nickel sample, the accuracy of the ratio-transformer and the gain of the amplifier. The equipment has been operated repeatedly with the same standard sample and stability has been found to be within 1 in 1000.

4.3.4 Sensitivity of the VSM

The sensitivity of a VSM is usually determined by the signal to noise ratio. But because of comparatively low sensitivity of the lock-in-amplifier used in this equipment, the noise level could not be measured. The maximum sensitivity of the lock-in-amplifier is 10 microvolt (rms). So the differential method has been used to measure the sensitivity. It is found to be about 10^{-4} emu. It may be mentioned here that the sensitivity of a commercial VSM made by PARC (Princeton Applied Research Corporation USA) is 5×10^{-5} emu. With the sensitivity so far achieved of the VSM can be used for investigation of only ferromagnetic, ferrimagnetic and strongly paramagnetic materials at room temperature. In order to extend its usefulness, a more sensitive lock-in-amplifier, a sample oven and cryostat are needed. Under the present conditions, however, routine measurements at room temperature can be performed for the materials mentioned above.

4.3.5 Working Procedure of the VSM

The sample is fitted to the drive rod assembly and then positioned at about the midpoint of the sample coils by eye estimation. The switches of the electromagnet power supply unit, the signal generator, the audio amplifier and the phase-shifter are turned on. Nearly half an hour is spent for the warming up of all the component units. The frequency of the sine wave from the signal generator is set at 80 Hz. The gain of the audio amplifier is adjusted to make the output signal driving the speaker about 3 volts peak to peak. The signal makes the rod assembly vibrate with sufficiently large amplitude. The signal produced in the reference coil-system is found to be about 5 mV peak to peak. The rod - assembly is made vertical by adjusting leveling screws. About 2 amperes or more current is passed through the electromagnet depending on the size and materials of the specimen. The sample signal alone is first seen on the D.C meter of the lock-in-amplifier. The meter reading is maximized by changing the phase of the locking signal in the reference channel. The sample signal is then optimized i.e. it is maximized by moving the sample in the Z-direction (vertical) and in the Y-direction and then minimized by moving it in the X-direction (field direction).

The locking signal in the reference channel is brought in exact quadrature with the sample signal to give a correct null reading on the meter. The two signals are then brought in the same phase to give a maximum reading on the meter to the right. Similarly, the reference coil signal alone is next seen on the meter . The signal is first brought in quadrature with the locking signal with the help of the external phase shifter in such a manner that it gives a deflection to the left on the meter when it is again brought in phase with the sample signal. The lock-in-amplifier is then set in the differential mode. The null-reading is obtained by correctly equalizing the decade transformer output with the sample

signal. The reading on the decade transformer is then multiplied by the calibration constant to obtain the sample moment.

4.3.6 Measurements of the Magnetization

The measurements of magnetization of Mn-Zn ferrite samples with and without dopants , total nine in number, were performed using a vibrating sample magnetometer as shown in fig.4.4. Samples in the form of thin disc of diameter about 5 mm were prepared from the disc shaped Mn-Zn ferrite samples. They were then weighed. The specimens were then glued to the lower end of the sample holder of the VSM. The measurements of magnetization were taken at room temperature for different values of the magnetic field in the range 0.1 KG to 4 KG. The strength of the applied magnetic field was simultaneously monitored with the help of a Digital Gauss-Meter (Model 811 A), keeping the tip of the Gaussmeter closed to a pole of the electromagnet . The accuracy in determining the field was estimated to be within one percent.

4.4 PERMEABILITY MEASUREMENT

For high frequency application, the desirable property of a ferrite is the high permeability with low loss. The present goal of most of the recent ferrite researches is to fulfil this requirement. Before going into the complexity of permeability measurement, we take a detour through the theories and mechanisms involved in permeability.

4.4.1 Theories of Permeability

Permeability is namely defined as the proportional constant between the magnetic field induction B and applied intensity H:

$$B=\mu H \quad (1)$$

This naive definition needs further sophistications. If a magnetic material is subjected to an ac magnetic field as given bellow:

$$H = H_0 e^{i\omega t} \quad (2)$$

Then it is observed that the magnetic flux density B experiences a delay. The delay is caused due to presence of various losses and is thus expressed as

$$B = B_0 e^{i(\omega t - \delta)} \quad (3)$$

where δ is the phase angle and marks the delay of B with respect to H. The permeability is then given by

$$\begin{aligned} \mu &= \frac{B}{H} = \frac{B_0 e^{i(\omega t - \delta)}}{H_0 e^{i\omega t}} \\ &= \frac{B_0 e^{-i\delta}}{H_0} \\ &= \frac{B_0}{H_0} (\cos\delta - i\sin\delta) \\ &= \mu' - i\mu'' \end{aligned} \quad (4)$$

$$\text{where } \mu' = \frac{B_0}{H_0} \cos\delta, \mu'' = \frac{B_0}{H_0} \sin\delta \quad (5)$$

The real part μ' of complex permeability μ as expressed in equation (4) represent the component of B which is in phase with H, so it corresponds to the normal permeability. If there are no losses, we should have $\mu = \mu'$. The imaginary part μ'' corresponds to that part of B which is delayed by phase angle 90° from H. The presence of such a component requires a supply of energy to maintain the alternating magnetization, regardless of the origin of delay.

The ratio of μ'' to μ' , as is evident from equation (5) gives

$$\frac{\mu''}{\mu'} = \frac{(B_0/H_0)\sin\delta}{(B_0/H_0)\cos\delta} = \tan\delta \quad (6)$$

This $\tan\delta$ is called the *LOSS FACTOR*. The Q-factor or quality factor is defined as the reciprocal of this loss factor, i.e.

$$Q = \frac{1}{\tan\delta} \quad (7)$$

4.4.2 Mechanisms of Permeability

The mechanisms can be explained as follows: A demagnetized magnetic material is divided into number of weiss domains separated by Bloch walls. In each domain all the magnetic moments are oriented in parallel and the magnetization has its saturation value M_s . In the walls the magnetization direction changes gradually from the direction of magnetization in one domain to that in the next. The equilibrium positions of the walls result from the interactions with the magnetization in neighboring domains and from the influence of pores, crystal boundaries and chemical inhomogeneities which tend to favour certain wall positions.

4.4.3 Wall permeability

The mechanism of wall permeability arises from the displacement of the domain walls in small fields. Lets us consider a piece of material in the demagnetized state, divided into weiss domains with equal thickness L by means of 180° Bloch walls (as in the fig. 4.5). The wall are parallel to the YZ plane. The magnetization M_s in the domains is oriented alternately in the $+Z$ or $-Z$ direction. When a field H with a component in the $+Z$ direction is applied, the magnetization in this direction will be favored. A displacement dx of the

walls in the direction shown by the dotted lines will decrease the energy density by an amount:

$$\frac{2M_s H_z dx}{L}$$

This can be described as a pressure $2M_s H_z$ exerted on each wall. The pressure will be counteracted by restoring forces, which for small deviations may assumed to be kdx per unit wall surface. The new equilibrium position is then given by

$$d = \frac{M_s H_z dx}{L}$$

From the change in the magnetization

$$\Delta M = \frac{2M_s d}{L}$$

the wall susceptibility χ_w may be calculated. Let H makes the angle θ with z direction. The magnetization in the θ direction becomes

$$(\Delta M)_\theta = \frac{2M_s d}{L} \cos \theta, \text{ and with } H_z = H \cos \theta \text{ and}$$

$$d = \frac{2M_s H_z}{K}$$

We obtain

$$\chi_w = \frac{(\Delta M)_\theta}{H} = \frac{4M_s^2 \cos^2 \theta}{KL}$$

4.4.4 Rotational Permeability

The rotational permeability mechanism arises from rotation of the magnetization in each domain. The direction of M can be found by minimizing the magnetic energy E as a function of the orientation. Major contributions may be due to the stress and shape anisotropy. The stress may influence the magnetic energy via the magnetostriction. The shape anisotropy is caused by the boundaries of the sample as well as by pores, nonmagnetic inclusions and inhomogeneities. For small angular deviations α_x and α_y or M , where

$$\alpha_x = M_x / M_s \text{ \& } \alpha_y = M_y / M_s$$

from the equilibrium Z - direction may be expressed as

$$E = E_0 + 1/2 \alpha_x^2 E_{xx} + 1/2 \alpha_y^2 E_{yy}.$$

Where it is assumed that x and y are the principal axes of the energy minimum. Instead of E_{xx} & E_{yy} , the anisotropy field H_X^A and H_Y^A are often introduced. Their magnitude is given by

$$H_X^A = E_{xx} / 2M_s \text{ and } H_Y^A = E_{yy} / 2M_s$$

H_X^A & H_Y^A represents the stiffnesses with which the magnetization is bound to the equilibrium direction for deviations in the X and Y direction, respectively. The rotational susceptibilities $\chi_{r,x}$ and $\chi_{r,y}$ for fields applied along X and Y directions, respectively are

$$\chi_{r,x} = M_s / H_X^A$$

$$\chi_{r,y} = M_s / H_Y^A$$

For cubic materials it is often found that H_x^A and H_y^A are equal. For $H_x^A = H_y^A = H^A$ and a field H which makes an angle θ with the Z-direction (as shown in Fig.4.5) the rotational susceptibility, $\chi_{r,c}$ in one crystallite becomes

$$\chi_{r,c} = M_s / H^A \sin^2 \theta$$

A polycrystalline material consisting of a large number of randomly oriented grains of different shapes, with each grain divided into domains in a certain way. The rotational susceptibility χ_r of the material has to be obtained as a weighted average of $\chi_{r,c}$ of each crystallite, where the mutual influence of neighboring crystallites has to be taken into account. If the crystal anisotropy dominates other anisotropies, then H^A will be constant throughout the material, so only the factor $\sin^2 \theta$ (equation 9) has to be averaged. Snoek [5] assuming a linear averaging of $\chi_{r,c}$ and found

$$\chi_r = \frac{2 M_s}{3 H^A}$$

The total internal susceptibility

$$\chi = \chi_\omega + \chi_r = \frac{4 M_s^2 C \cos^2 \theta}{K L} + \frac{2 M_s}{3 H^A}$$

If the shape and stress anisotropies can not be neglected, H^A will be larger. Any estimate of χ_r will then be rather uncertain as long as the domain structure, and the pore distribution in the material are not known. A similar estimate χ_ω would require knowledge of the stiffness parameter k and the domain width L . These parameters are influenced by such factors as imperfection, porosity and crystallite shape and distribution are essentially unknown

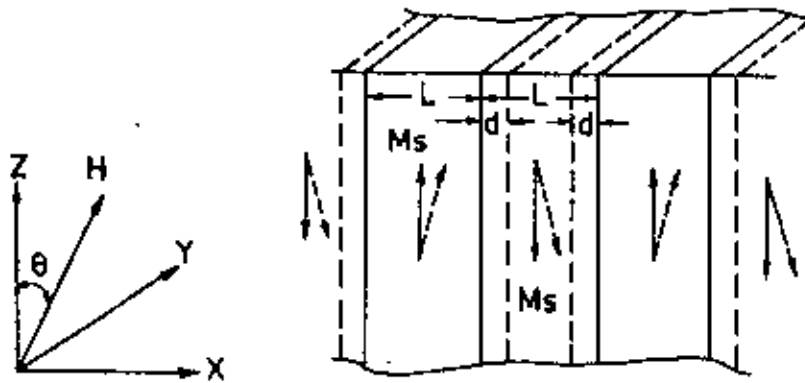


Fig. 4.5: Magnetization by wall motion and spin rotation

4.4.5 Techniques of Measurements of Permeability

Measurements of permeability normally involves the measurements of the change in self inductance of a coil in presence of the magnetic core. The behaviour of a self inductance can now be described as follows. Suppose we have an ideal lossless air coil of inductance L_0 . On insertion of magnetic core with permeability μ , the inductance will be μL_0 . The complex impedance Z of this coil can be expressed as

$$Z = R + jX = j\omega L_0\mu = j\omega L_0(\mu' - j\mu'') \quad (12)$$

where the resistive part is

$$R = \omega L_0\mu'' \quad (13)$$

and the reactive part is

$$X = \omega L_0\mu' \quad (14)$$

The r.f permeability can be derived from the complex impedance of a coil Z (equation 12). The core is usually toroidal to avoid demagnetizing effects. The quantity L_0 is derived geometrically.

4.4.6 Measurement of Frequency Characteristics of Mn-Zn ferrite Samples

The frequency characteristics of the Mn-Zn ferrite samples i.e. the permeability spectra were investigated using an Hewlett Packart Impedance Analyzer of model no-4192ALF. The mean diameter and the thickness of the samples are given in table 1.2 and 1.3. The measurement of inductances were taken in the frequency range of 5 KHz to 13 MHz. The values of measured parameters obtain as a function of frequency and the real and imaginary part of permeability and the loss factor are given in table 5.1 to 5.18. μ' is calculated by using the following formula

$$L_s = L_0 \mu'$$

and

$$\tan \delta = \mu'' / \mu'$$

where L_s is the self-inductance of the sample core and

$$L_0 = \frac{\mu_0 N^2 s}{d}$$

where L_0 is the inductance of the winding coil without the sample core and N is the number of turns of coil (here $N = 10$), s is the area of cross section as given below

$$s = dh$$

$$\text{where } d = (d_1 + d_2) / 2$$

$$h = \text{height}$$

and \bar{d} is the mean diameter of the sample given as follows

$$\bar{d} = \frac{d_1 + d_2}{2}$$

4.5 THE MICROSTRUCTURE STUDY

Microstructure

The microstructure study of the Mn-Zn ferrite samples with and without dopants were performed in order to have an insight of the grain structures. The samples of different compositions and sintered at different temperatures were chosen for this purpose. The samples were polished using the conventional metallurgical process. Then they were etched. The etching solution contained H_2SO_4 (concentration was 95%-98%), $C_2H_2O_4$ (concentration was 10%) and water. They were mixed in the ratio of 2 : 1 : 1 respectively. While etching the

samples in the etching solution, the temperature of the solution was kept at about 70°C to 80°C , and the samples were kept in the solution for 30 min. to 40 min. The etched samples were then visualized under a polarizing microscope and then photographed.

REFERENCES

1. M. A. Mazid, M. Amanullah Chowdhury and Shireen Akhtar. Internal Report 1986.
2. G.W. Van Oesterhout, Appl. Sci. Rev. B6 101 (1965)
3. S. Foner, Rev. Sci. Instr. 30, 584-557 (1965).
4. S. Foner, Rev. Sci. Instr. 27, 578 (1955)
5. J L. Snoek, Physica, 14, 207 (1948).

CHAPTER-5

RESULTS AND DISCUSSION

5.1 X-ray Diffraction

The X-ray diffraction patterns for the different Mn-Zn ferrite samples are shown in fig.-5.1 to fig.-5.9. The 2θ values of the diffraction peaks corresponding to different planes are shown in table 2.1. The calculated values of lattice parameter 'a' for different samples are given in table 2.2 and table 2.3. An increase was evidenced in the lattice parameters (Table 2.2) with the addition of V_2O_5 , TiO_2 and CoO additives. The lattice parameters (Table 2.3) is found to decrease with the increase of Cu^{2+} content except for the sample for copper content $x=0.03$.

The X-ray diffraction patterns of both the groups of samples clearly indicate their single and spinel phase formation. Analyzing the XRD patterns we notice that the position of the peaks comply with the reported value[1] within experimental error. The sharp peaks reveals that the samples are in good crystalline form. Also the clear peaks exhibit the presence of single phase in the samples. The bulk density ρ_B was measured by usual mass and dimensional consideration. The X-ray densities ρ_x for different samples were calculated by using the lattice parameter as stated in 4.1 of chapter 4. The porosity P of the samples was calculated from the values ρ_B and ρ_x by using the following expression [2]

$$P = 1 - \rho_B / \rho_x$$

In Table 2.2 and 2.3 the results for porosity, bulk density and x-ray density are summarized. By substituting Cu^{2+} ion for Mn^{2+} ion into Mn-Zn ferrites a relatively higher density was obtained. The increase in density with Cu substitution in Mg-Zn ferrites have been reported [3]. The density increase is

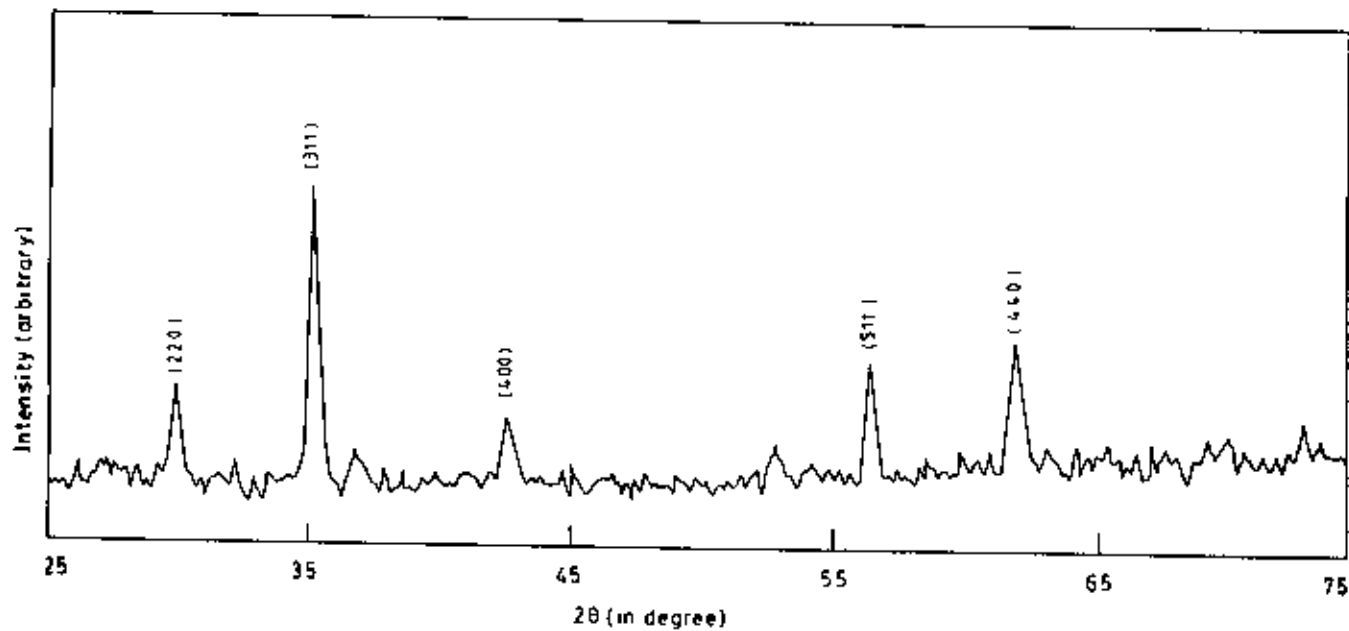


Fig. 5.1 XRD pattern for sample (A-1) $Mn_{0.51}Zn_{0.44}Fe_{2.05}O_4$ without additives

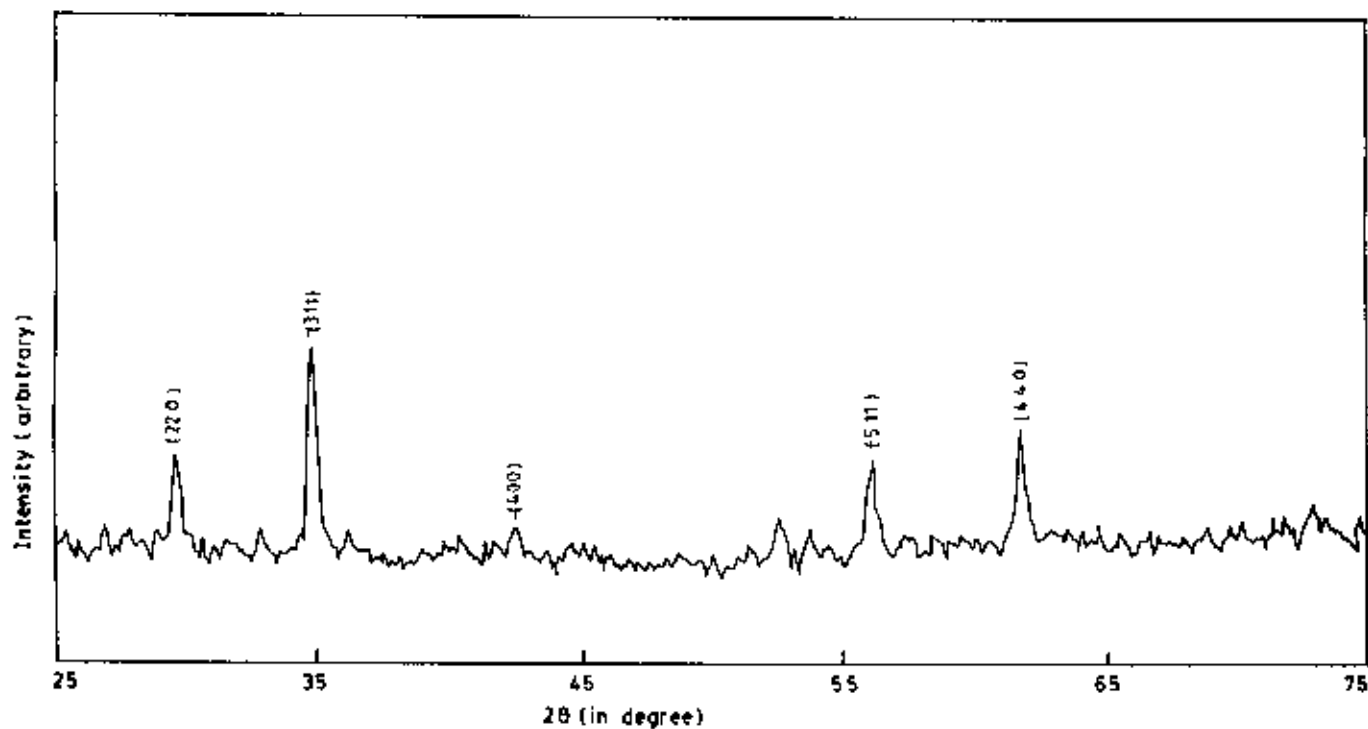


Fig. 5.2: XRD pattern for sample (A-2) $Mn_{0.51}Zn_{0.44}Fe_{2.05}O_4$ with 1 mole % additives of V_2O_5

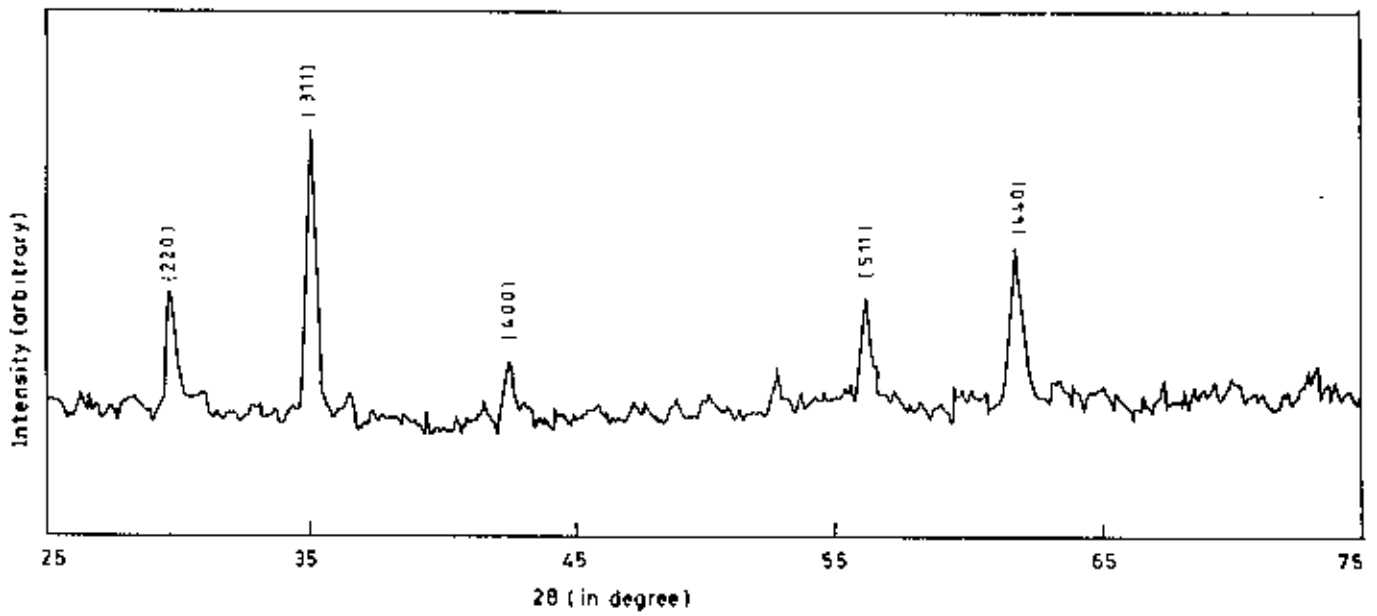


Fig 5.3. XRD pattern for sample (A-3) $Mn_{0.51}Zn_{0.44}Fe_{2.05}O_4$ with 1 mole % additives of TiO_2

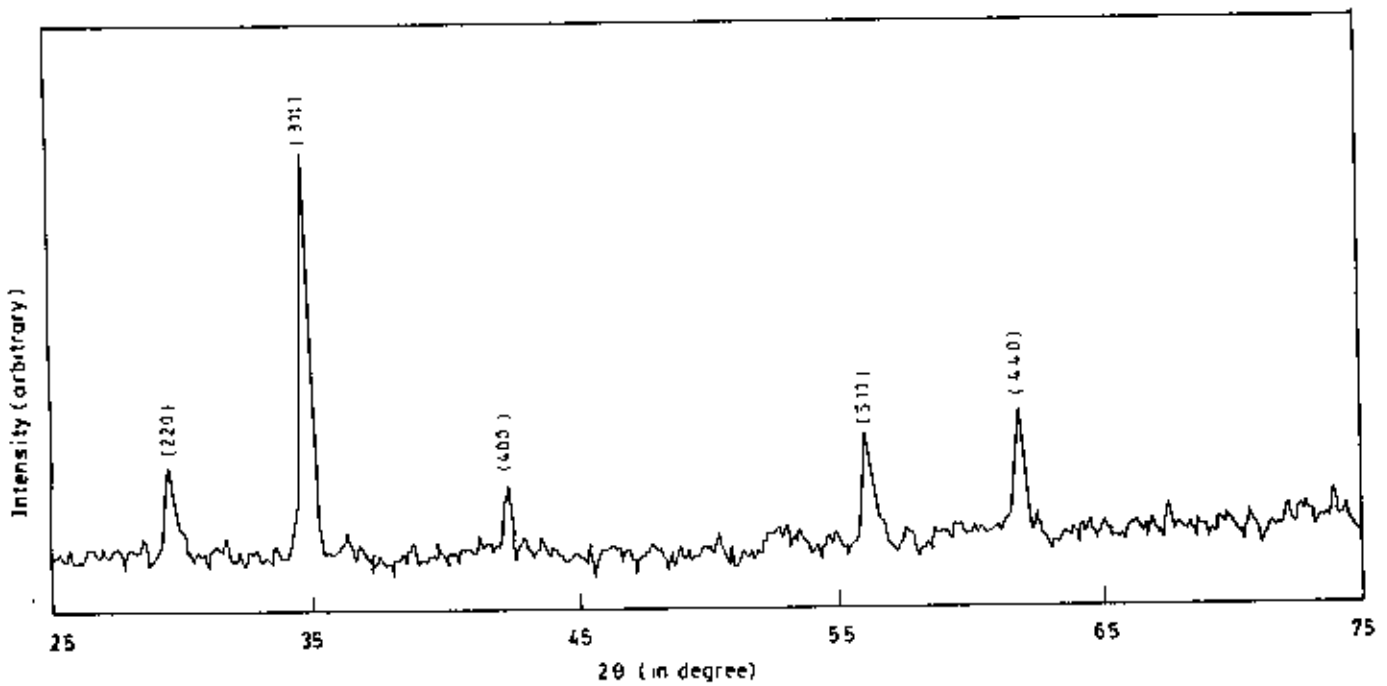


Fig.5.4 XRD pattern for sample (A-4) $Mn_{0.51}Zn_{0.44}Fe_{2.05}O_4$ with 1 mole % additives of CoO

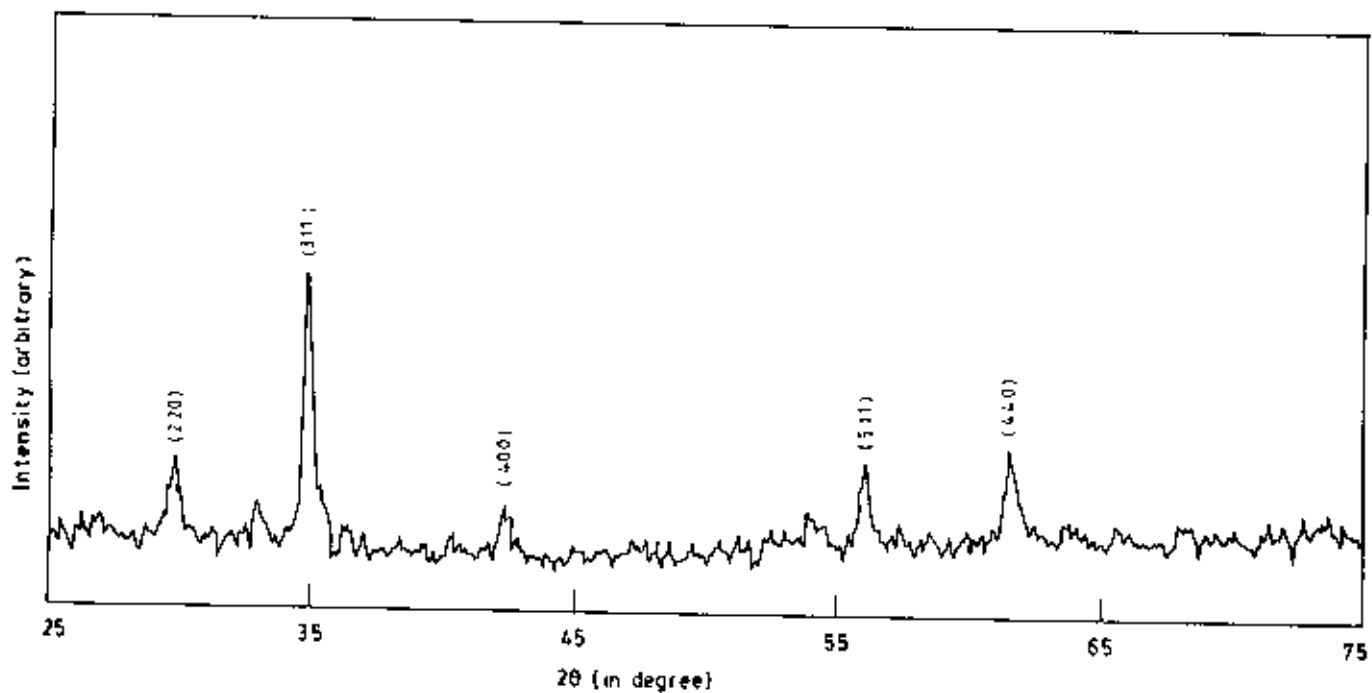


Fig 5.5. XRD pattern for sample (B-1) $Mn_{0.7}Cu_{0.0}Zn_{0.22}Fe_{2.08}O_4$

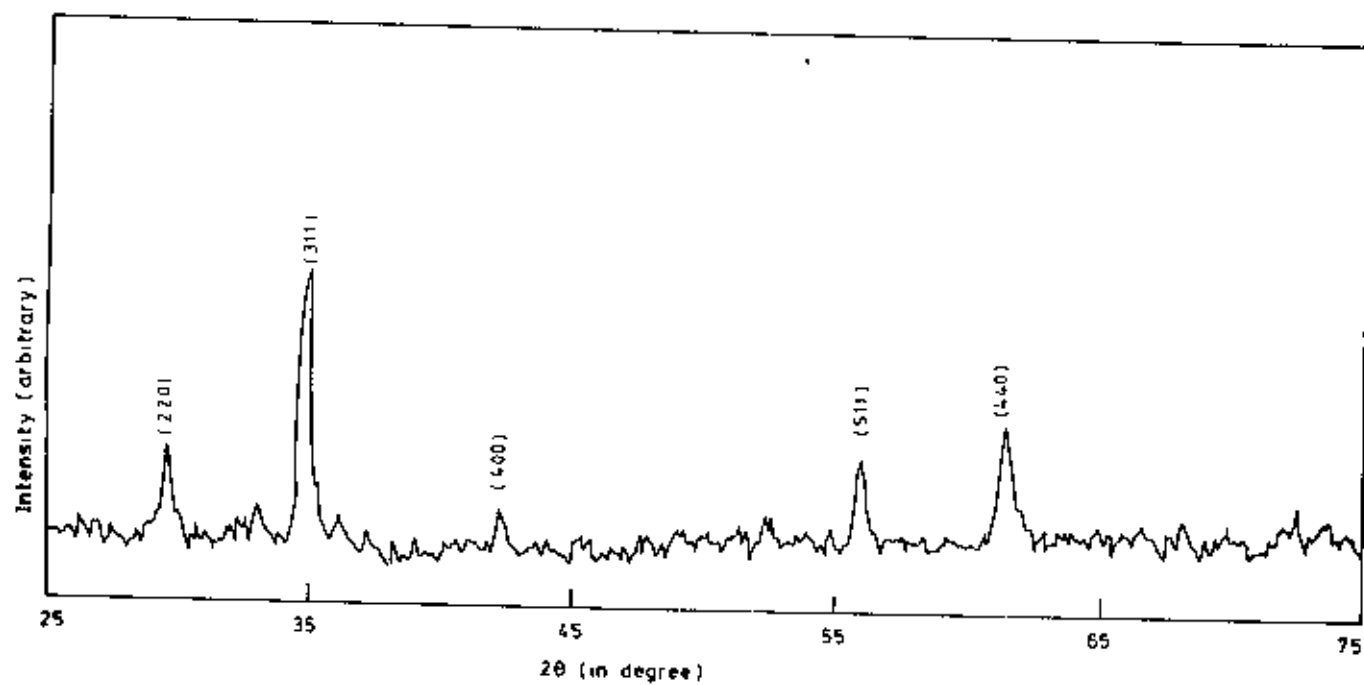


Fig 5.6 XRD pattern for sample (B-2) $Mn_{0.67}Cu_{0.03}Zn_{0.22}Fe_{2.08}O_4$.

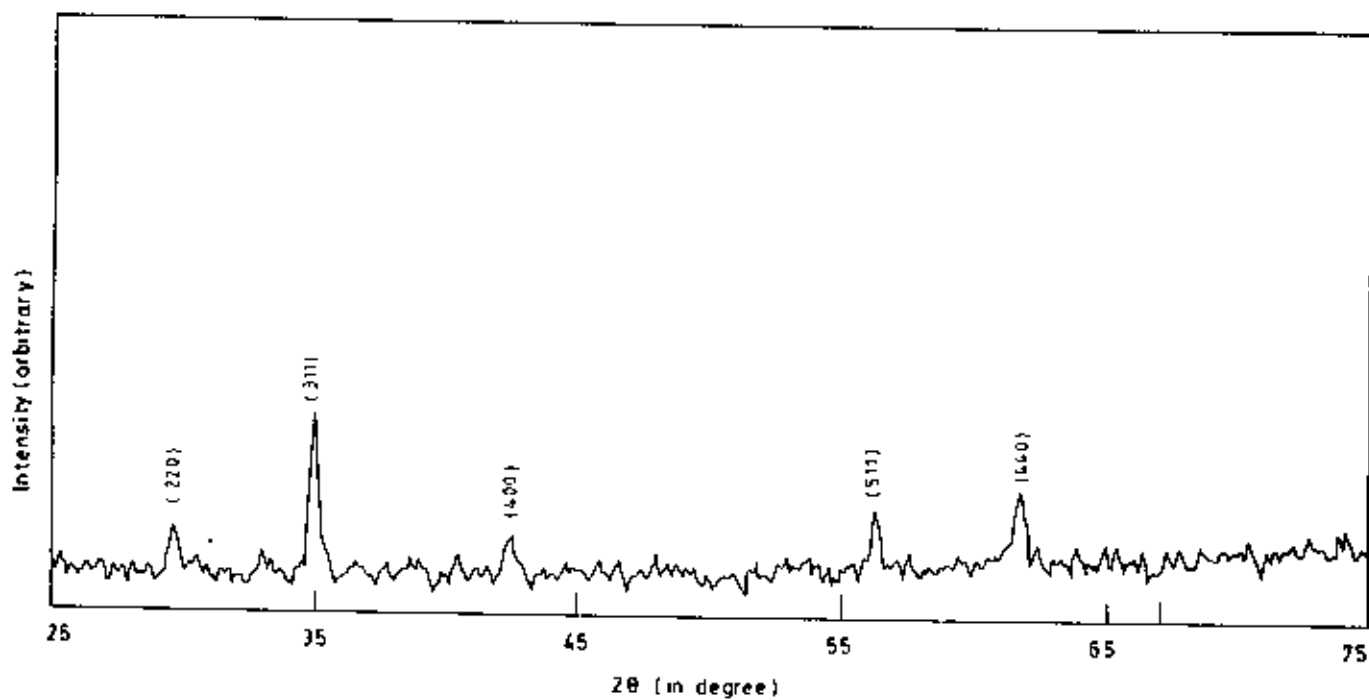


Fig. 5.7 - XRD pattern for sample (B-3) $Mn_{0.64}Cu_{0.06}Zn_{0.22}Fe_{2.08}O_4$

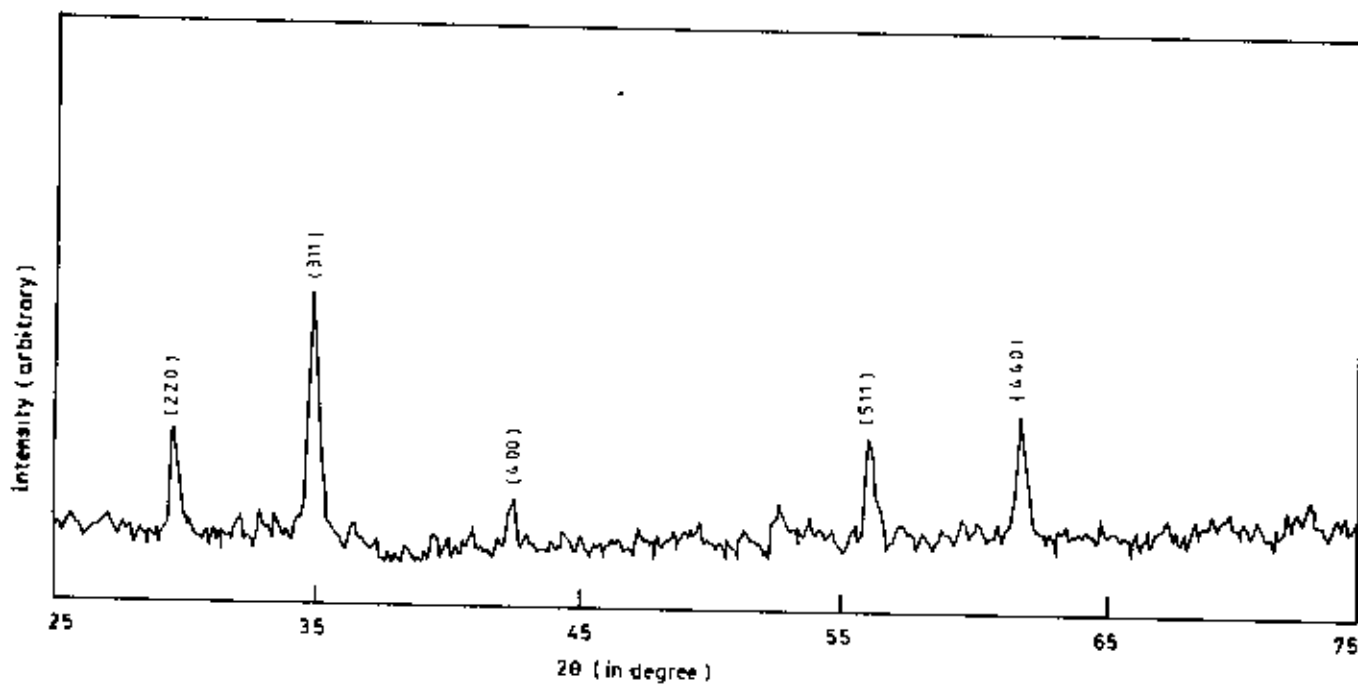


Fig. 5.8 XRD pattern for sample (B-4) $Mn_{0.60}Cu_{0.10}Zn_{0.22}Fe_{2.08}O_4$

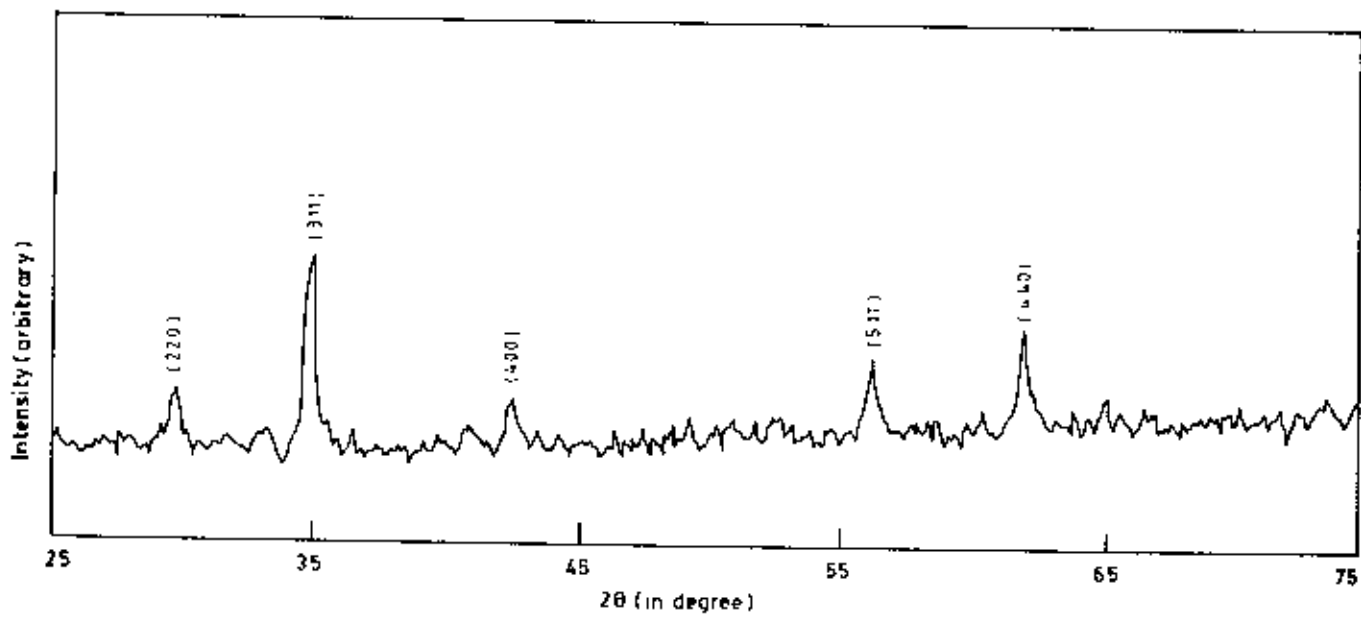


Fig 5.9 XRD pattern for sample (B-5) $\text{Mn}_{0.55}\text{Cu}_{0.15}\text{Zn}_{0.22}\text{Fe}_{2.08}\text{O}_4$

caused by the lowering of the porosity and by the segregated layer. It is interesting to observe from the table 2.3 that the porosity values are found to decrease with increasing Cu^{2+} substitution, thereby giving an impression that copper substitution might be helping in the densification of the materials. In the case of samples with additives it is observed that the density of the specimen rather decreases and this effect is drastic for the CoO additives compared to V_2O_5 and TiO_2 .

5.2 Curie Temperature Measurement

Curie temperature is a measure of exchange force in ferrimagnetics. It is the temperature at which the thermal energy KT tending to disorder the system just wins over the exchange energy tending to order the system magnetically. At this temperature, ferrimagnetic substance thus changes over to a paramagnetic substance.

It has been observed that, whenever diamagnetic ions are introduced in the sublattice, the Curie temperature decreases. Zn substituted mixed ferrites are examples of this. The exchange integral for A-site i.e. J_{AA} is almost negligible. So, Zn substitution only weakens the A-B interaction effectively. If the number of substituted ions is not too high, the overall ferrimagnetic arrangement is not destroyed even though some loosely bounded spins may become locally canted or distorted, at temperature $T < T_C$. For larger substitution, the A-B interactions may become comparable to or even weaker than B-B interaction. In this way the collinear ferrimagnets often change to canted ones. Both the local canting and long range non-collinear structures were reported [4]. Owing to this reduced A-B exchange interaction with increasing Zn^{2+} content, the Curie temperature will drop. This was first found out by Forestier [5].

Our Curie temperature measurements involved the measurement of permeability μ , while varying the temperature, as already stated before. At Curie temperature T_C the permeability μ showed abrupt fall. The curves for μ

vs T for our two series of samples are shown in fig.5.10 to fig.5.11. It is noted that the samples of two series contain different Zn^{2+} contents. In A-series Zn^{2+} contents is 0.44 mole% while in B-series it is 0.22 mole %. It is observed from the figures 5.10 and 5.11 that when mole % of ZnO was higher, the Curie temperature T_c is lower. This is expected because of the inclusion of higher concentration of non-magnetic Zn in the material. This is in harmony with the theoretical and experimental findings.

Figure 5.10 shows the variation of μ with temperature T for A-series. It is observed that when 1 mole % TiO_2 was added the Curie temperature decreases as compared with that of the non-additives samples. It appears that the addition of non-magnetic tetravalent Ti^{4+} have an indirect effect on the properties is that the Fe^{2+} content is increased. Since Fe^{2+} on an octahedral sites contributes a positive anisotropy, the addition of Ti^{4+} will effect a decrease in the Curie temperature[6]. But when 1 mole% CoO is added instead of TiO_2 Curie temperature increases. This can be explained on the basis of A-B interaction. In the presence of strong A-B interactions, greater thermal energy is required to offset the spin alignment which results in higher Curie temperature[7]. Here A-B interaction between $Fe_A^{3+} - Co_B^{2+}$ and $Mn_A^{2+} - Co_B^{2+}$ ions may play a significant role in increasing the strength of magnetic interactions. In the case of V_2O_5 additive sample the permeability dropped drastically (nearly 1/5th the value of the non-additive sample) and the change in permeability with temperature was not significant. As a result T_c for the V_2O_5 added sample could not measured.

Figure 5.11 shows the variation of μ with temperature T for Cu-substitutes samples of the general composition $Mn_{0.70-x}Cu_xZn_{0.22}Fe_{2.08}O_4$, where x= 0.0, 0.03, 0.06, 0.10, 0.15 etc. It is noteworthy that the shape of the μ - T curves strongly depend on the substitute composition. It also depends strongly on the preparation condition since these ferrites are in polycrystalline form and are prepared by ceramic technique. The Curie temperatures show a decreasing

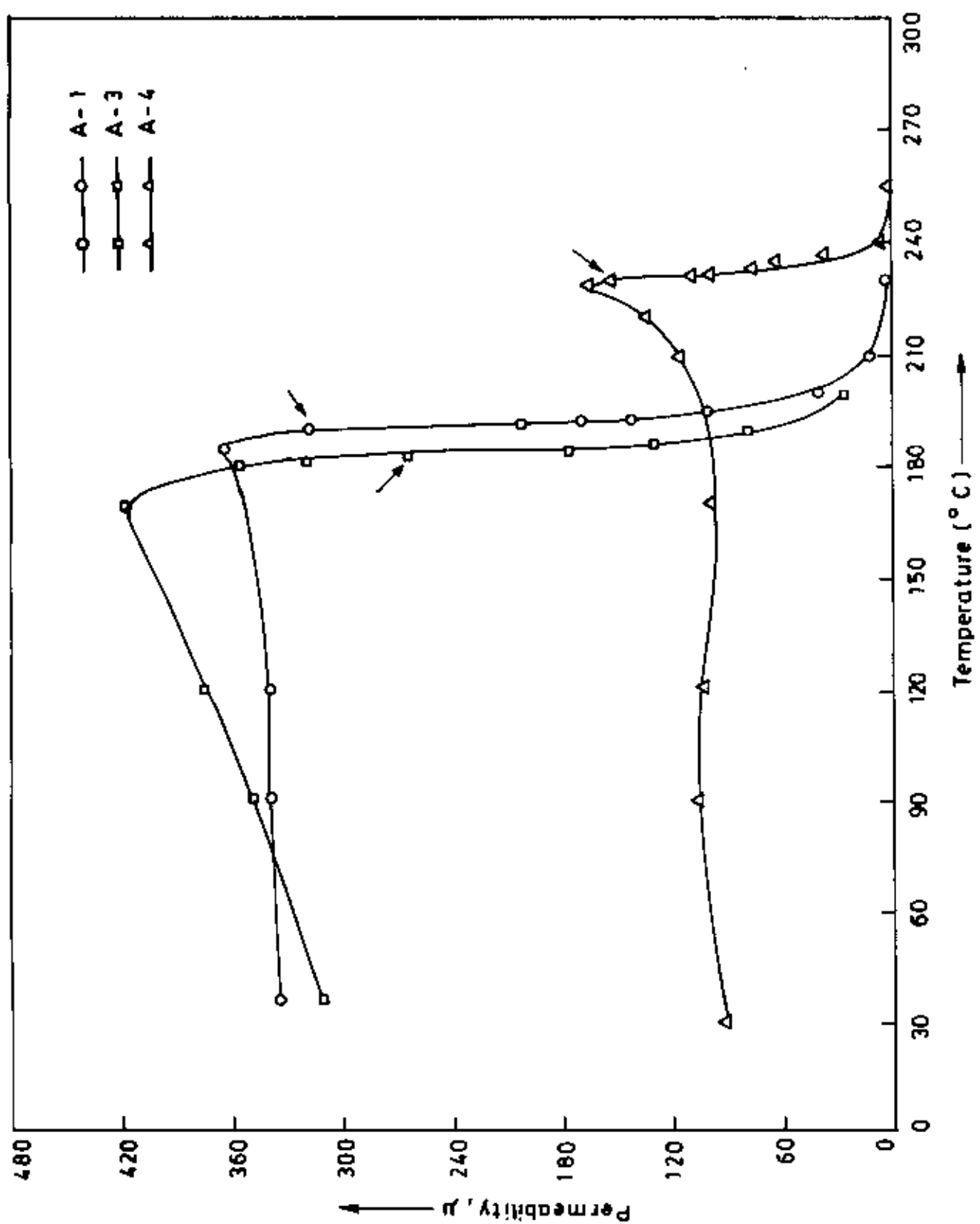
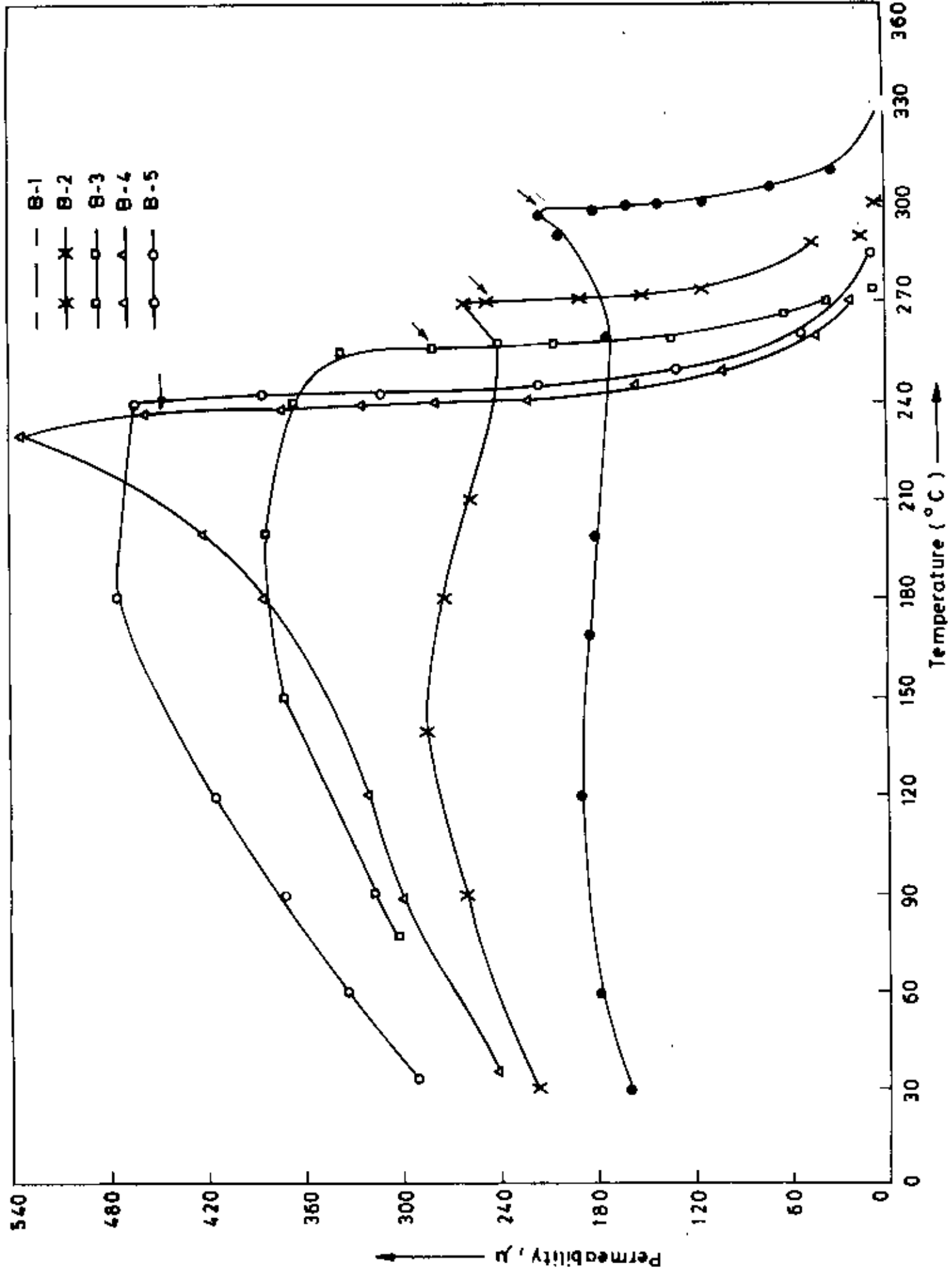


Fig. 5.10: The variation of μ with temperature for A-series



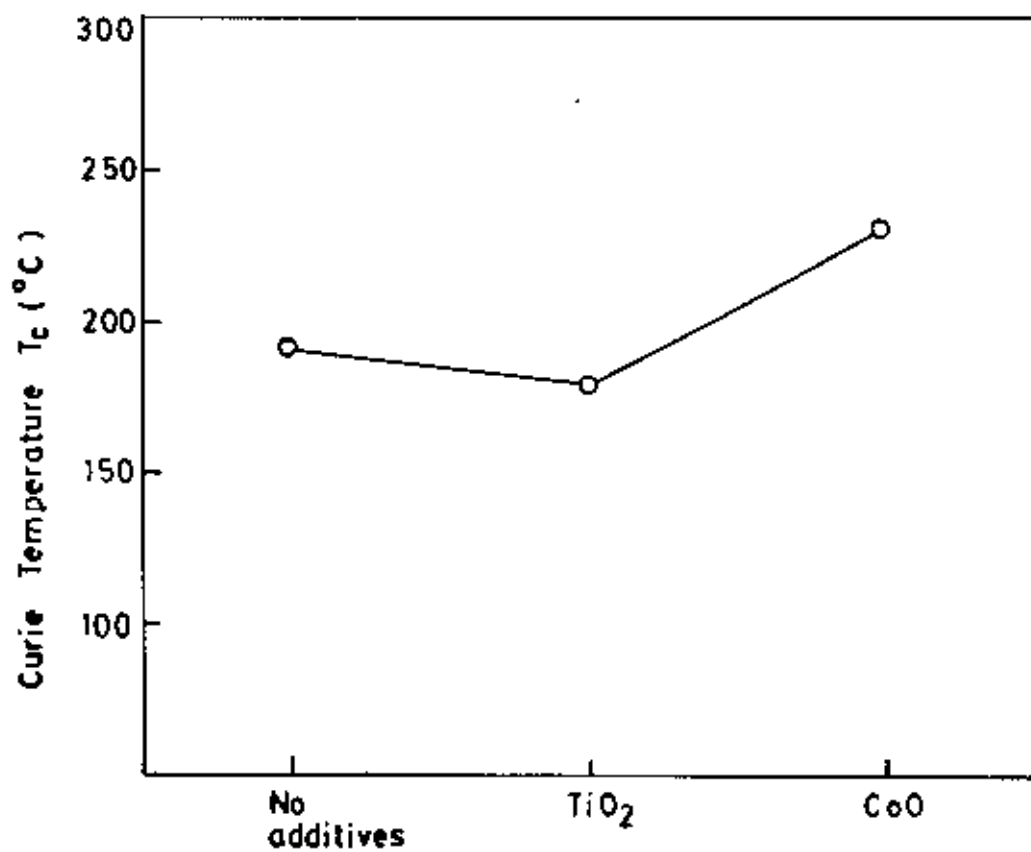


Fig. 5.12 The effect of additives (1 mole %) on curie temperature in $Mn_{0.51}Zn_{0.44}Fe_{2.05}O_4$

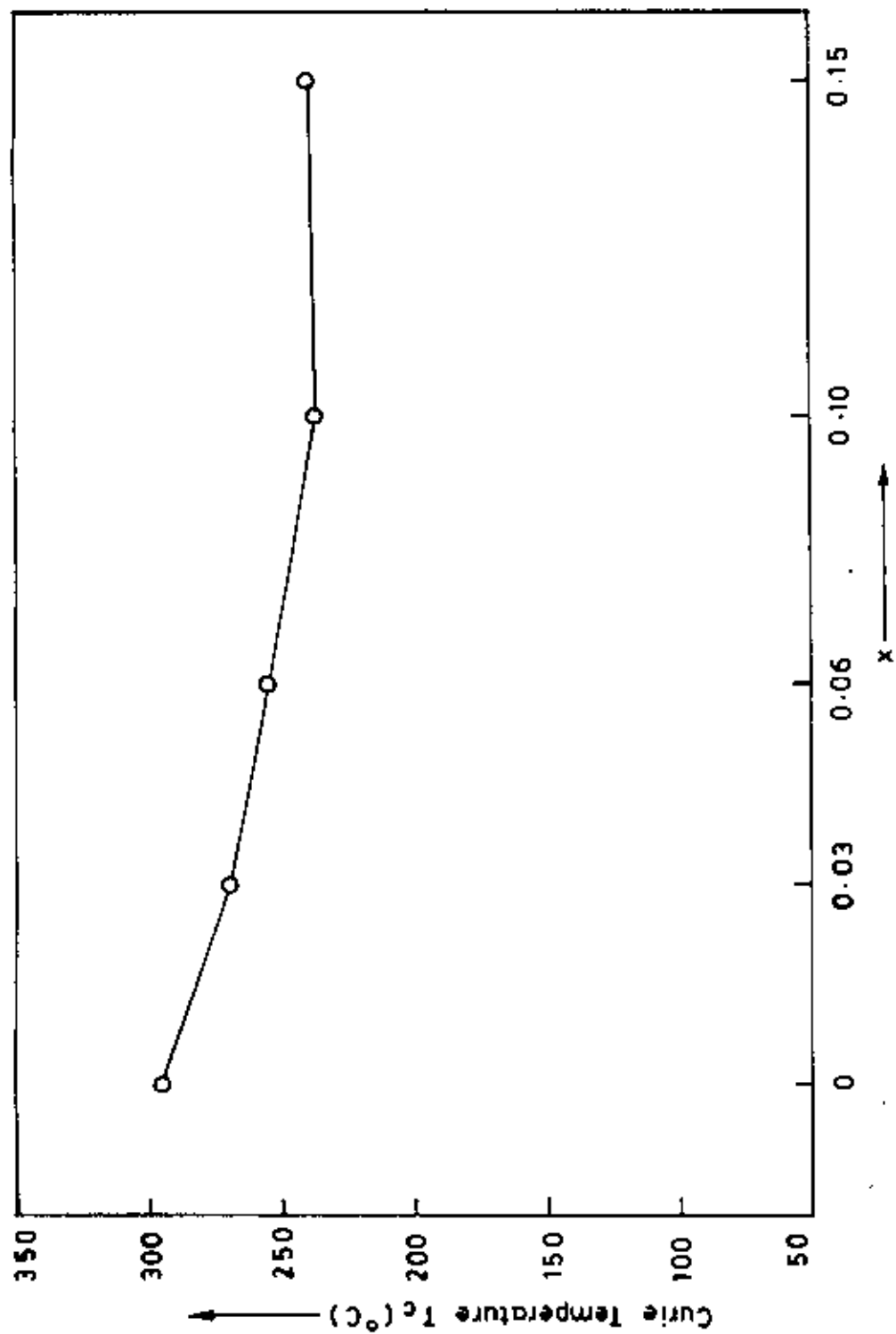


Fig. 5.13: The variation of curie temperature with Cu-content x in $Mn_{0.70-x}Cu_xZn_{0.22}Fe_{2.08}O_4$

trend on substitution of Cu^{2+} for Mn^{2+} (fig-5.13). The decrease of T_c with an increasing Cu^{2+} content may be explained by a modification of the A-B exchange interaction strength due to the change of the Fe^{3+} distribution between A and B sites. The decrease of the Curie temperature is due to the weakening of the A-B interaction.

5.3 Magnetization Measurements

Magnetization curve for the ferrite samples are shown in fig.-5.14 to fig.-5.15. The measurements for V_2O_5 , TiO_2 and CoO doped samples are shown in fig.-5.14 and for CuO substituted samples are shown in fig. 5.15.

Magnetization in ferrite samples originate due to the difference in the magnetic moments of the two sub-lattices. The larger the difference, the greater is the resultant magnetization, because of the anti-parallel arrangements of the moments in two sub-lattices. The magnetic moment of each sub-lattice arises due to the presence of magnetic ions such as Fe^{2+} , Fe^{3+} , Mn^{2+} , Zn^{2+} , Cu^{2+} , Ti^{4+} , V^{5+} , Co^{2+} etc (as in our case) in them. Different magnetic ions occupy different sites. So, as a whole, the two sub-lattices have their individual resultant magnetic moments. The differences in magnetic moment between the two sub-lattices give rise to net magnetic moment which in turn yields magnetization. Now the site preference of the magnetic ions is rather complex since it is governed by many competing factors. The principal dominating factors are:

(a) The ionic radius: Due to the small size of tetrahedral site, smaller ions prefer to stay there. Ionic radii normally decrease with increasing valency. As a result, divalent ions are bigger than the trivalent ones. So, it is expected that A site will be dominated by trivalent cations.

(b) The electronic configuration: Certain ions show special site preferences due to their electronic configuration. For example, Zn^{2+} ions show

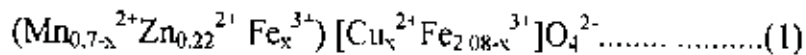
special preference to A site where their 4s, 4p electrons can form a covalent bond with 6 2p electrons of oxygen ions.

(c) The electrostatic energy: This is another factor which plays substantial role in deciding a site for a cation. The electrostatic energy of spinel lattice or the Madelung energy is the energy gained when ions are brought from infinite distance to the spinel lattice. In normal arrangements the metal ions with smallest positive charge are surrounded by 4 O₂ ions and the metal ions with higher positive charge are by 6 O₂ ions. This is electrostatically most favourable.

The above stated discussions reveal that, magnetization of ferrites can be seriously affected by preparation procedure, sintering condition, composition etc. This is so in our measurements too. In figure 5.18 it can be seen that the magnetization measured at 1280°C sintering temperature varies with the additives. This dependence may be explained by taking into account the cation distribution between tetrahedral and octahedral sites of the ferrites. The highest magnetization corresponds to Co²⁺ added samples. Since all the Mn²⁺ ions and Zn²⁺ ions occupy tetrahedral sites while almost all the Fe³⁺ ions are present at octahedral sites, the strength of A-B exchange interaction, due to Fe³⁺ ions, is very weak. As suggested by Yafet and Kittel [8], a strong antiferromagnetic B-B interaction may, therefore, be present due to Fe³⁺ ions at B sites which decreases the magnetization of the B sites yielding lowest value of M_s for Mn_{0.6}Zn_{0.4}Fe₂O₄. Mossbauer study of CoFe₂O₄ [9] shows that Co²⁺ ions having a magnetic moment of 3.5 μ_B, have a preference for octahedral sites. Co²⁺ ions may, therefore, lead to migration of Fe³⁺ ions from B-sites to A-sites due to preference of Co²⁺ ions for B-sites. The strength of A-B interaction thus starts increasing which disturbs the balance of anti-parallel spins at B-sites thus increasing magnetization of B sites resulting in a significant increase in the net magnetization. When 1 mole % TiO₂ is added then magnetization decreases slightly. It is known that Ti⁴⁺ ions have strong preference for B-sites. As non-

magnetic Ti^{3+} ions replace Fe^{3+} ions of magnetic moment $5\mu_B$ in B-sites, the net magnetic moment $M=M_B-M_A$ decreases, hence decreasing the magnetization. In the case of V_2O_5 the magnetization decreases significantly. If like Ti^{3+} , the V^{5+} ions prefer B-site, the magnetic moment is expected to decrease. However, the effect is found to be drastic for V_2O_5 doped samples than for TiO_2 ones.

Figure 5.19 shows the variation of magnetization with Cu-substitution of the composition $Mn_{0.70-x}Cu_xZn_{0.22}Fe_{2.08}O_4$. The saturation magnetization increases for $x=0.03$ and this starts decreasing with further increase of Cu^{12} ions. Neutron diffraction studies of $Mn_{0.6}Zn_{0.4}Fe_2O_4$ ferrites [10] yield the cation distribution as $(Mn_{0.6}^{2+}Zn_{0.4}^{2+}) [Fe_2^{3+}]O_4^{2-}$, it shows that all the Mn^{2+} ions and Zn^{2+} ions occupy tetrahedral sites while all the Fe^{3+} ions occupy octahedral sites. For the present ferrites, the cation distribution can be written as



By substituting Mn^{2+} ions with Cu^{2+} , having a magnetic moment of $1\mu_B$, on the octahedral sites (B-sites), an increase of the magnetization of B sublattice takes place. Thus, the initial increase of saturation magnetization for 0.03 mole% of CuO substitution may be explained as the reinforcement of the A-B interaction thus helping the suppression of negative B-B interaction. The magnetization at B-sites is, therefore, increased thus increasing the net value of M_s . For Cu content, $x>0.03$, decrease of M_s is observed and the following explanations have been proposed:

- the cation distribution differs from (1) i.e., when the value of x exceeds 0.03, M_s again starts decreasing because the number of Fe^{3+} ions migrating to A-sites increases thus decreasing M_B and increasing M_A ,
- some of the iron ions behave paramagnetically in the B-sites [11, 12];
- the formation of $CuFe_2O_4$ nonmagnetic solid phase, nondetectable by means of qualitative x-ray analysis.

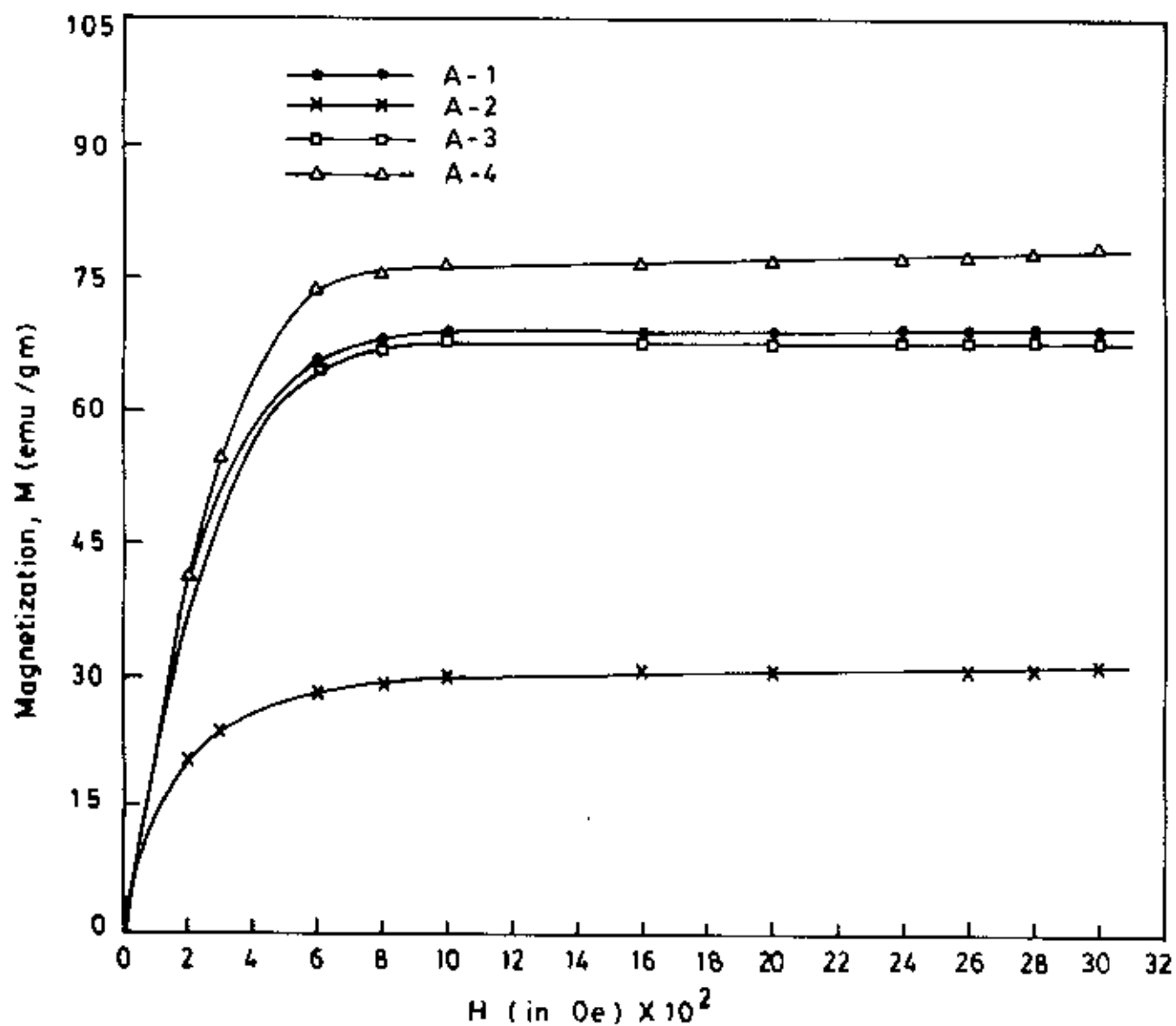


Fig.5.14: Magnetization curves for the samples $Mn_{0.51}Zn_{0.44}Fe_{2.05}O_4$ without and with 1 mole % additives of V_2O_5 , TiO_2 and CoO .

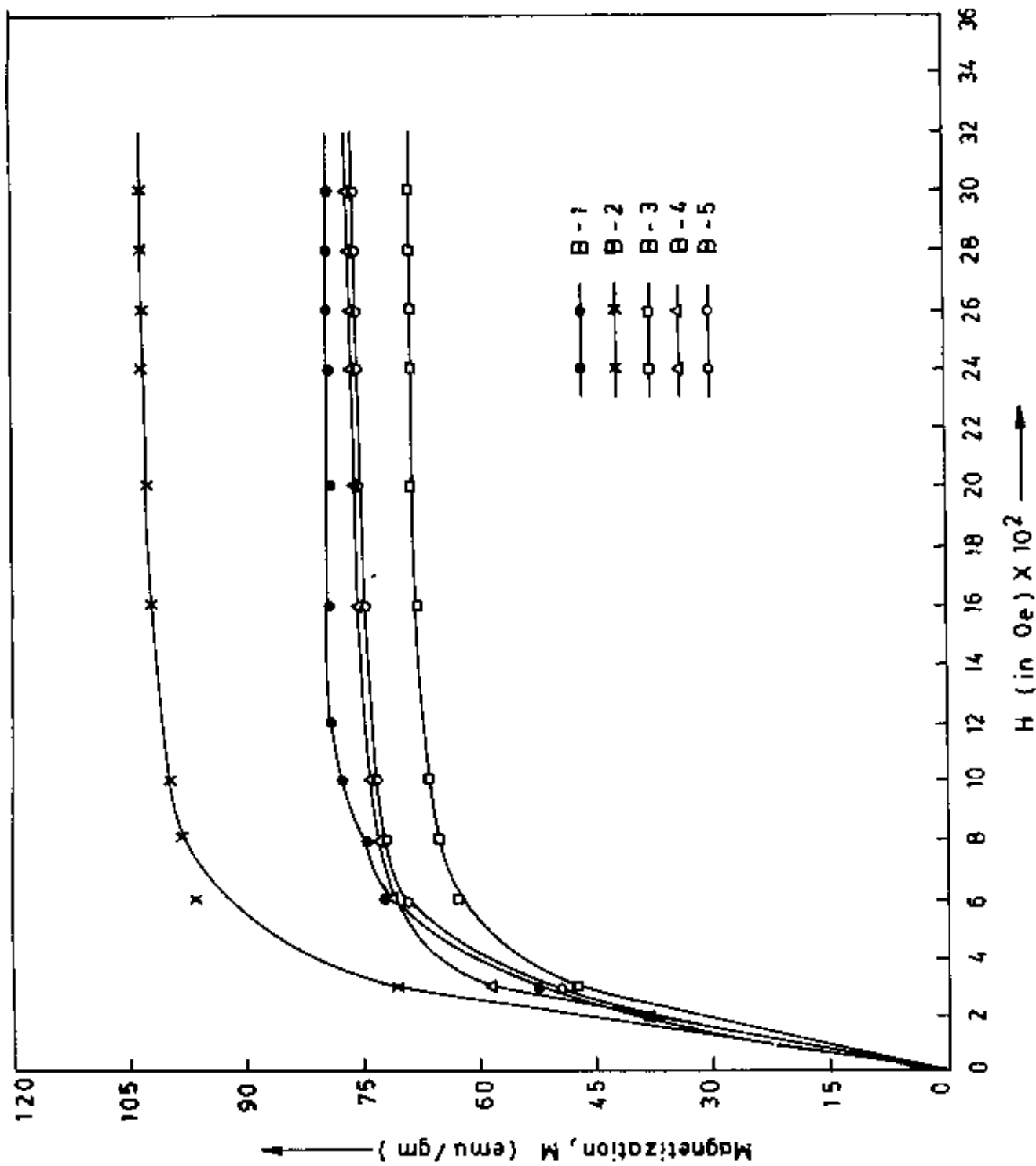


Fig. 5. 15: Magnetization curves for the samples $Mn_{0.75}Cu_xZn_{0.22}Fe_{2.08}O_4$ with $x=0.0, 0.03, 0.06, 0.10, 0.15$.

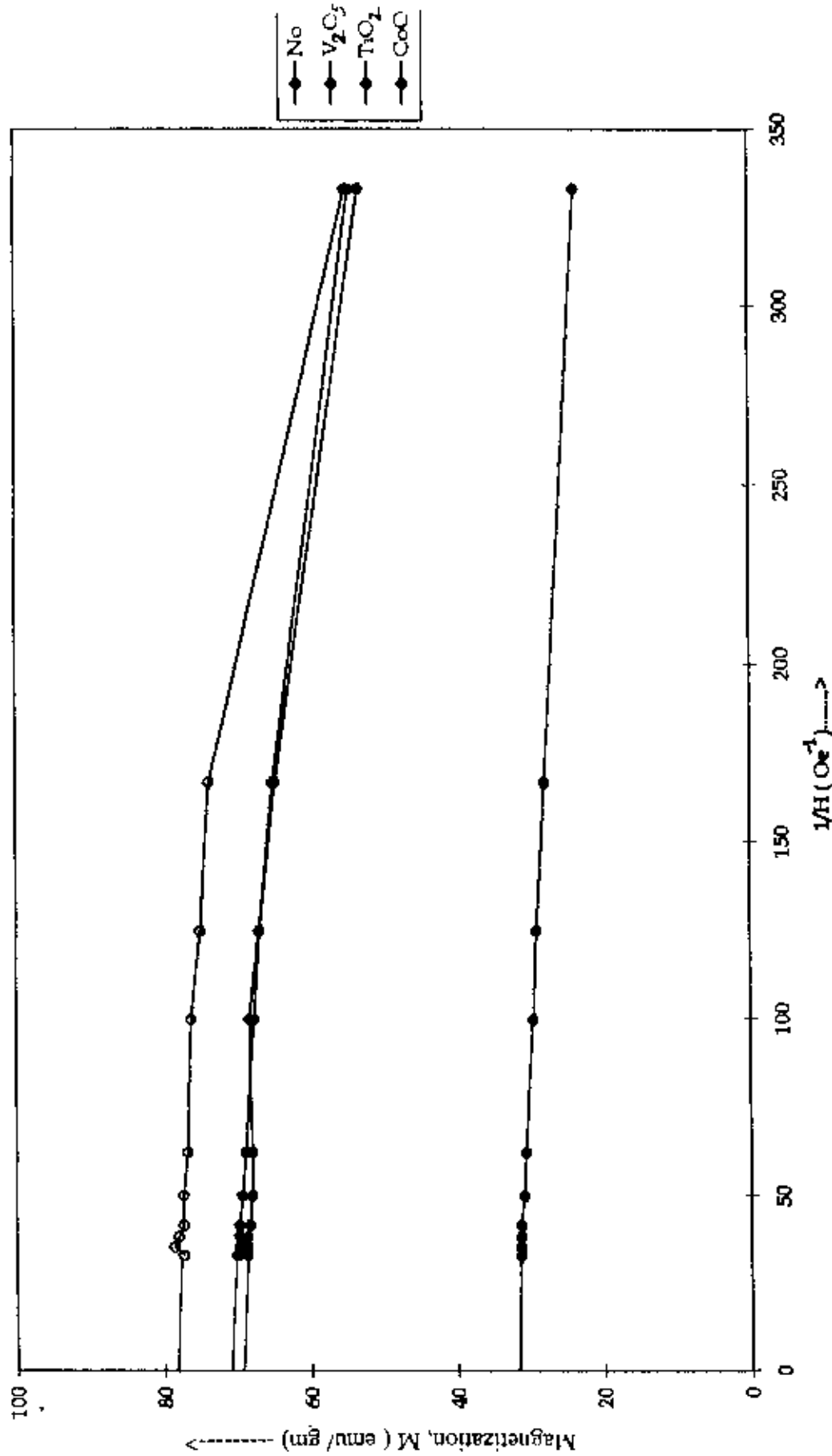


Fig. 5.16: Magnetization against $1/H$ curves for the samples $Mn_{0.51}Zn_{0.44}Fe_{2.02}O_4$ without and with 1 mole % additives of V_2O_5 , TiO_2 and CoO Magnetization at $1/H=0$, is taken as the value at saturation.

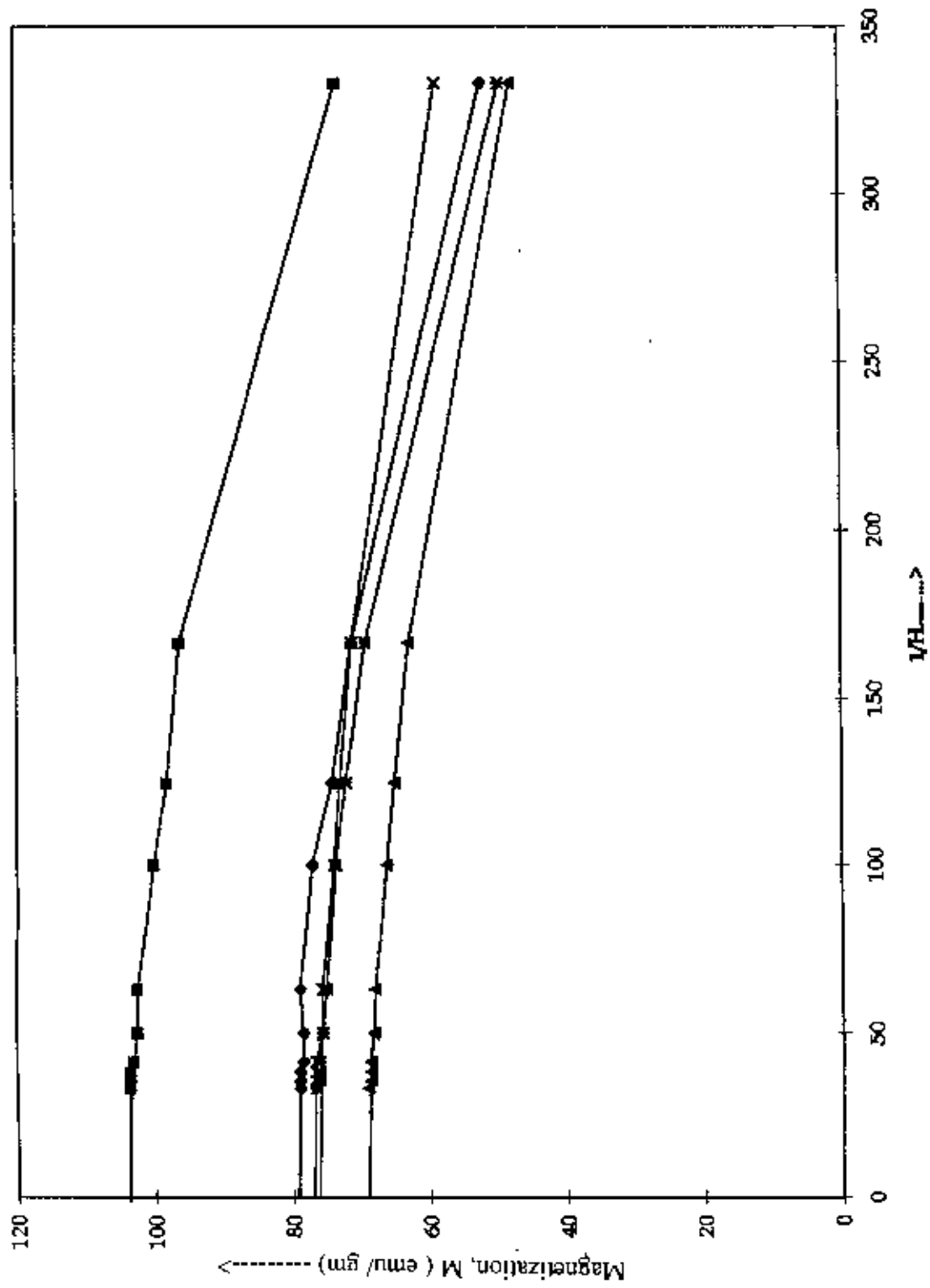


Fig 5.17: Magnetization curves for the samples $Mn_{0.7-5}Cu_xZn_{0.22}Fe_{2.08}O_4$ with

$x=0.0, 0.03, 0.06, 0.10, 0.15$. Magnetization at $1/H=0$, is taken as the value at

saturation.

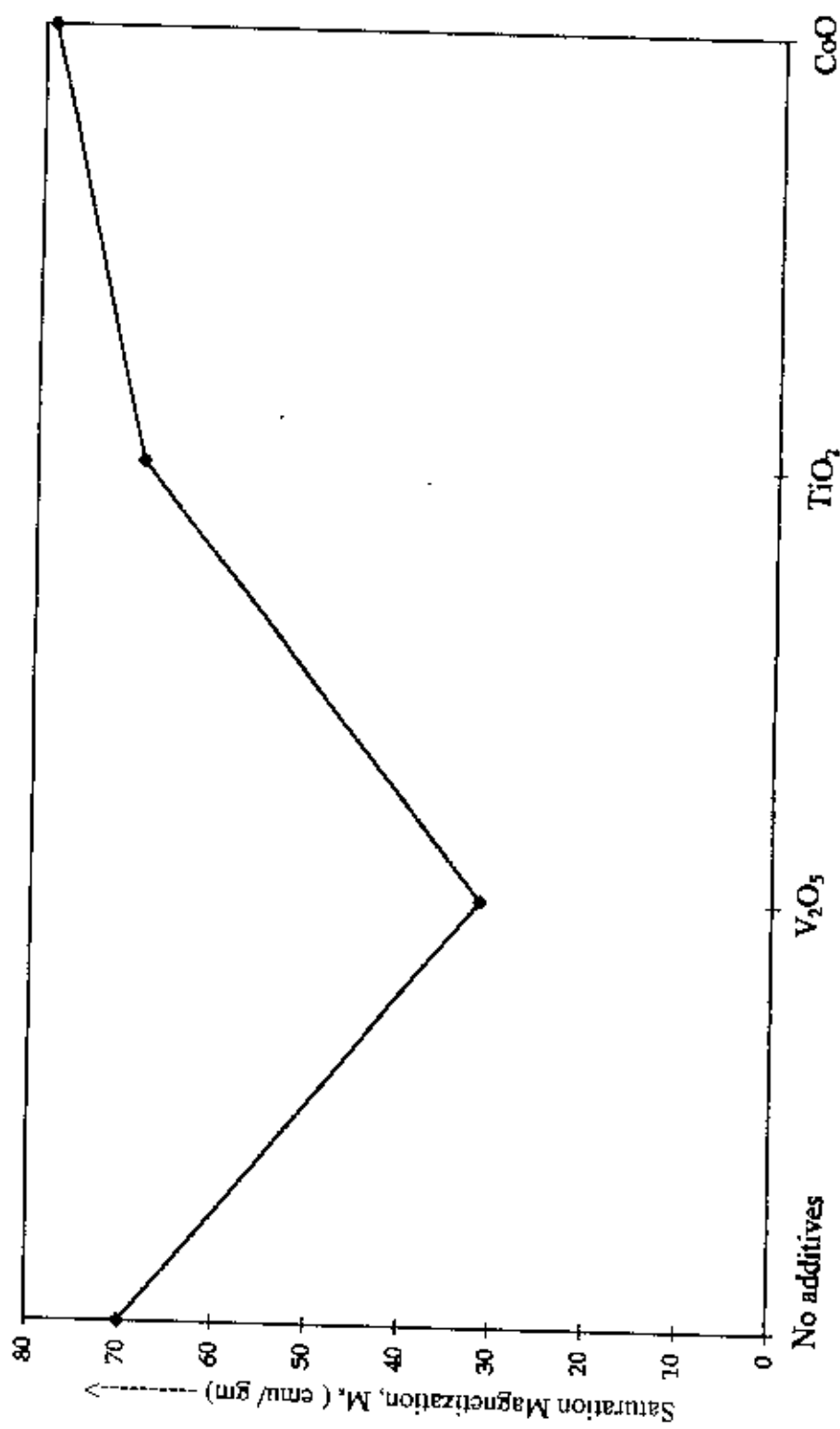
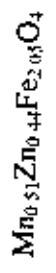


Fig.5.18. The effect of additives (1 mole %) on the Saturation magnetization in



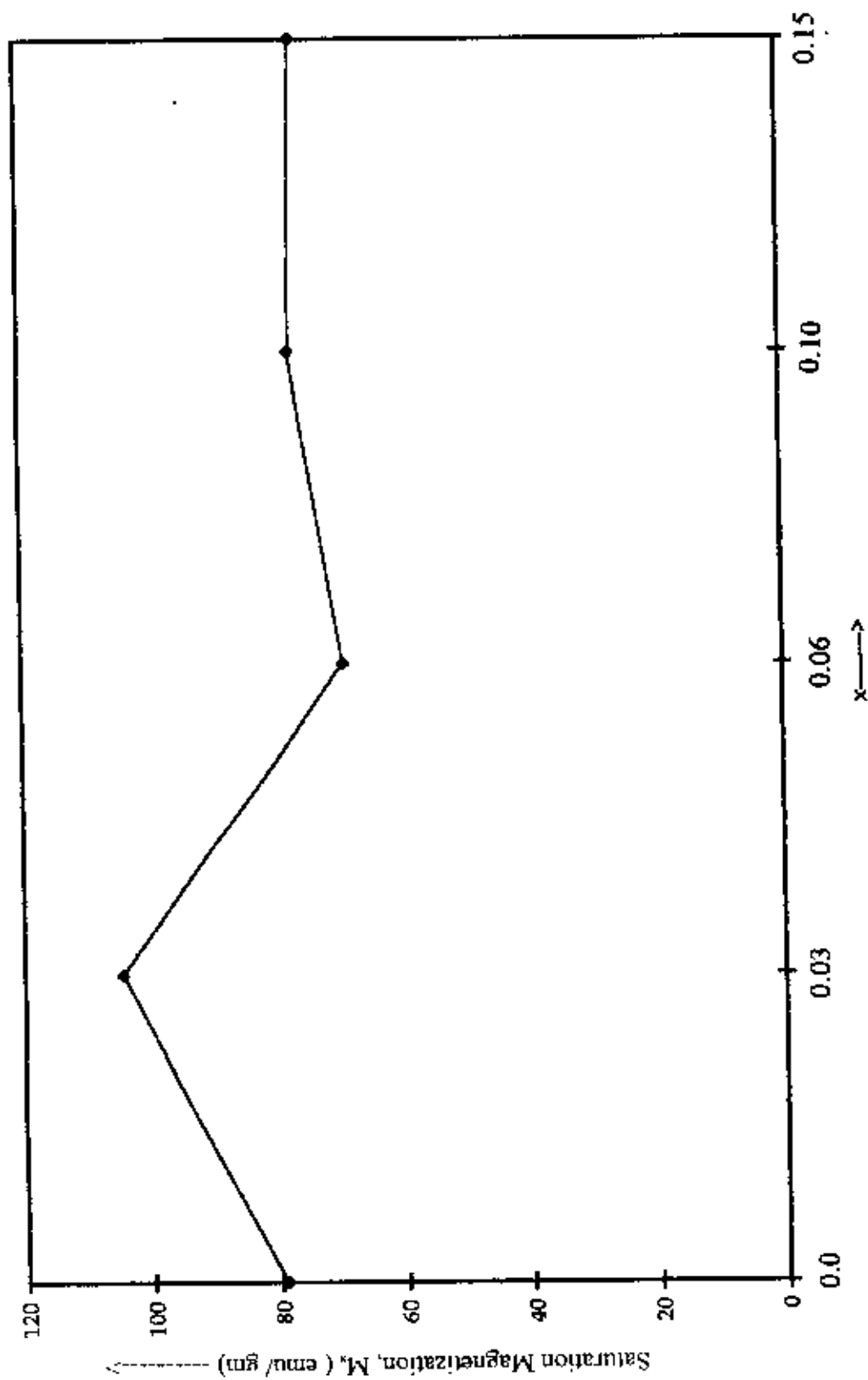
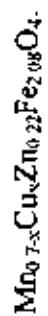


Fig.5.19: The variation of Saturation Magnetization with Cu-content x in



5.4 Microstructure Study

It is well known that most of the electromagnetic characteristics of a ferrite material strongly depend on the microstructure of the fired body. Core loss, as one of the most important characteristic to any ferrite materials for switching power supplies, is dependent on the microstructure as well. Desired magnetic properties of ferrites could be achieved by the control of microstructure

The microphotographs of the samples are shown in fig 5.20 to fig.5.40. All the photographs were taken by polarizing microscope at the Department of Material and Metallurgical, BUET. The pictures were taken at 400X magnification.

Figs. 5.20 to 5.31 are for the samples of the composition $Mn_{0.51}Zn_{0.44}Fe_{2.05}O_4$ with different additives like V_2O_5 , TiO_2 and CoO . Again Figs. 5.32 to 5.40 are for the samples of the composition $Mn_{0.7-x}Cu_xZn_{0.22}Fe_{2.08}O_4$ where $x=0.0, 0.03, 0.06, 0.10$ and 0.15 . All these photographs for samples sintered at temperatures $1227^{\circ}C, 1188^{\circ}C, 1365^{\circ}C$ and quenched at $1300^{\circ}C$

The general conclusions that can be drawn from these photographs are as follow:

1. The sintering procedure have great influence on the microstructure. The grain size of all the samples increased with sintering temperature. But for quenched samples we had small grains. This is because the grains did not get enough time to grow.
2. Uniform grain distribution is observed for the quenched samples. This uniform distribution also corresponds to high permeability. Our permeability spectra supports this result.
3. It seems that, for samples sintered at lower temperature, relatively larger number of pores was formed. This is deleterious to μ .

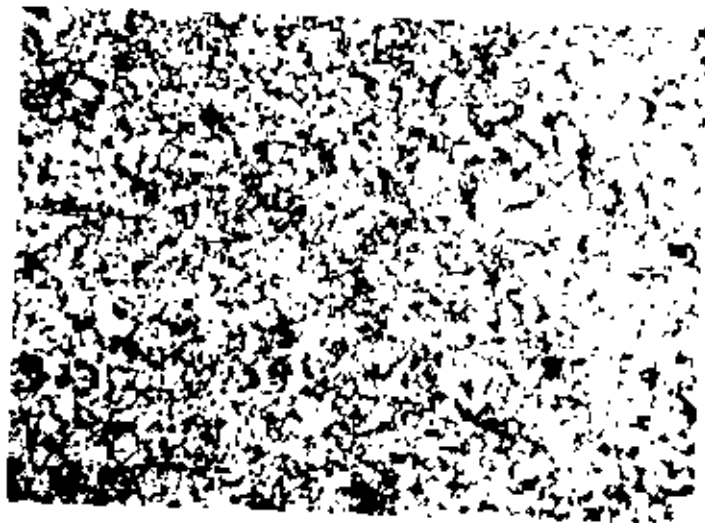


Fig 5.20: Microphotograph for the sample $Mn_{0.51}Zn_{0.44}Fe_{2.05}O_4$ sintered at $1227^{\circ}C$
(Magnified 400 times)



Fig.5.21: Microphotograph for the sample $Mn_{0.51}Zn_{0.44}Fe_{2.05}O_4$ sintered at $1365^{\circ}C$
(Magnified 400 times)

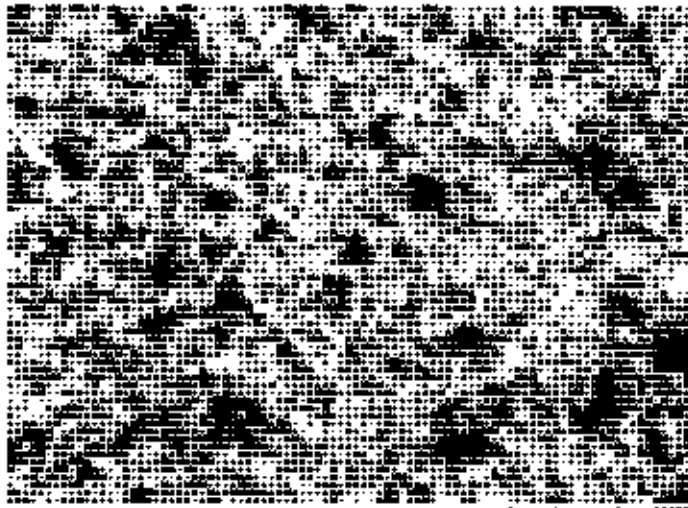


Fig.5.22: Microphotograph for the sample $Mn_{0.51}Zn_{0.44}Fe_{2.05}O_4$ sintered at $1300^{\circ}C$
(Magnified 400 times)

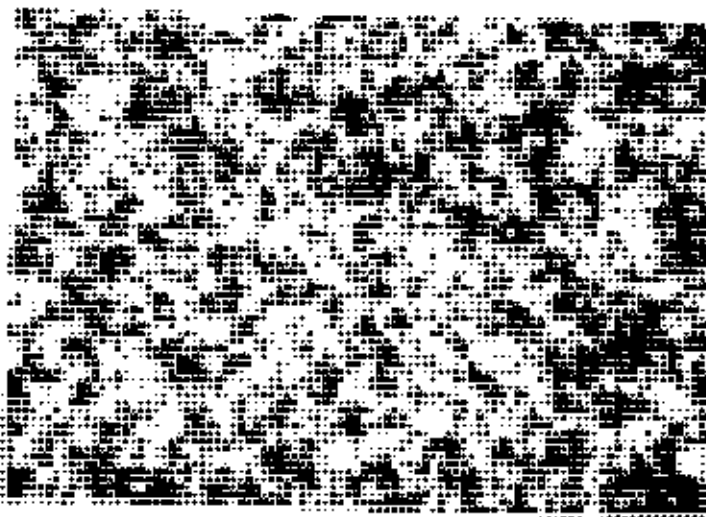


Fig.5.23. Microphotograph for the sample $Mn_{0.51}Zn_{0.44}Fe_{2.05}O_4$ with 1 mole %
additives of TiO_2 sintered at $1227^{\circ}C$ (Magnified 400 times)

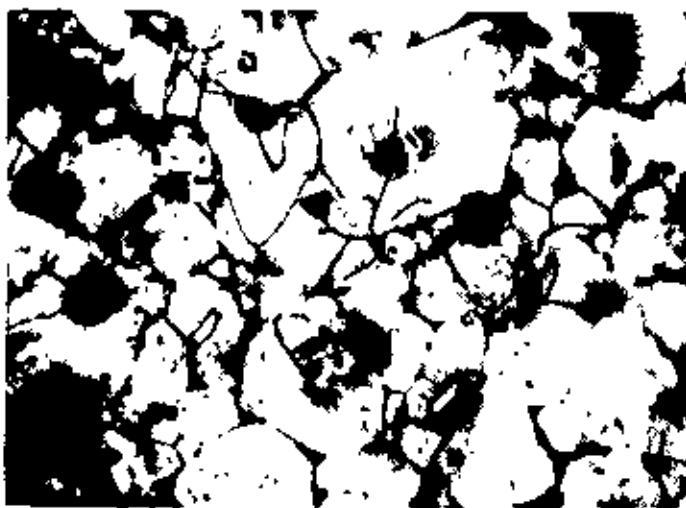


Fig 5.24: Microphotograph for the sample $Mn_{0.51}Zn_{0.44}Fe_{2.05}O_4$ with 1 mole % additives of TiO_2 sintered at $1365^{\circ}C$ (Magnified 400 times)

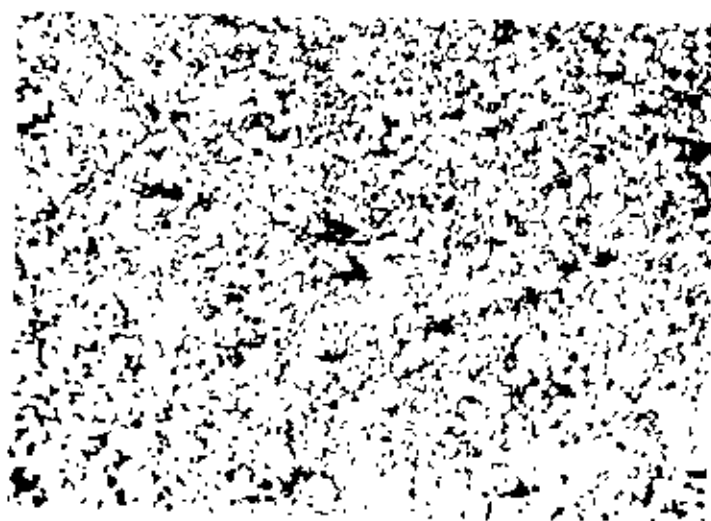


Fig.5 25: Microphotograph for the sample $Mn_{0.51}Zn_{0.44}Fe_{2.05}O_4$ with 1 mole % additives of TiO_2 sintered at $1300^{\circ}C$ (Magnified 400 times)

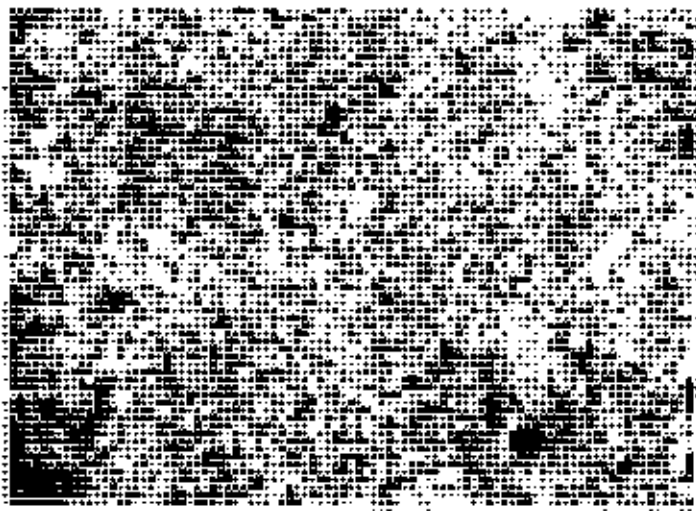


Fig.5.26: Microphotograph for the sample $Mn_{0.31}Zr_{0.44}Fe_{2.05}O_4$ with 1 mole % additives of CoO sintered at $1227^{\circ}C$ (Magnified 400 times)



Fig.5.27: Microphotograph for the sample $Mn_{0.31}Zr_{0.44}Fe_{2.05}O_4$ with 1 mole % additives of CoO sintered at $1365^{\circ}C$ (Magnified 400 times)

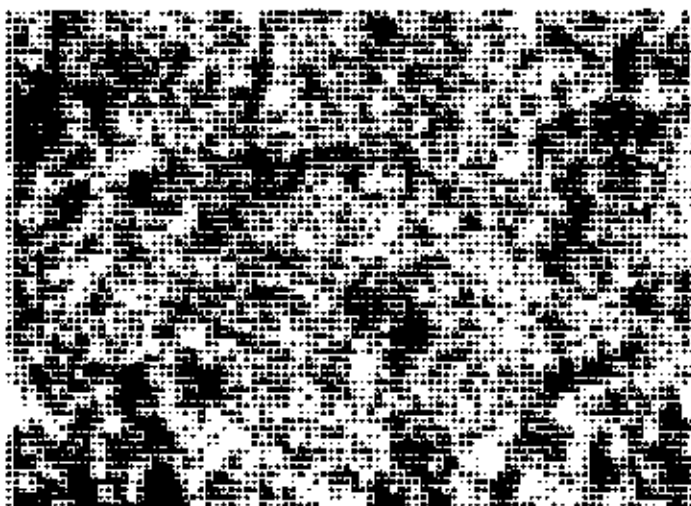


Fig 5.28: Microphotograph for the sample $Mn_{0.51}Zn_{0.44}Fe_{2.05}O_4$ with 1 mole % additives of CoO sintered at $1300^{\circ}C$ (Magnified 400 times)

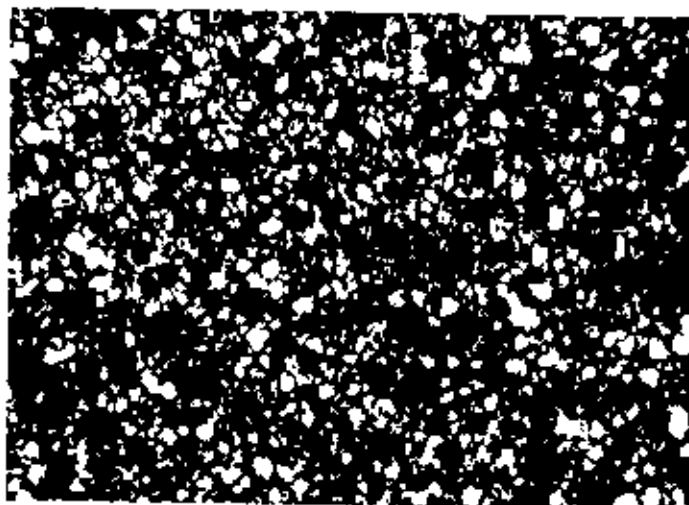


Fig.5 29: Microphotograph for the sample $Mn_{0.7x}Cu_{0.2y}Zn_{0.2z}Fe_{2.48}O_4$ with $x=y=z=0$ sintered at $1188^{\circ}C$ (Magnified 400 times)

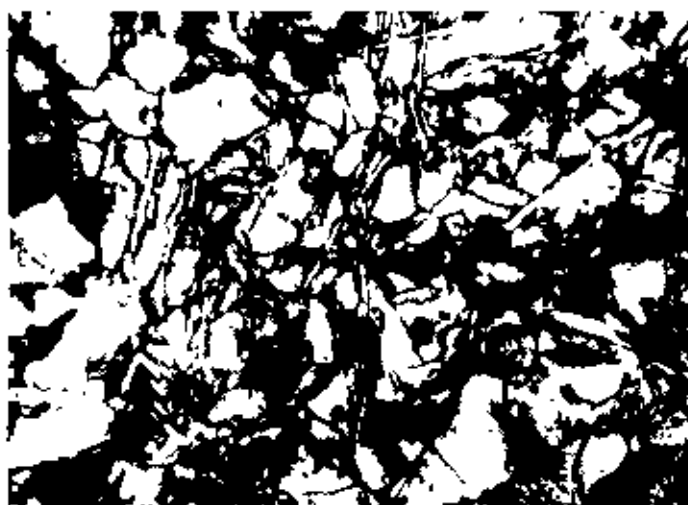


Fig 5.30 Microphotograph for the sample $Mn_{0.7-x}Cu_xZn_{0.22}Fe_{2.08}O_4$ with $x=0.0$ (
sintered at $1365^{\circ}C$ (Magnified 400 times)

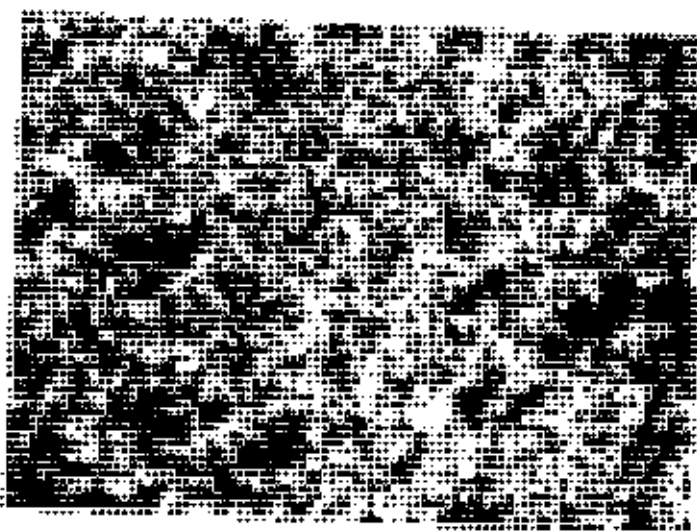


Fig.5.31. Microphotograph for the sample $Mn_{0.7-x}Cu_xZn_{0.22}Fe_{2.08}O_4$ with $x=0.0$ (
sintered at $1300^{\circ}C$ (Magnified 400 times)

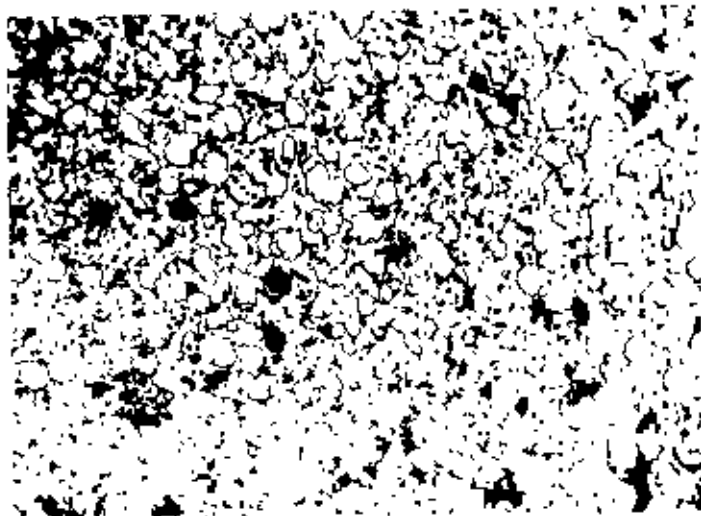


Fig.5.32 Microphotograph for the sample $Mn_{0.7-x}Cu_xZn_{0.22}Fe_{2.08}O_4$ with $x=0.03$
sintered at $1188^{\circ}C$ (Magnified 400 times)

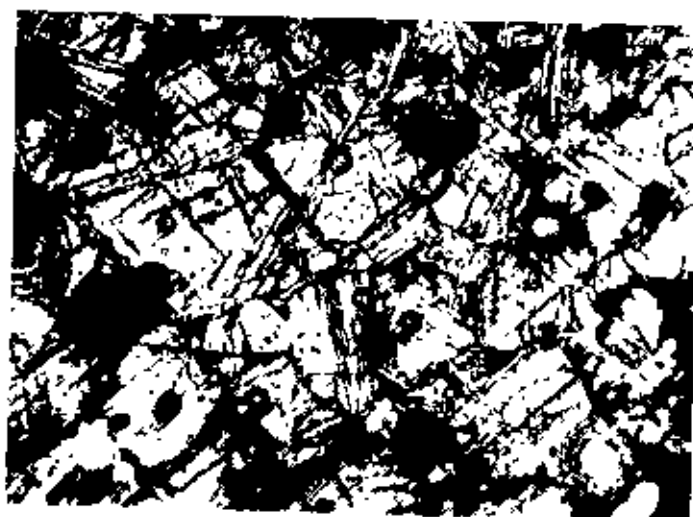


Fig 5.33. Microphotograph for the sample $Mn_{0.7-x}Cu_xZn_{0.22}Fe_{2.08}O_4$ with $x=0.03$
sintered at $1365^{\circ}C$ (Magnified 400 times)

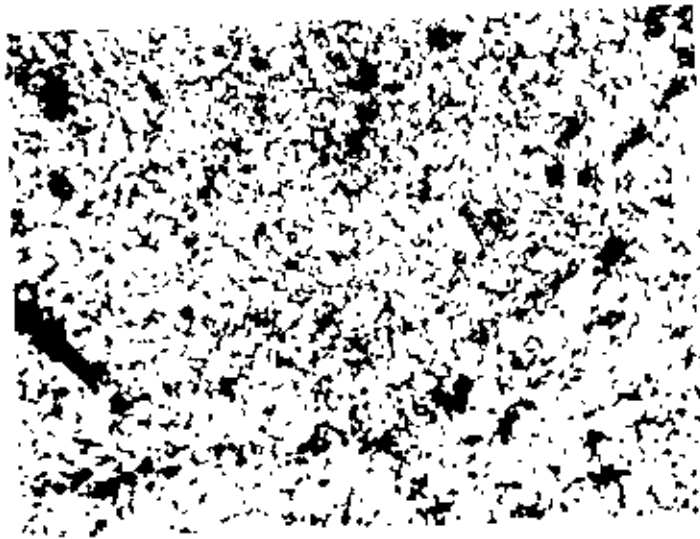


Fig.5.34: Microphotograph for the sample $Mn_{0.7-x}Cu_xZn_{0.22}Fe_{2.08}O_4$ with $x=0.03$ sintered at $1300^{\circ}C$ (Magnified 400 times)

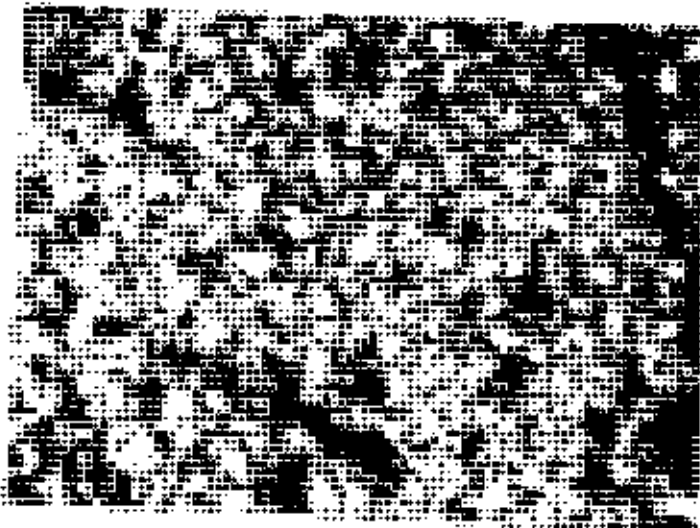


Fig 5.35: Microphotograph for the sample $Mn_{0.7-x}Cu_xZn_{0.22}Fe_{2.08}O_4$ with $x=0.06$ sintered at $1188^{\circ}C$ (Magnified 400 times)

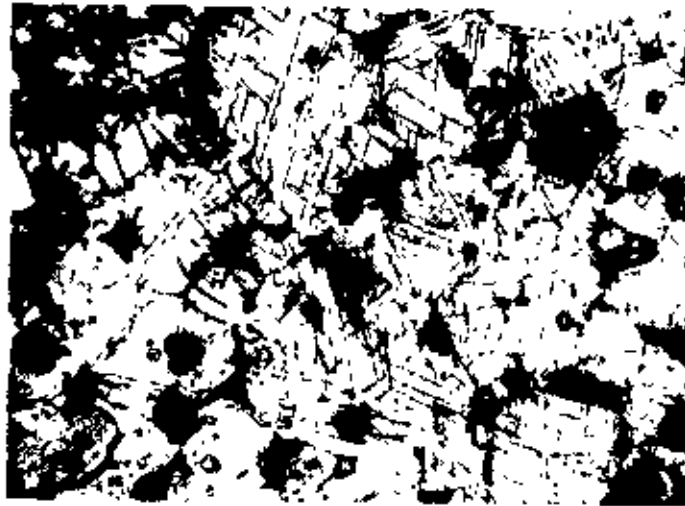


Fig.5.36: Microphotograph for the sample $Mn_{0.75}Cu_{0.25}Zn_{0.22}Fe_{0.08}O_4$ with $x=0.06$ sintered at $1365^{\circ}C$ (Magnified 400 times)

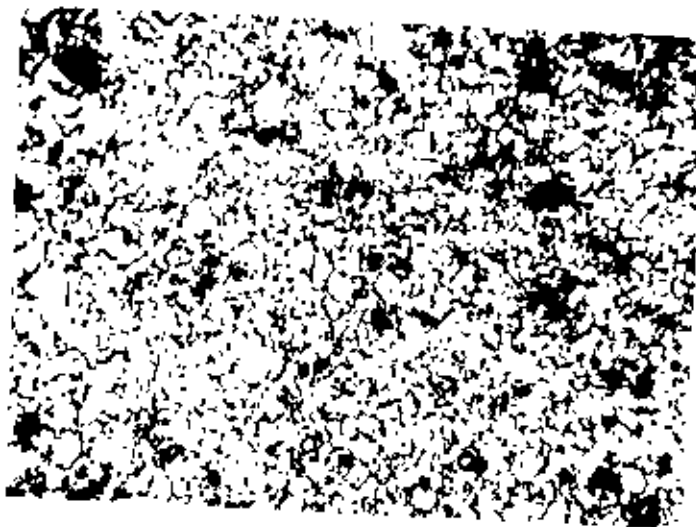


Fig.5.37: Microphotograph for the sample $Mn_{0.75}Cu_{0.25}Zn_{0.22}Fe_{0.08}O_4$ with $x=0.06$ sintered at $1300^{\circ}C$ (Magnified 400 times)

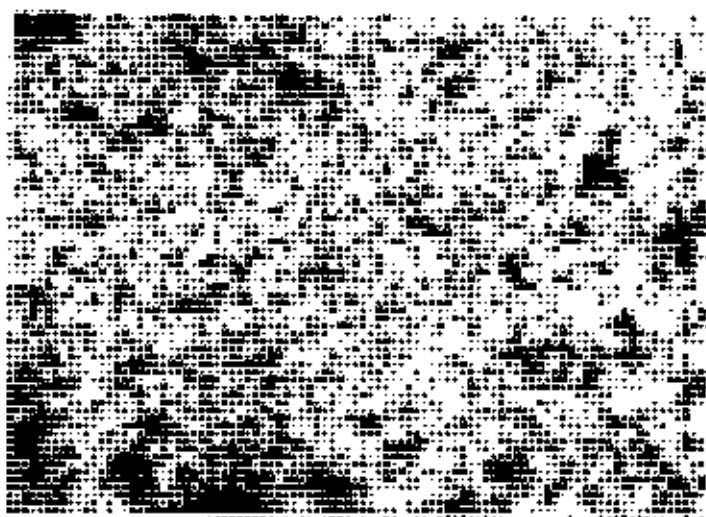


Fig.5.38: Microphotograph for the sample $Mn_{0.75}Cu_{0.22}Fe_{0.08}O_4$ with $x=0.15$
sintered at $1188^{\circ}C$ (Magnified 400 times)



Fig.5.39: Microphotograph for the sample $Mn_{0.75}Cu_{0.22}Fe_{0.08}O_4$ with $x=0.15$
sintered at $1188^{\circ}C$ (Magnified 400 times)



Fig.5 40: Microphotograph for the sample $Mn_{0.75}Cu_{0.25}Zn_{0.25}Fe_{2.00}O_4$ with $x=0.15$ sintered at $1188^{\circ}C$ (Magnified 400 times)

5.5 Permeability Measurements

Permeability curves for the two series of samples doped and substitution ones are shown in fig.-5.41 to fig.-5.56. Fig.-5.41 to fig.-5.49 are the curves of μ' and μ'' against frequency for samples sintered at different temperature and fig.-5.50 to fig.-5.53 are the curves for the samples of different dopant percentages and fig. 5.54 to fig 5.56 are the curves for the sample sintered at different times.

Permeability measurement comprises one of the most important part of the present work. Actually, we were looking for an optimum composition in Mn-Zn ferrite, as well as the best sintering condition. Our aim was to attain the following goals:

1. Optimum composition
2. Optimum sintering condition.
3. Maximum permeability.
4. Uniformity of permeability over a large frequency range

Looking at the permeability spectra we search for the above mention properties in different samples. Fig.-5.41 to fig.-5.56 depicts the permeability spectra over the frequency range from 5 KHz to 13 MHz. The real part μ' and imaginary part μ'' of complex permeability are shown in solid lines and dotted lines respectively. It is to be mentioned that, there are a large number of factors associated with the domain motion and hence the magnetization process related to our measured

permeability of the ferrite samples. First and foremost comes the contribution from domain wall movement and spin rotation in domains. The uncertainty of the contribution from each of the mechanism, however makes the theoretical interpretation of the experimental results difficult. For a spherical grain with diametral and spherically bulging walls, Globus (1975) [13] shows that the intrinsic rotational permeability μ^R and 180° wall permeability μ^w may be written as:

$$\begin{aligned}\mu^R &= 1 + \frac{2\pi M_s^2}{K} \\ \mu^w &= 1 + \frac{3}{4} \cdot \frac{1}{\gamma} \cdot \pi M_s^2 D\end{aligned}\quad (1)$$

where M_s is the saturation magnetization, K is total anisotropy, D is grain diameter and γ is the wall energy.

Total anisotropy $K = K_1 + \lambda_s \sigma$

where σ is the internal stress. Since the wall energy $\gamma \cong K\delta_w$, where δ_w is the wall thickness, Then

$$\mu^w = 1 + (3\pi/4\delta_w) (M_s^2/K)D.$$

The rotational permeability is dependent only on intrinsic properties such as M_s , K_1 and λ_s which are controlled by chemistry. In addition the wall permeability is microstructurally sensitive to grain size and intragranular defects such as porosity, second phase, inclusions and dislocations that affect the wall energy. So, there are too many parameters involved and in many ways they affect the permeability. It is thus difficult to explain the permeability spectra quantitatively.

In present work, the measurements done by changing the sintering temperatures for a particular sample given in fig.-5.41 to fig.5.49 show a common feature.

With the increase of sintering temperature T_s , μ' is found to increase at first and then decreases. This is explained as due to lowering of domains wall energy by easy domain wall movements. This explanation is supported by our microstructure study. Since increase in grain size is associated with lower grain boundary area which varies proportionally with the square of the linear dimensions of grain, while magnetization increases is proportional to volume, which increases as cube of the linear dimensions of the grain. So for smaller grain size the major contribution should come from rotational permeability. This is also supported by Joseph Pankert [14]. In his paper titled "Influence of grain boundaries on complex permeability in Mn-Zn ferrite" he suggested that proceeding to smaller grains leads to monodomain state where no domains wall can exist inside single grain. The microstructure study disclosed that with the increase in T_s , the grain size is increased. Thus for a large grain permeability should increase as it varies proportionally with grain diameter. Thus higher μ for higher T_s can be accounted for. The grain diameter D depends on the sintering time as the following relation hold good

$$\bar{D} = kt^n$$

where \bar{D} is the average grain diameter, k is the proportionality constant, $n=1/3$ and t is the sintering time. All the samples were sintered at different temperatures. The sintering temperatures were 1188^oC, 1280^oC, 1365^oC and 1300^oC. The sintering time for the samples varies from 1.5 to 2 to 4 hours. In case of all the samples except that treated at 1365^oC shows expected increase in permeabilities. For the samples heat treated at 1365^oC though the grain size was observed to increase the permeability was found to decrease drastically. We believe that the reason behinds this phenomena is that the samples heat treated at higher temperature contains increase number of pores within the grains which results sharp decrease in permeability. Similar phenomena was observed by Guillard [15]. He demonstrated that the permeability of a NiZn

ferrite drastically decreased with increasing percentage of grains possessing pores despite increasing grain size.

It is interesting to note that for all the samples, 'quenched' from 1300°C gives the highest permeability. Quenching phenomenon needs special attention. When we quenched the samples the grain size of the samples were found to be small. Because they did not get enough time to grow. The grains were also uniform in size. When the materials are quenched from an elevated temperature, the condition of the sample at the elevated temperature is normally 'frozen in'. As a result we get uniformly distributed and microscopically more homogeneous materials with small grains which could rotate more easily due to the small value of shape anisotropy. Thus a higher value of μ for quenched materials can be accounted for.

Except for very low frequency the real part of the permeability μ' for the heat treated samples is found to show constant uniform value over the frequency range 10KHz to 2MHz. It is observed that as the permeability started to decrease, the resonance frequency f_r (i.e. the frequency at which μ' shows peak) gets higher. This really confirms with Snoek's relation stated as

$$\mu f_r = \text{constant}$$

E. G Visser [16] reported that below 1 MHz μ is dominated by wall motion. Between 1 and 3 MHz μ' is determined by rotational susceptibility χ'_r and μ'' by wall susceptibility χ'_w . Above 3 MHz wall motion is strongly damped and the relation becomes dominating process in Mn-Zn ferrites. T. Kimura et. al [16] suggested earlier that, there should be a transition frequency between 0.5 to 2 MHz above which the rotational process dominates. This feature is attributed to natural resonance. This ceramic is thought to be a good candidate for use in multilayer chip inductors

We now look at the effect of additives and substitutes on the permeability i.e. the initial permeability μ' . Fig.-5.50 to fig.5.53 show the variation of μ' and μ'' with frequency for different dopants. The effect of additives i.e. dopants are

- to change the densification of the ferrites thereby changing the mechanical properties like hardness, erosion etc.,
- the additive can control the mobility of the porosity and
- it can segregate all the grain boundaries and control the grain growth.

The effect of additives, however, is not monotonous because two apparently opposite effects are produced by additives in respect of coercivity and initial permeability. When the grains are homogeneous and free of porosities the coercivity gets lower and permeability increases. However this positive effect on permeability is countered by the smaller size of the crystallites. On the other hand, with increasing additives the growth of grain can be favoured with associated increase in permeability. But these grains may be separated by the random segregation of additives which hinder the domain wall movement. It is also noted that the effects of additives on the magnetic properties could not be separated from the influence of compositional inhomogeneity.

We now concentrate our focus towards Fig 5.50 to 5.51. Permeability at all frequencies was effectively reduced by addition of CoO. The presence of Co^{2+} ions is expected to significantly modify its anisotropy and consequently the measured permeability[17]. Globus[18] has given the following approximate relation for μ' :

$$\mu' = M_s^2 \text{ dm} / K_1$$

Where dm is the average grain diameter and K_1 is the magnetocrystalline anisotropy constant. Since addition of Co^{2+} ions increases the value saturation magnetization M_s , and grain size does not change significantly, an increase in

the value of K_1 may be responsible for decrease of μ' . Co^{2+} ions, when present in small quantity, contribute to the positive value of K_1 and hence reduce μ as the host lattice possesses negative anisotropy[19,20]. It was shown that permeability value was slightly reduced by addition of 1 molc% TiO_2 . A low value of μ' is attributed to high porosity of these samples. It is also dependent on other factors like domain wall motion, size and distribution of pores in the crystallite and solubility of Ti^{4+} ions. With the addition of 1 mole % V_2O_5 , permeability decreased significantly. This is due to the large effective grain boundary thickness compounded with the lower grain conductivity of the sample.

Fig.5.52 to 5.53 shows the influence of the copper ions substitution on permeability. One can observe that the permeability value increases with increasing copper content in the Mn-Zn-Cu ferrite. We tried to correlate this result with the influence of the copper content on the grain size. In general the permeability is related to two different magnetizing mechanisms: the spin rotational magnetization and the domain wall motion. Globus suggested that the domain-wall motion was affected by the grain size and enhanced with the increase of the grain size [21]. The grain growth being a result of interparticle mass transport. One explanation must be sought in terms of the influence of Cu^{2+} ions in the diffusion process. Of course, the grain boundary diffusion may play an important role in the grain growth during sintering, because the activation energy for lattice diffusion is higher than for grain boundary diffusion [22].

From our permeability measurements, we also calculated the loss factor $\tan\delta$ or D and the quality factor Q . Fig.-5.57 to fig.-5.67 show the variations of loss factors $\tan\delta$ or D with frequency of the two series of samples sintered at different sintering temperature T_s , D is minimum for frequency upto 1MHz. The rise in the value of D after that can be associated with resonance phenomenon occurring in the domains. Brockman *et al.* [23] first brought this

thing to notice. These investigations found that the loss factor D rises sharply i.e the permeability drops rapidly at frequency about 1.5 MHz. This frequency was found to be dependent on size of the core They explained this phenomenon in terms of the building up of an electromagnetic standing wave propagating in the material with relative permeability $\bar{\mu}$ and relative dielectric constant $\bar{\epsilon}$ reduced by the factor $\frac{1}{\sqrt{\epsilon\mu}}$ as compared with that in vacuum;

hence the wavelength is

$$\lambda = \frac{c}{f\sqrt{\epsilon\mu}}$$

where c is the velocity of light and f is the frequency. For Mn-Zn ferrite, $\bar{\mu} \sim 10^3$, $\bar{\epsilon} \sim 5 \times 10^4$; if we assume $f = 1.5$ MHz, the wave length is estimated to be $\lambda \cong 2.6$ cm. If therefore, the dimensions of the core is equal to an integer multiple of the wave length λ , the electromagnetic wave will resonant within the core, giving rise to a standing wave. This type of phenomenon is known as dimensional resonance. So the rise of D at frequency about 1 MHz can be attributed to this phenomenon. If we now search for any effect of additives on the value of D, we find from fig. 5.66 that the addition of 1 mole% Li_2O and V_2O_5 decreases the value of D but the addition of 1 mole% CoO increases the value of D. Figs 5.67 show that the substitution of Cu^{2+} ions for Mn^{2+} ions increase the value of D.

The quality factor or Q factor is shown in fig.-5.68 to fig.-5.78. Fig.-5.68 to fig.-5.76 are for the samples of two series sintered at different sintering temperature and fig.-5.77 to fig.-5.78 are for the variation of Q-value with different mole percentage of additives and CuO substitutes. We have already defined Q factor as the reciprocal of $\tan\delta$. So, these curves are mere a reciprocal representation of $\tan\delta$ values. We first consider figs. 5.72 to 5.76 for the Cu-substitutes samples of the composition $\text{Mn}_{0.75}\text{Zn}_{0.22}\text{Cu}_x\text{Fe}_{2-0.08x}\text{O}_4$. The results that can be extracted from these figure are as follows.

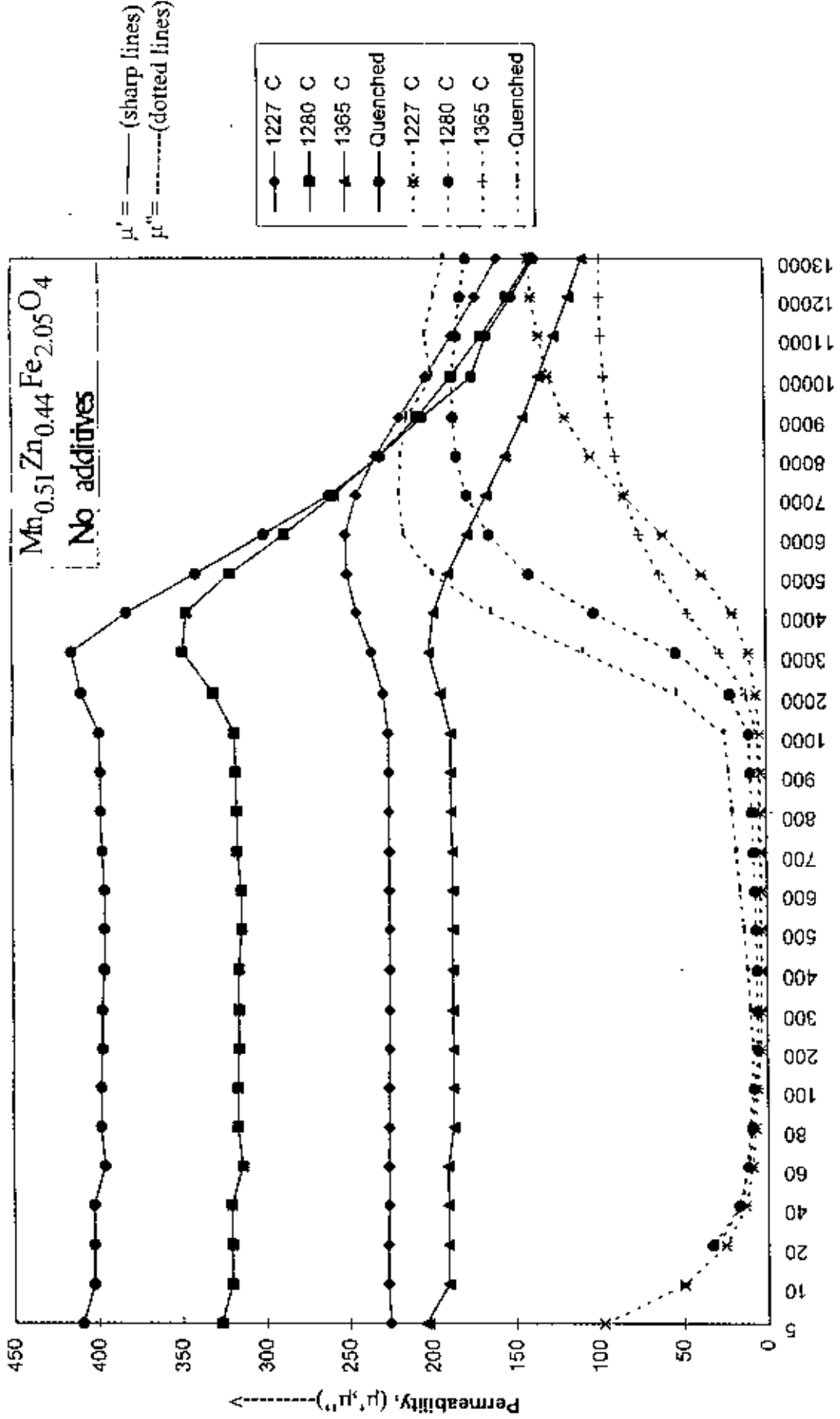


Fig 5.41: Dispersion curves for the samples $\text{Mn}_{0.51}\text{Zn}_{0.44}\text{Fe}_{2.05}\text{O}_4$ sintered at different temperatures.

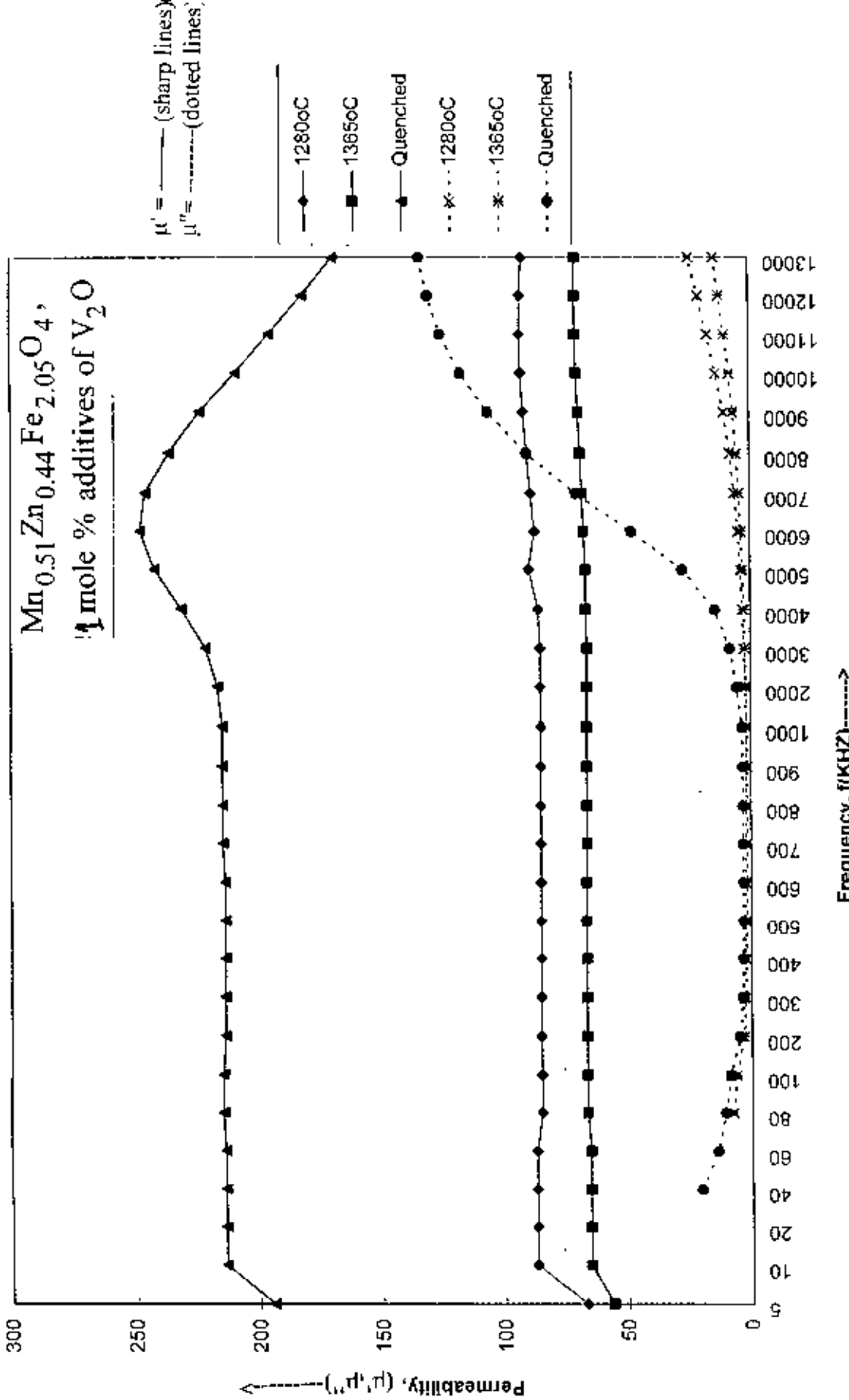


Fig 5.42: Dispersion curves for the samples $\text{Mn}_{0.51}\text{Zn}_{0.44}\text{Fe}_{2.05}\text{O}_4$ with 1 mole % additives of V_2O_5 sintered at different temperatures.

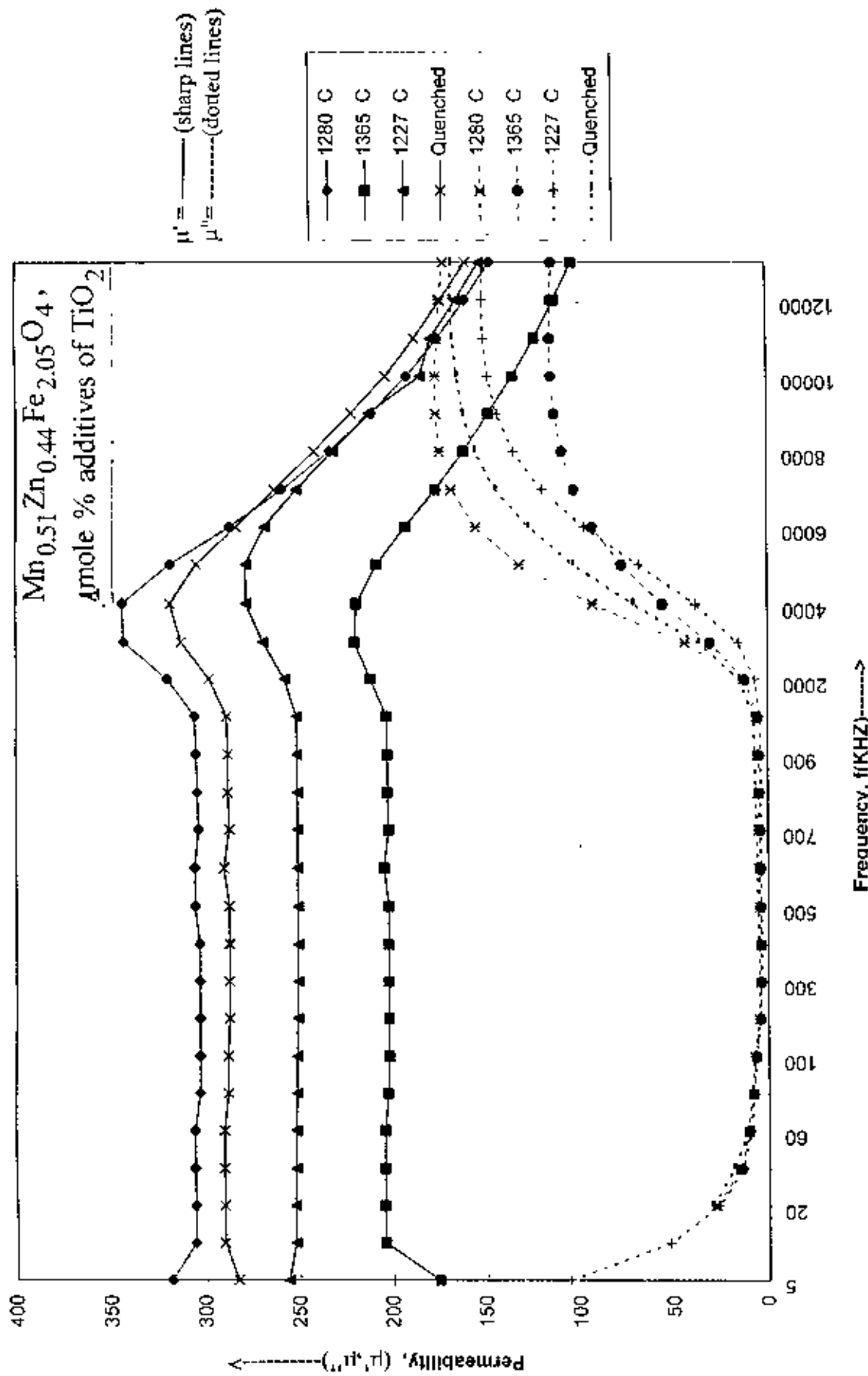


Fig 5.43: Dispersion curves for the samples $\text{Mn}_{0.51}\text{Zn}_{0.44}\text{Fe}_{2.05}\text{O}_4$ with 1 mole % additives of TiO_2 sintered at different temperatures.

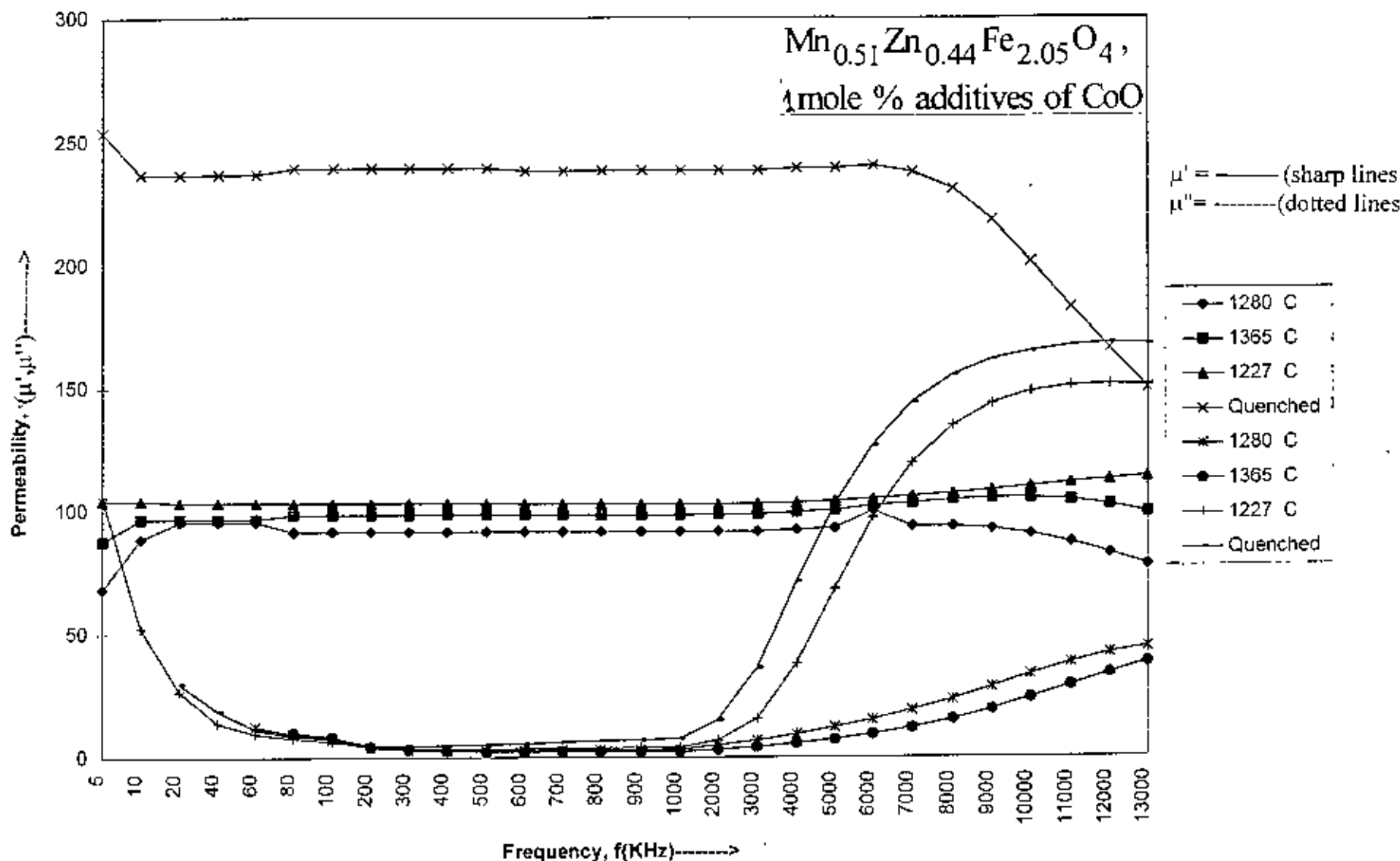


Fig 5.44: Dispersion curves for the samples $\text{Mn}_{0.51}\text{Zn}_{0.44}\text{Fe}_{2.05}\text{O}_4$ with 1 mole % additives of CoO sintered at different temperatures.

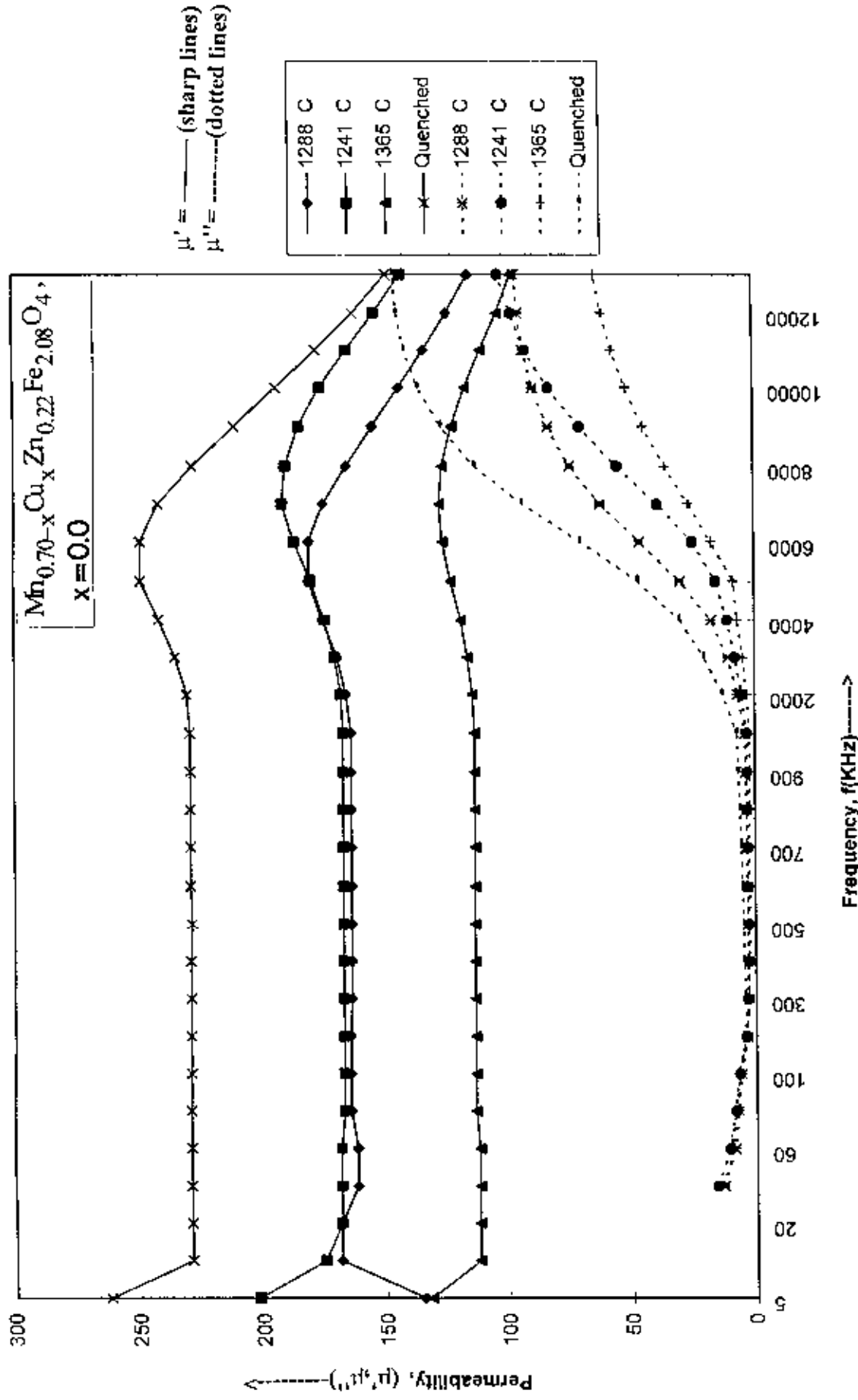


Fig 5.45: Dispersion curves for the samples $\text{Mn}_{0.70-x}\text{Cu}_x\text{Zn}_{0.22}\text{Fe}_{2.08}\text{O}_4$ with $x=0.0$ sintered at different temperatures

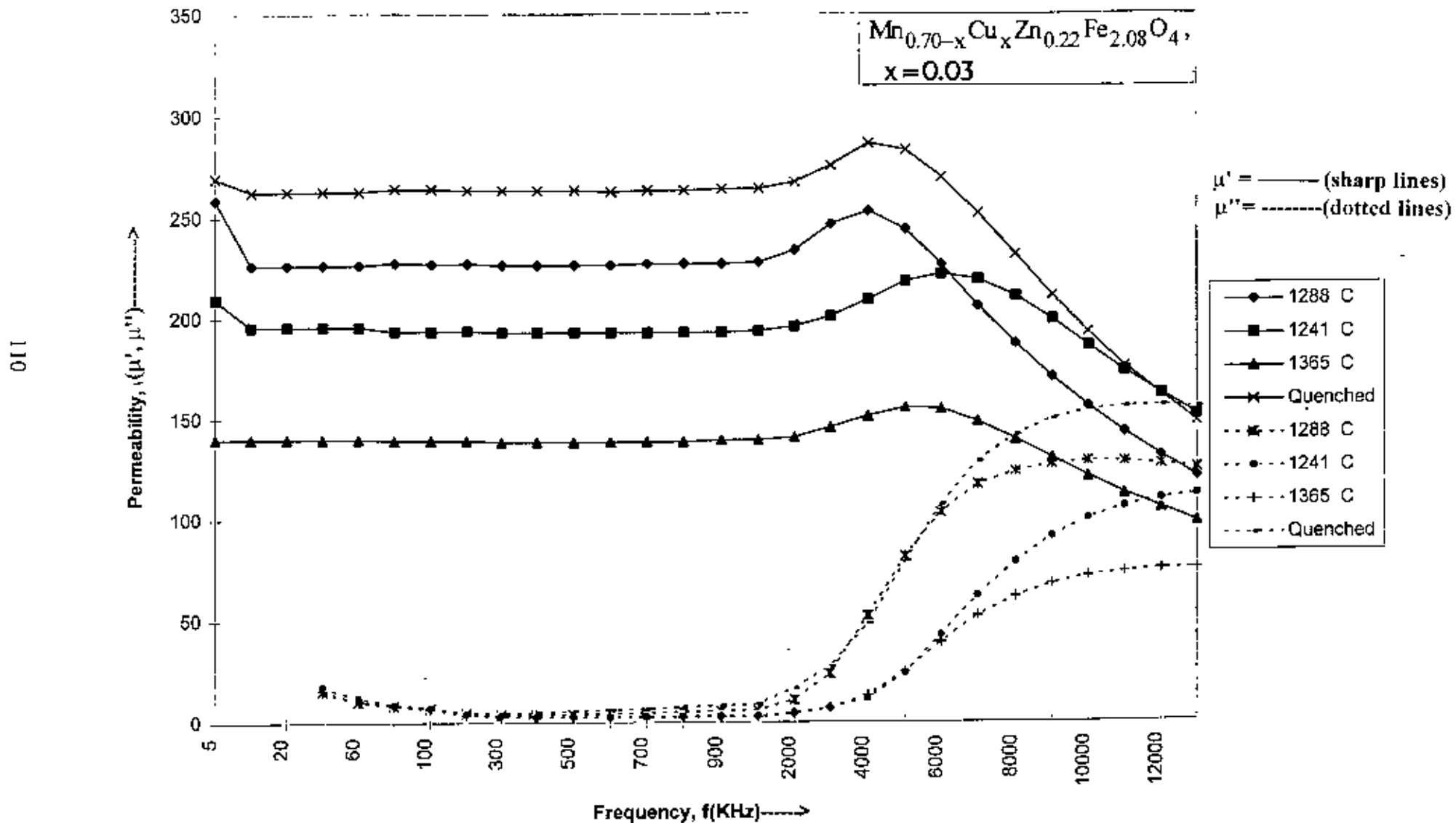


Fig 5.46: Dispersion curves for the samples $\text{Mn}_{0.70-x}\text{Cu}_x\text{Zn}_{0.22}\text{Fe}_{2.08}\text{O}_4$ with $x=0.03$ sintered at different temperatures

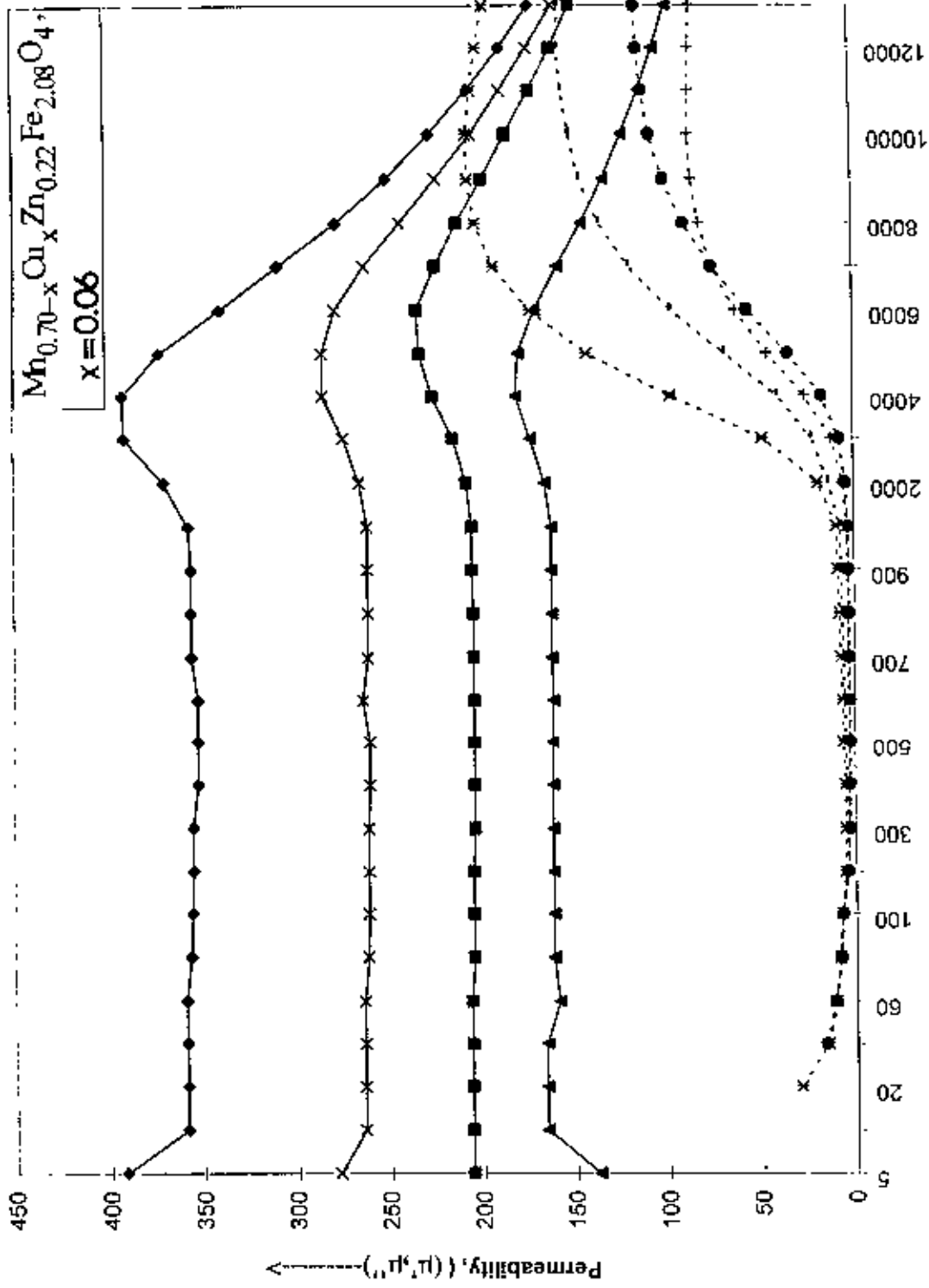


Fig 5.47: Dispersion curves for the samples $Mn_{0.70-x}Cu_xZn_{0.22}Fe_{2.08}O_4$ with $x=0.06$ sintered at different temperatures

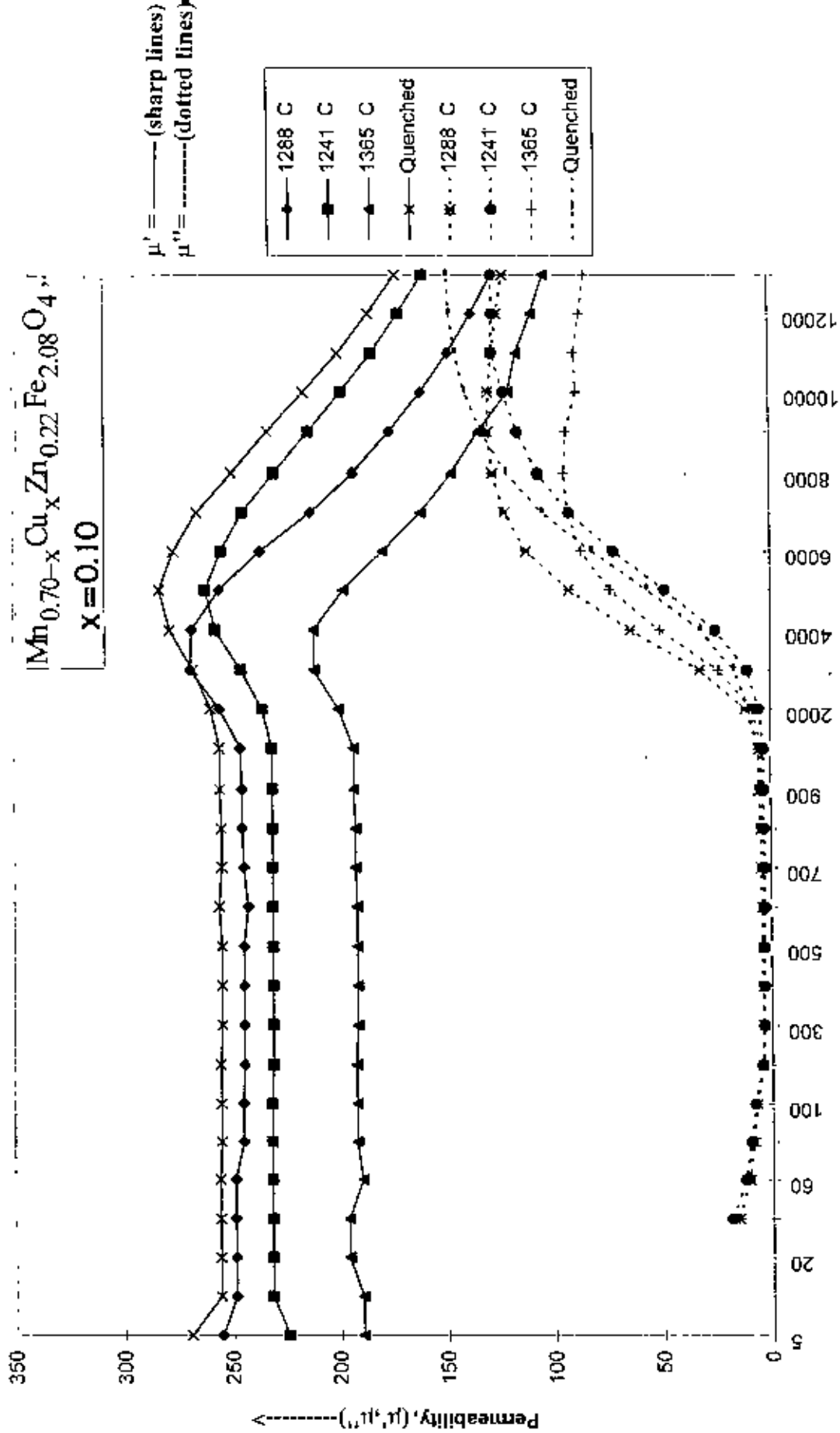


Fig 5.48: Dispersion curves for the samples $\text{Mn}_{0.70-x}\text{Cu}_x\text{Zn}_{0.22}\text{Fe}_{2.08}\text{O}_4$, with $x=0.10$ sintered at different temperatures

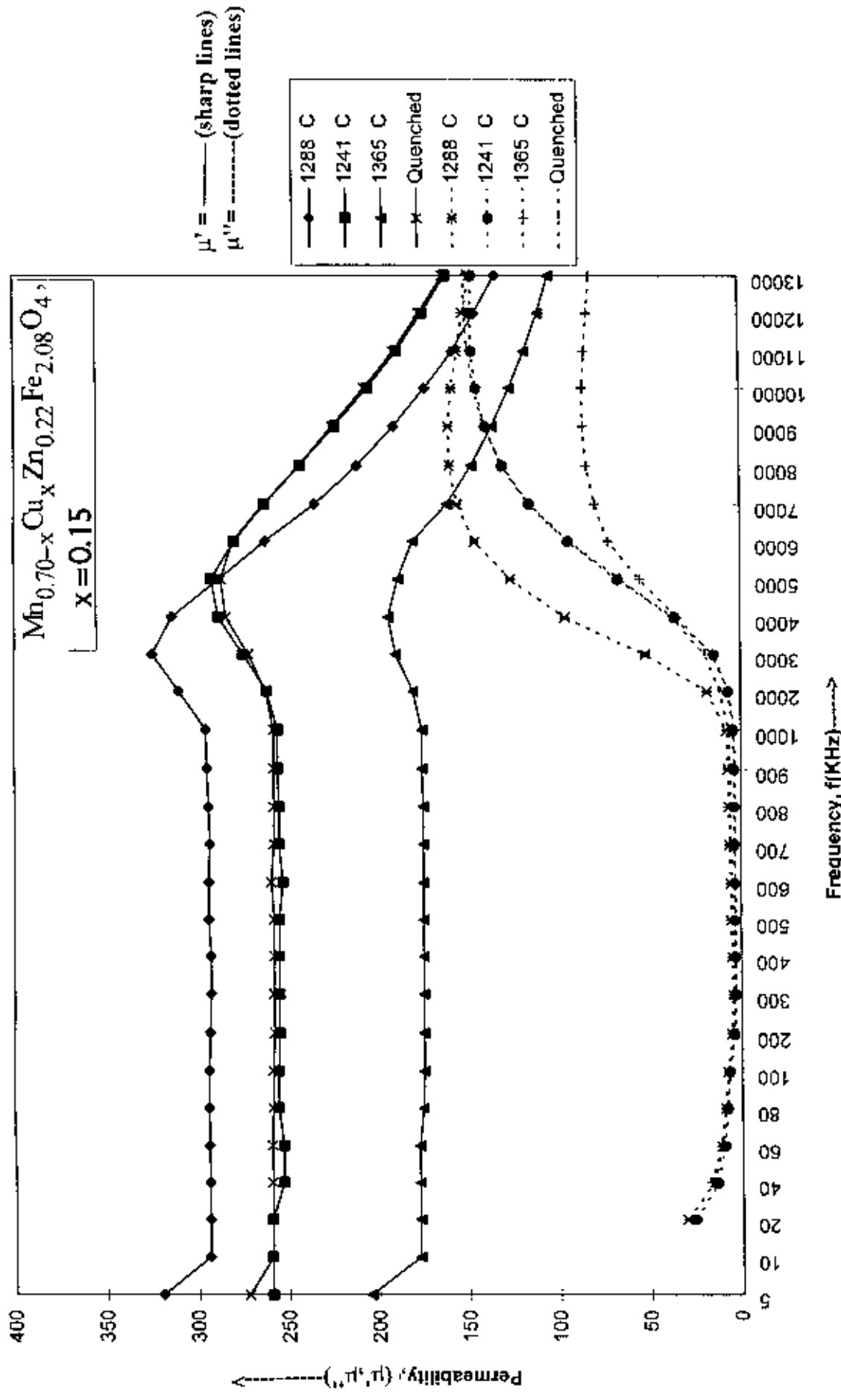


Fig. 5.49: Dispersion curves for the samples $\text{Mn}_{0.70-x}\text{Cu}_x\text{Zn}_{0.22}\text{Fe}_{2.08}\text{O}_4$ with $x=0.15$ sintered at different temperatures

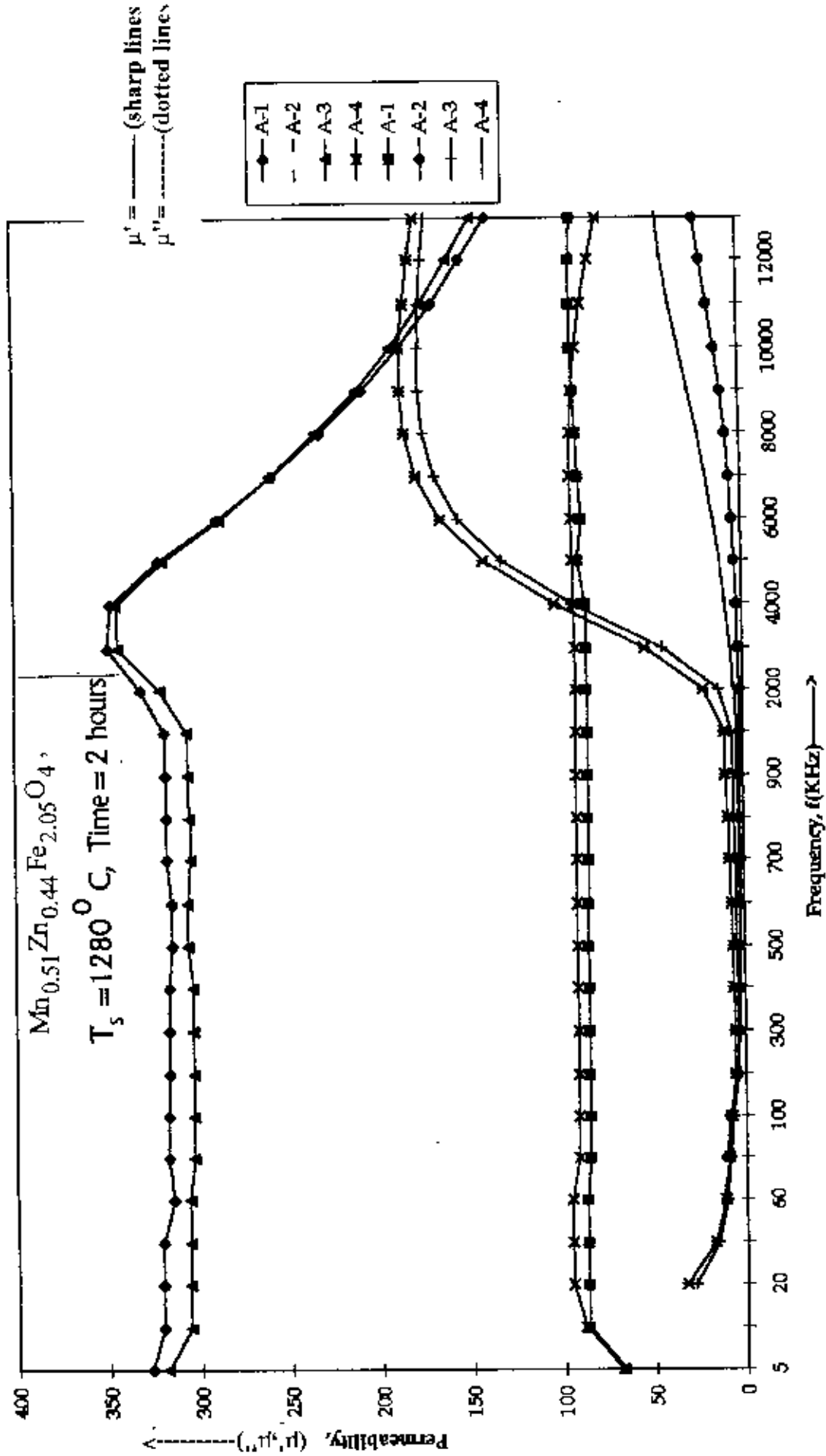


Fig. 5.50: Dispersion curves for the samples $\text{Mn}_{0.51}\text{Zn}_{0.44}\text{Fe}_{2.05}\text{O}_4$, without and with 1 mole % additives of V_2O_5 , TiO_2 and CoO sintered at 1280°C .

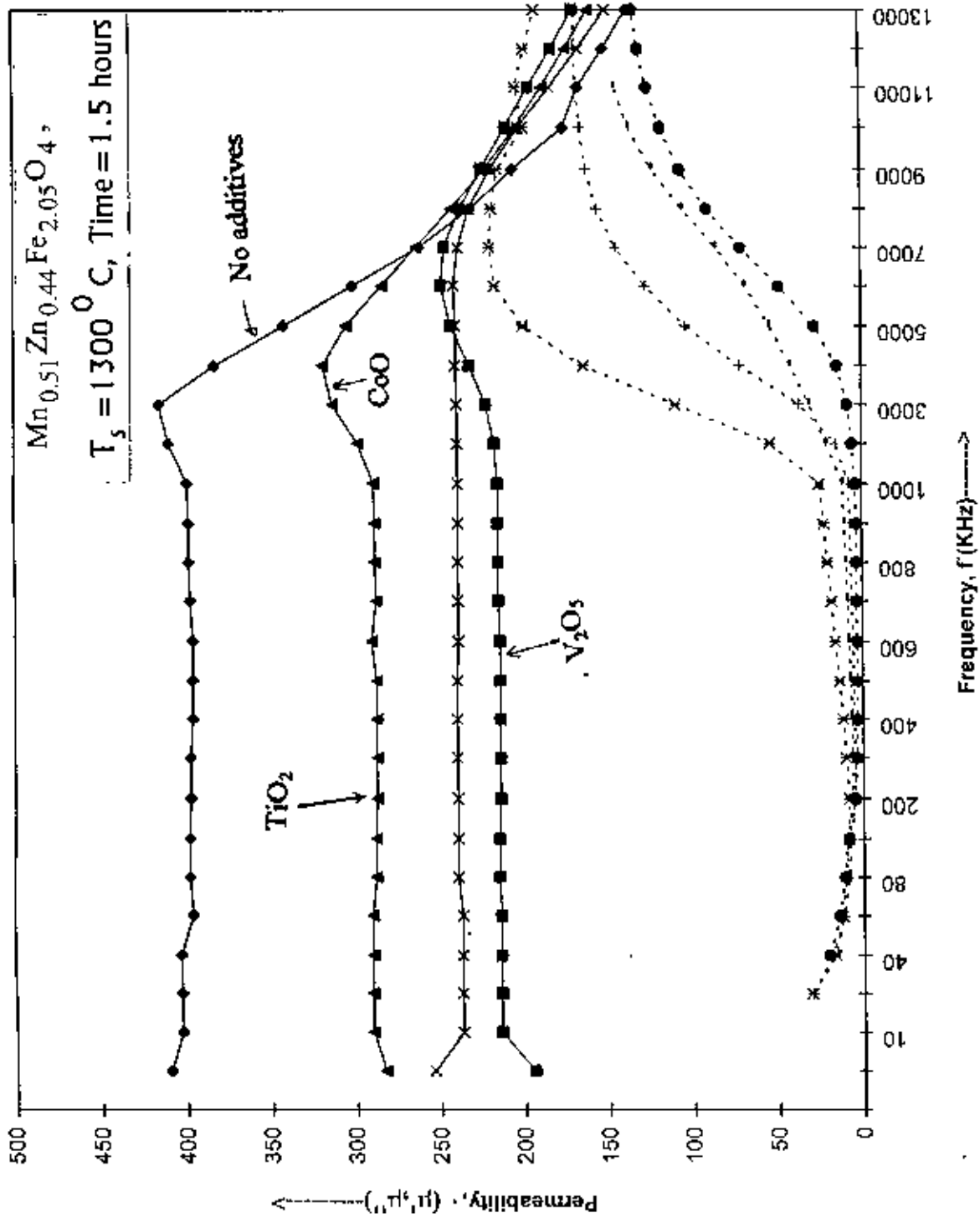


Fig 5.51: Dispersion curves for the samples $Mn_{0.51}Zn_{0.44}Fe_{2.05}O_4$ without and with 1 mole % additives of V_2O_5 , TiO_2 and CoO sintered at $1300^\circ C$.

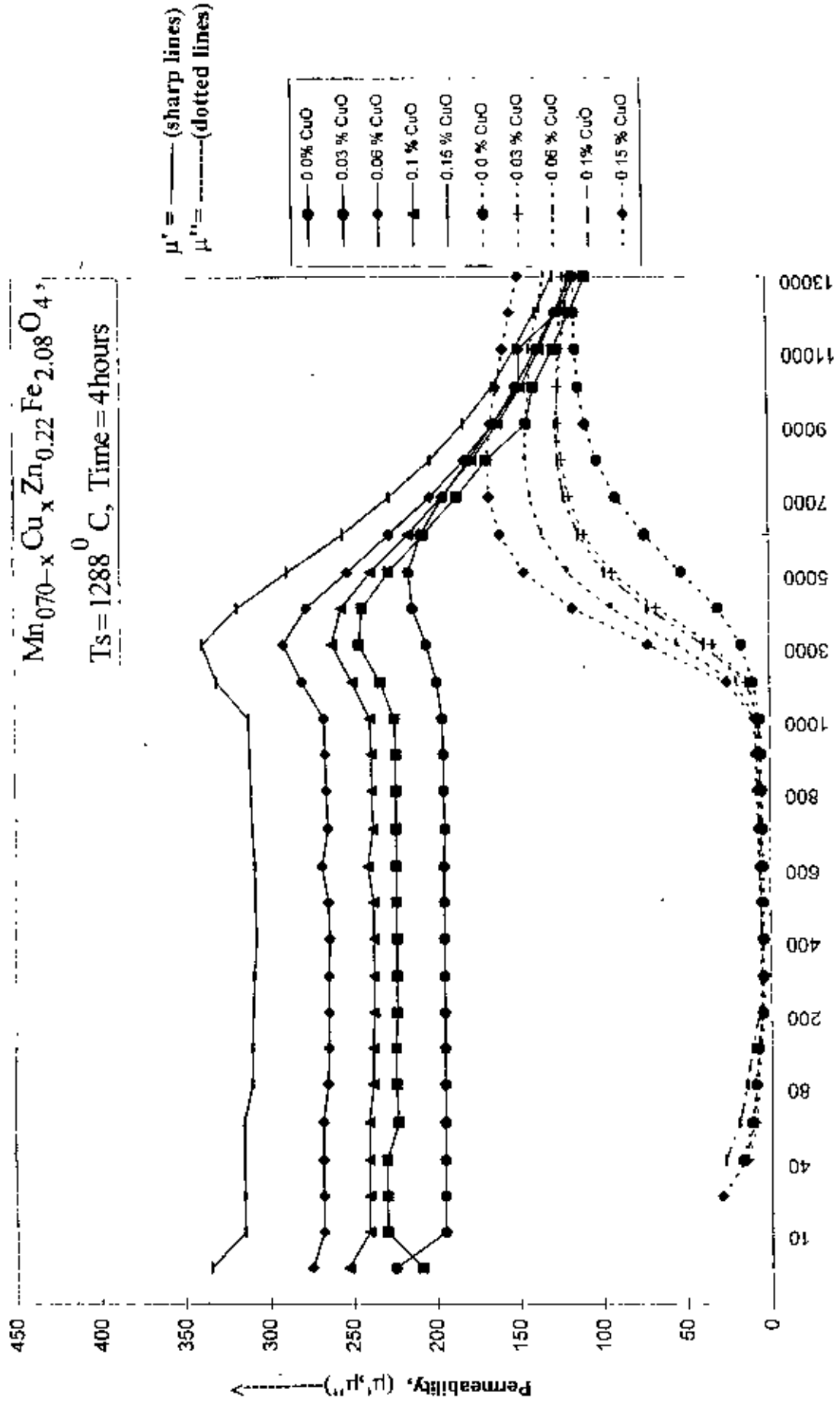


Fig 5.52: Dispersion curves for the samples $Mn_{0.7-x}Cu_xZn_{0.22}Fe_{2.08}O_4$ with $x=0.0, 0.03, 0.06, 0.10, 0.15$ sintered at $1288^{\circ}C$.

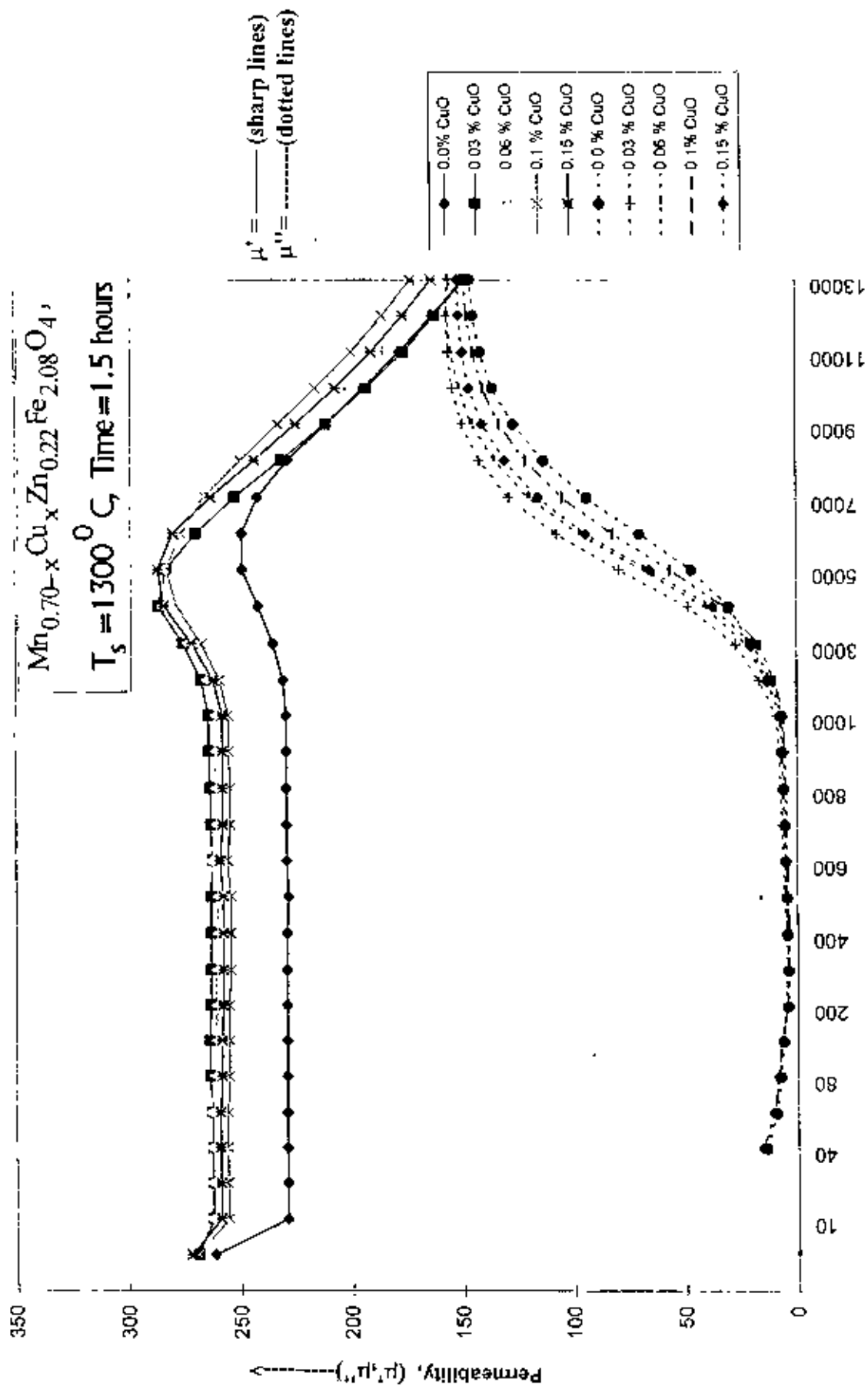


Fig. 5.53: Dispersion curves for the samples $Mn_{0.7-x}Cu_xZn_{0.22}Fe_{2.08}O_4$ with $x=0.0, 0.03, 0.06, 0.10, 0.15$ sintered at $1300^\circ C$

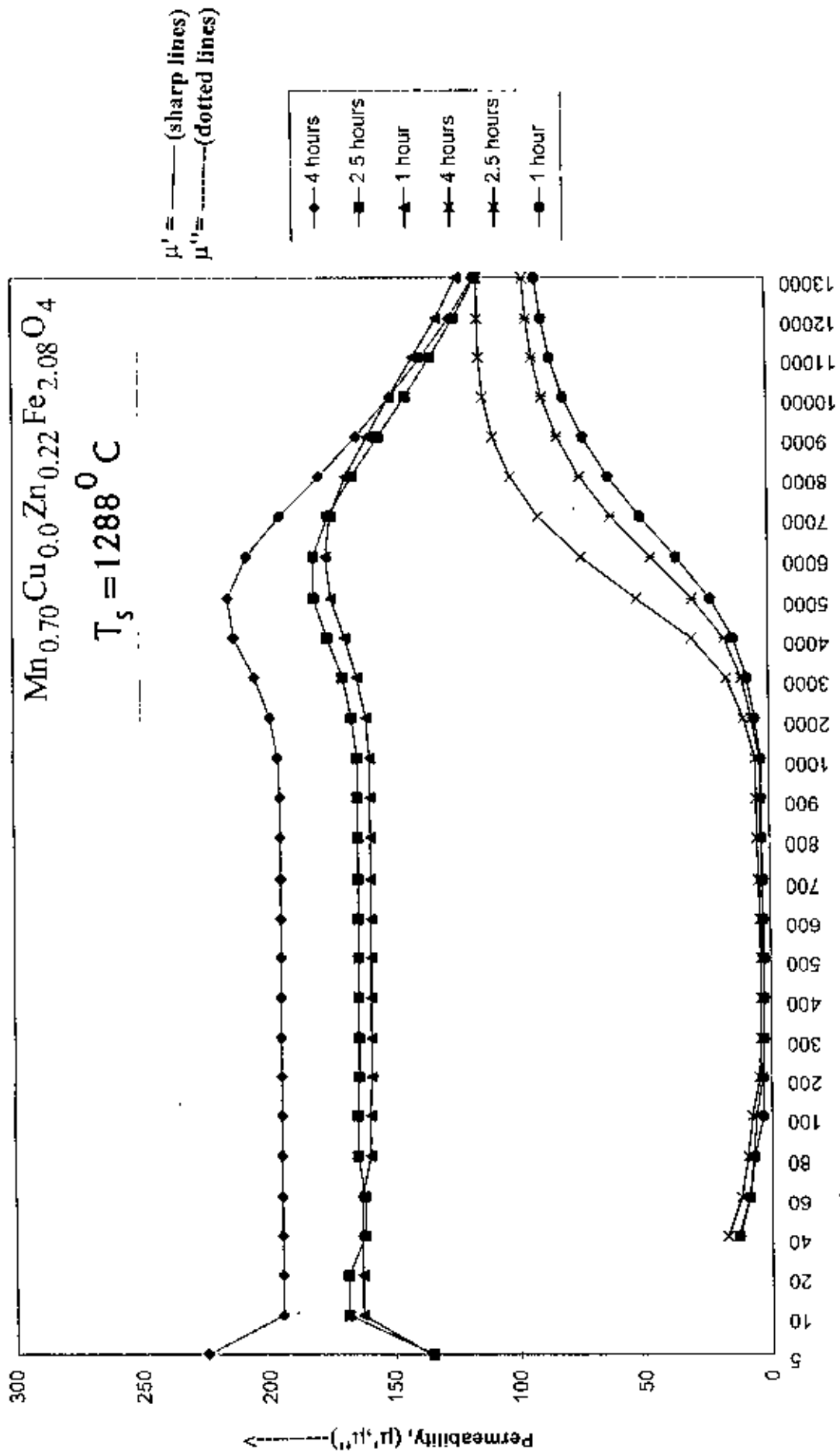


Fig. 5.54: Dispersion curves for the samples $\text{Mn}_{0.7-x}\text{Cu}_x\text{Zn}_{0.22}\text{Fe}_{2.08}\text{O}_4$ with $x=0.0$ sintered at different sintering times.

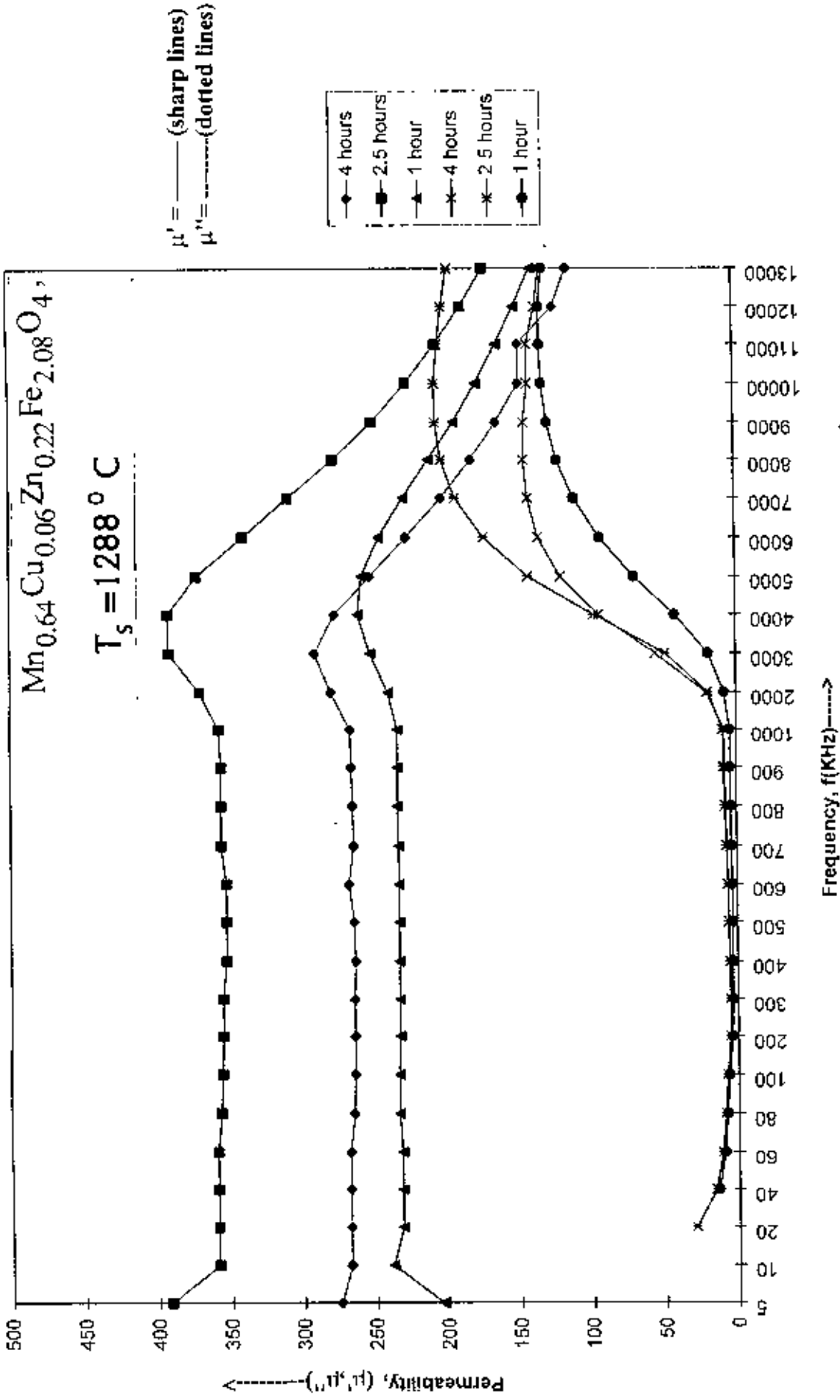


Fig. 5.55: Dispersion curves for the samples $\text{Mn}_{0.7-x}\text{Cu}_x\text{Zn}_{0.22}\text{Fe}_{2.08}\text{O}_4$ with $x=0.06$ sintered at different sintering times.

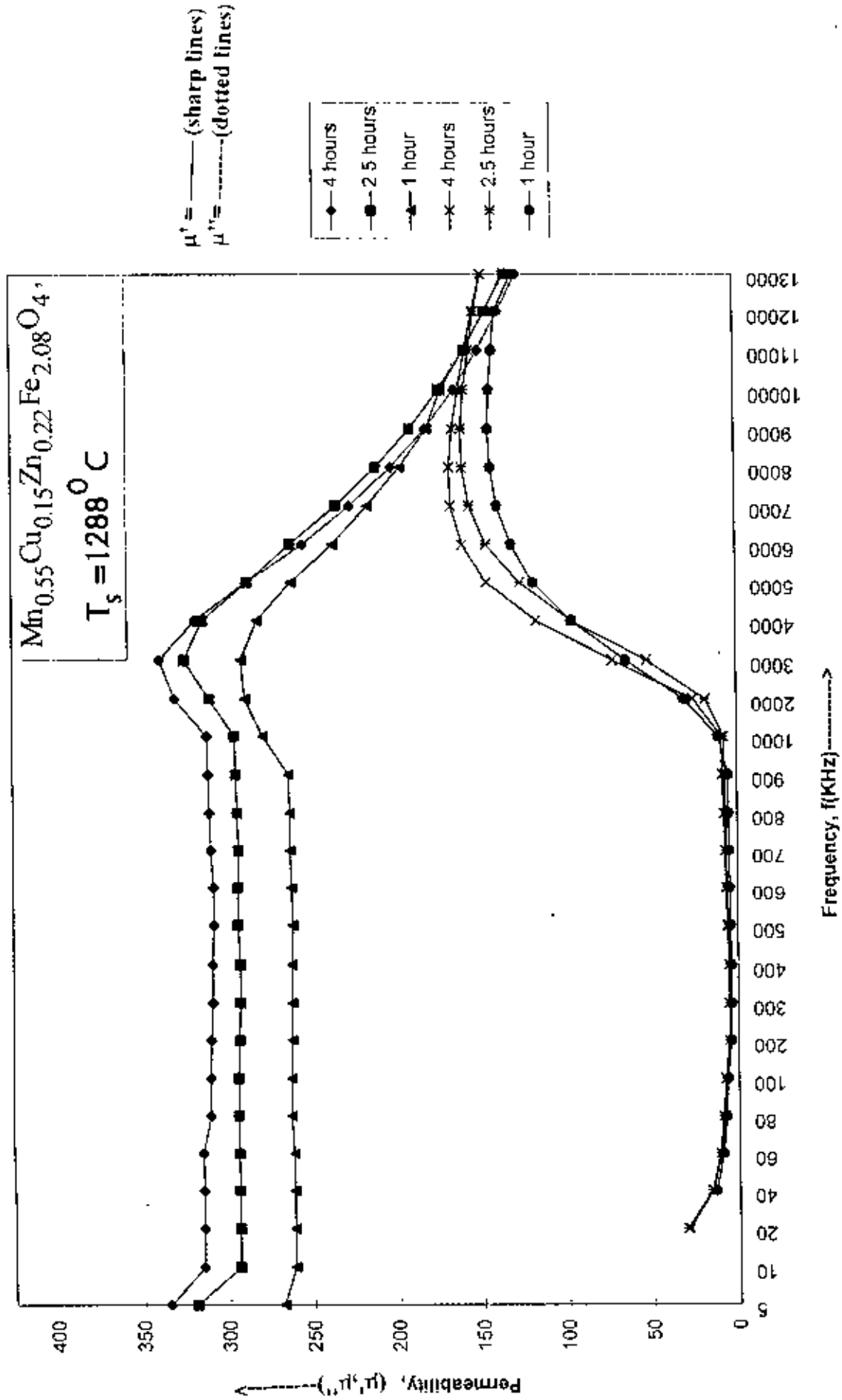


Fig. 5.56: Dispersion curves for the samples $\text{Mn}_{0.55}\text{Cu}_{0.15}\text{Zn}_{0.22}\text{Fe}_{2.08}\text{O}_4$ with $x=0.15$ sintered at different sintering times.

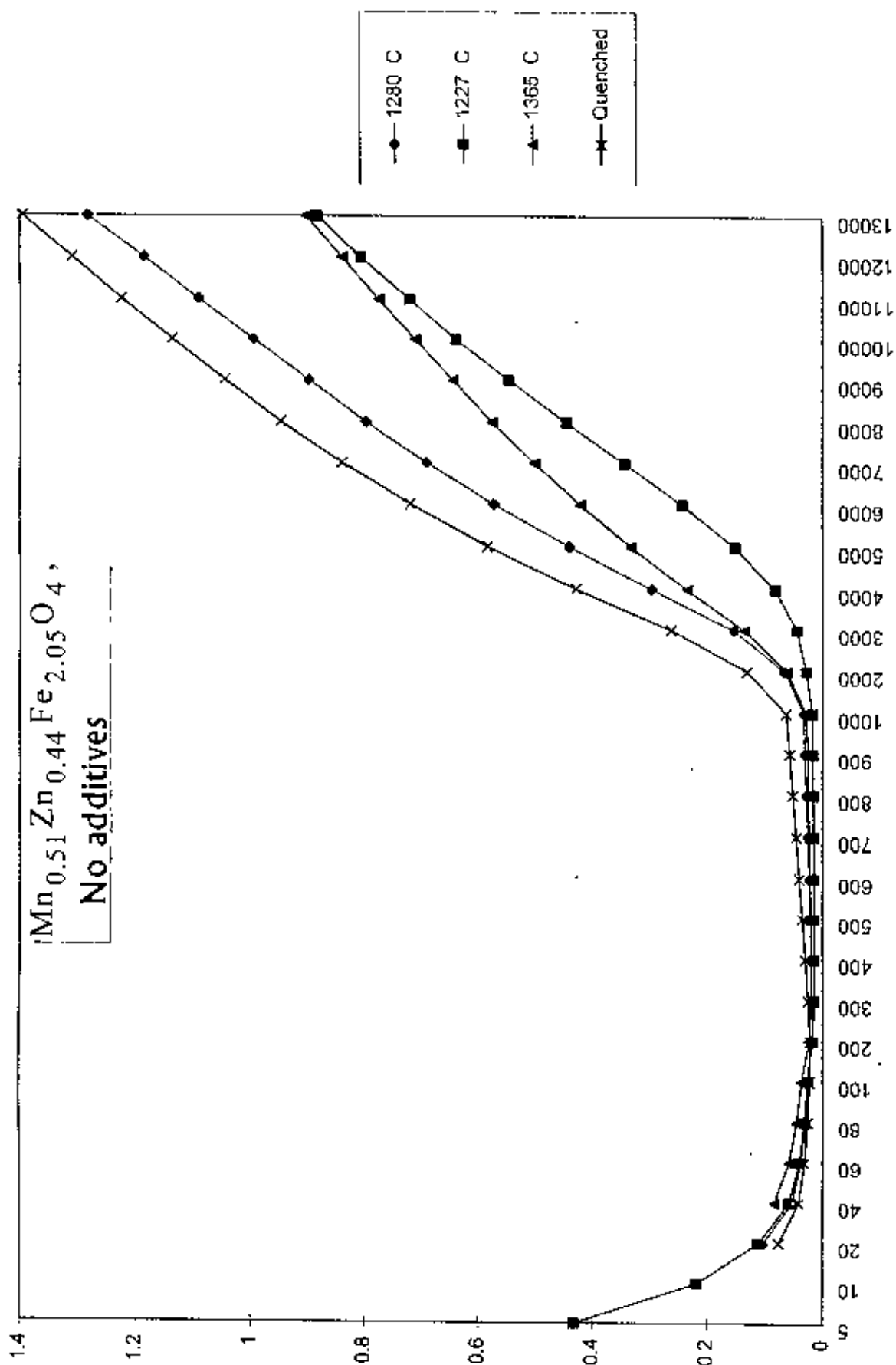


Fig. 5.57: The variation of $\tan \delta$ or D with frequency for the samples $\text{Mn}_{0.51}\text{Zn}_{0.44}\text{Fe}_{2.05}\text{O}_4$ sintered at different temperatures.

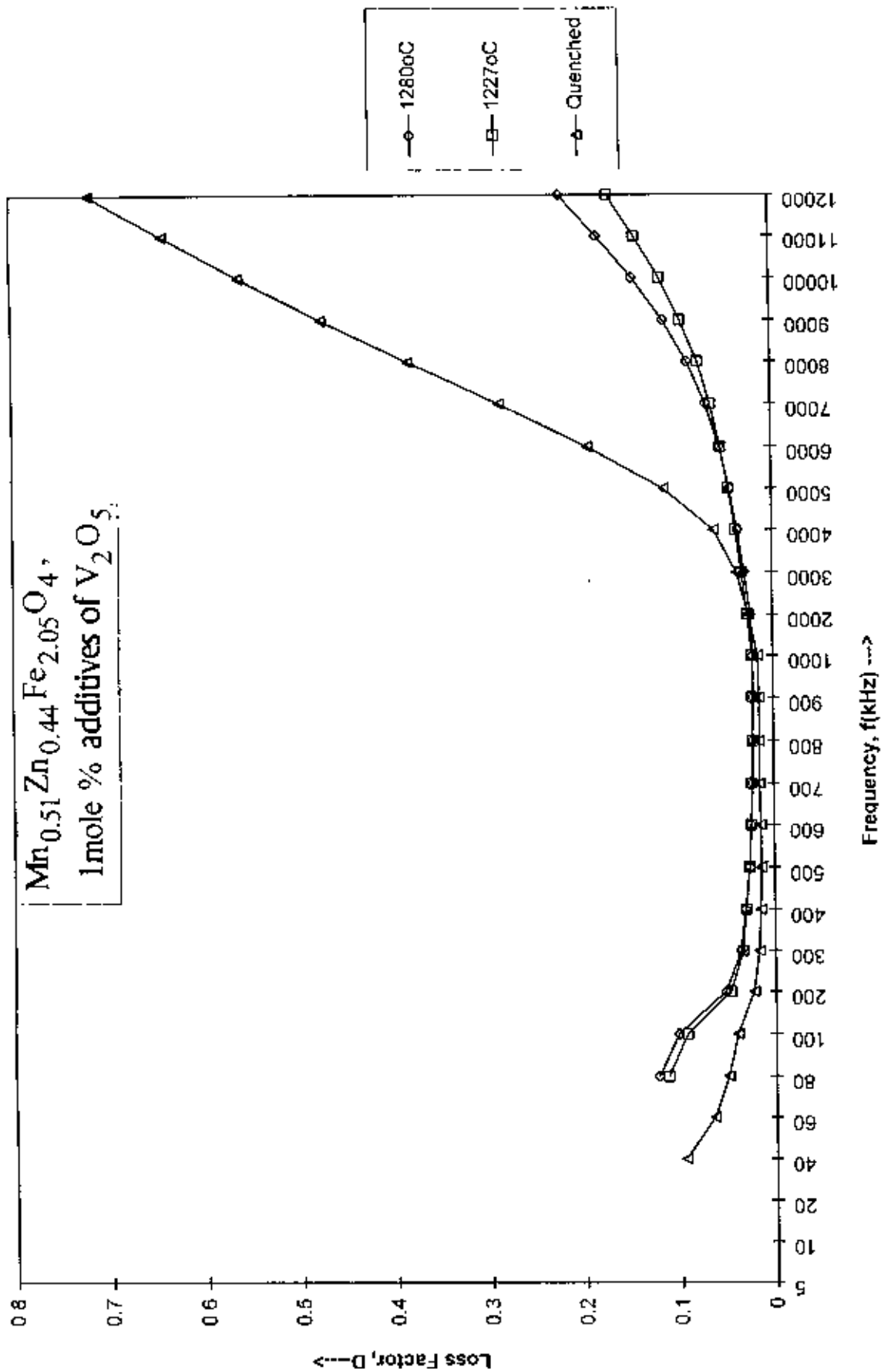


Fig 5.58: The variation of $\tan\delta$ or D with frequency for the samples $\text{Mn}_{0.51}\text{Zn}_{0.44}\text{Fe}_{2.05}\text{O}_4$ with 1 mole % additives of V_2O_5 sintered at different temperatures.

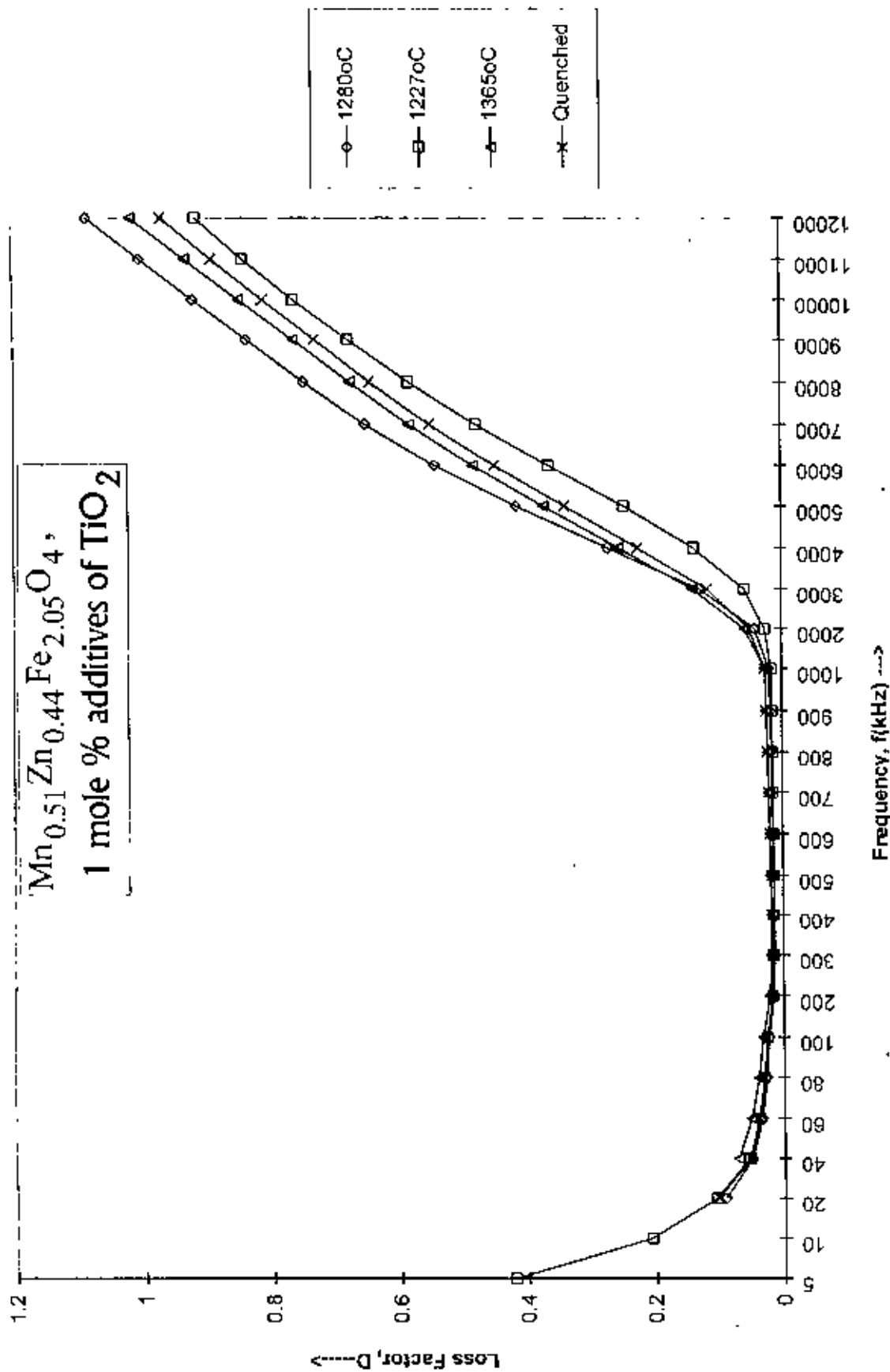


Fig. 5.59: The variation of $\tan\delta$ or D with frequency for the samples $\text{Mn}_{0.51}\text{Zn}_{0.44}\text{Fe}_{2.05}\text{O}_4$ with 1 mole % additives of TiO_2 sintered at different temperatures.

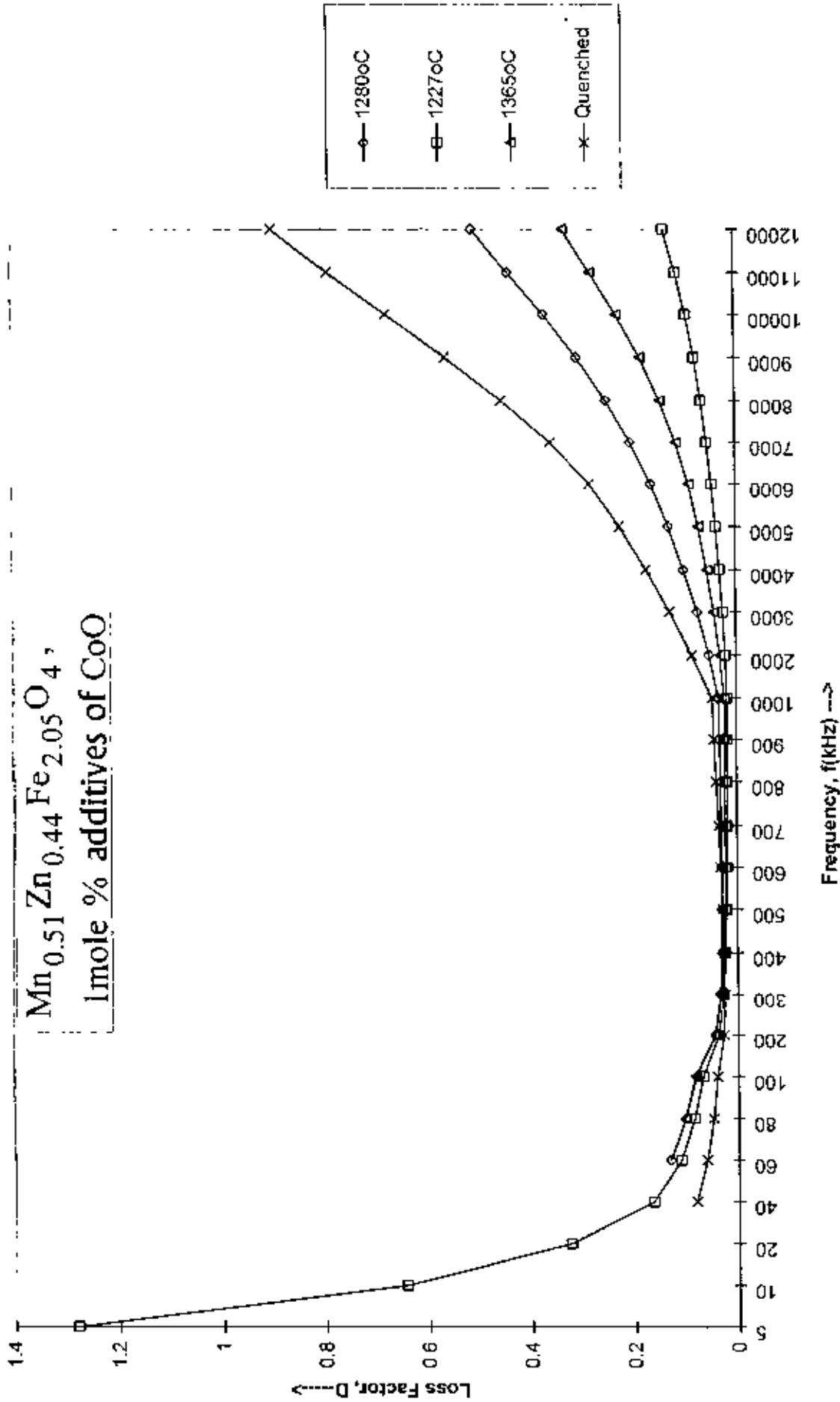


Fig. 5.60: The variation of $\tan\delta$ or D with frequency for the samples $\text{Mn}_{0.51}\text{Zn}_{0.44}\text{Fe}_{2.05}\text{O}_4$ with 1 mole % additives of CoO sintered at different temperatures.

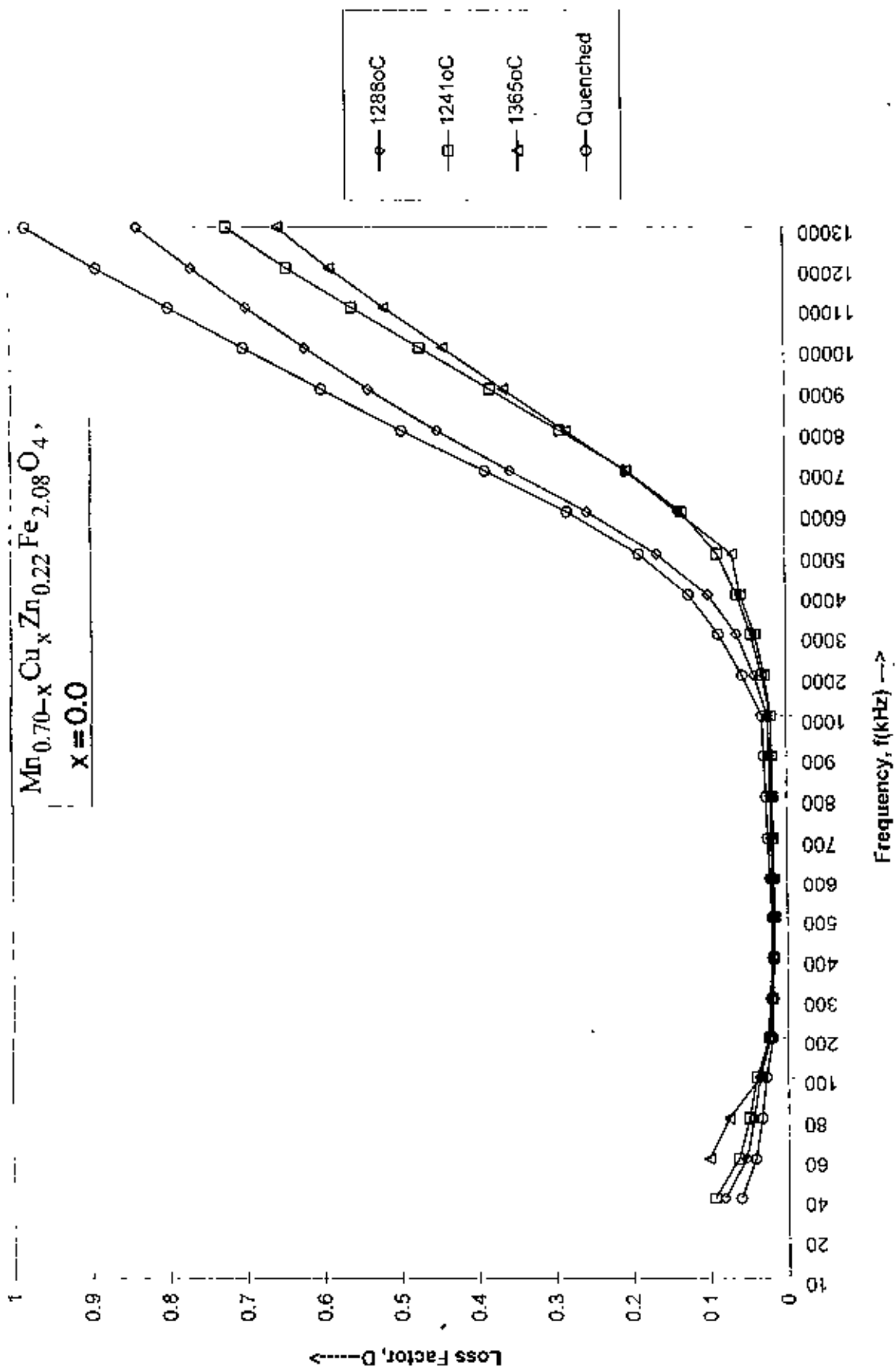


Fig.5.6.1: The variation of $\tan\delta$ or D with frequency for the samples $Mn_{0.7-x}Cu_xZn_{0.22}Fe_{2.08}O_4$ with $x = 0.0$ sintered at different temperatures.

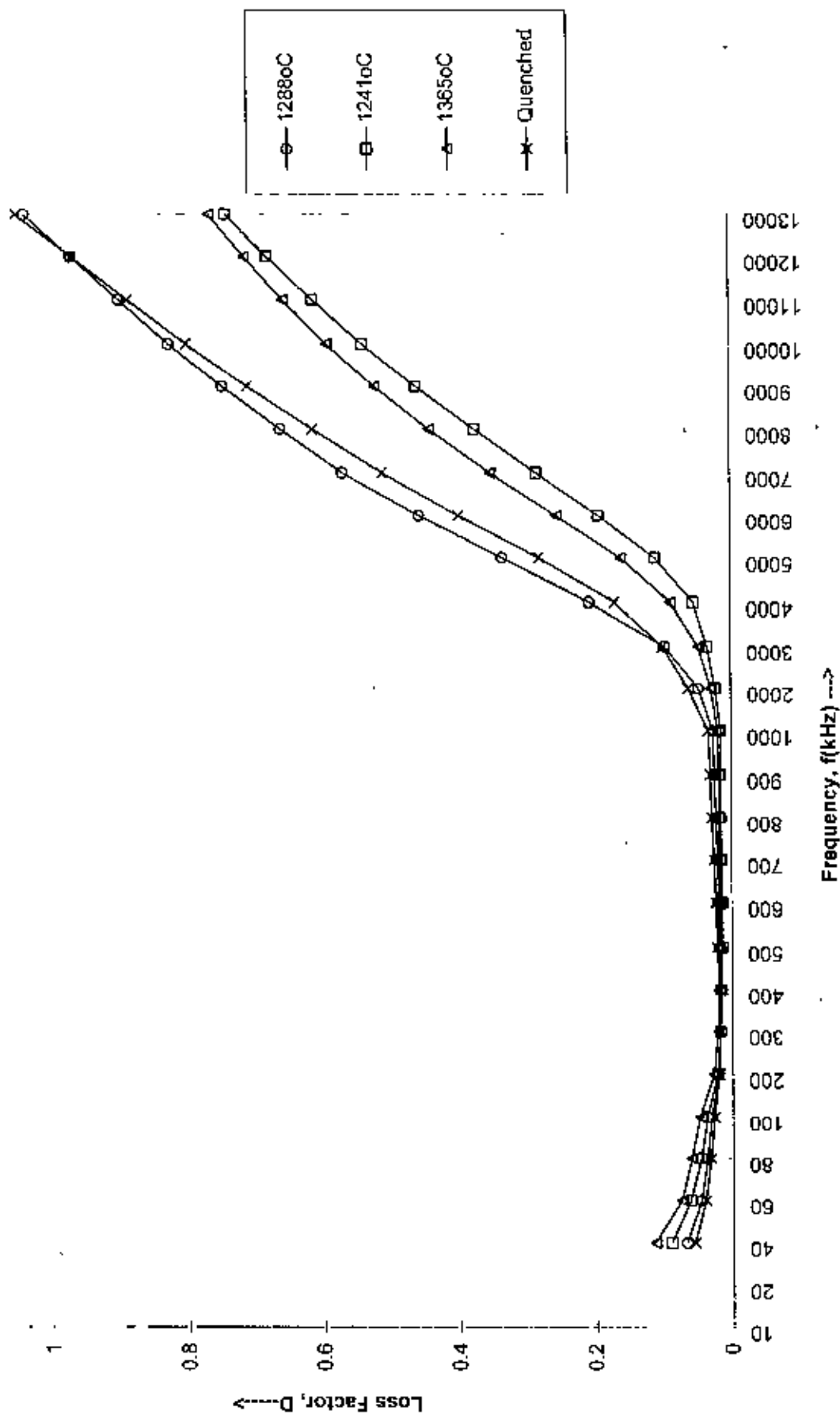
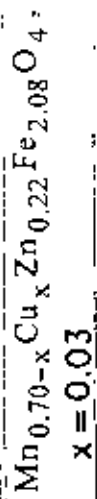


Fig5.62: The variation of $\tan\delta$ or D with frequency for the samples $\text{Mn}_{0.7-x}\text{Cu}_x\text{Zn}_{0.22}\text{Fe}_{2.08}\text{O}_4$ with $x = 0.03$ sintered at different temperatures.

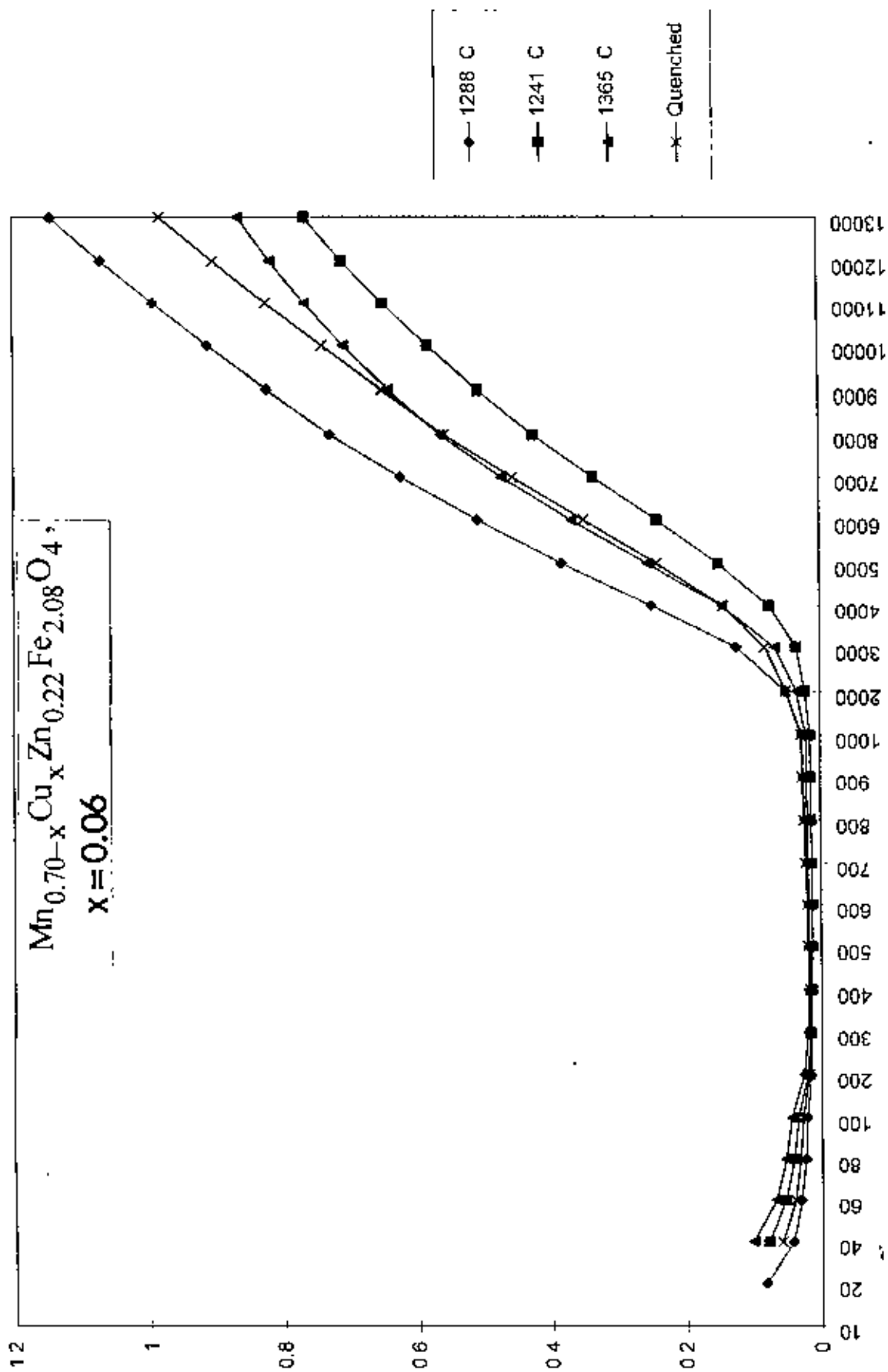


Fig. 5.63: The variation of $\tan\delta$ or D with frequency for the samples $\text{Mn}_{0.7-x}\text{Cu}_x\text{Zn}_{0.22}\text{Fe}_{2.08}\text{O}_4$ with $x = 0.06$ sintered at different temperatures.

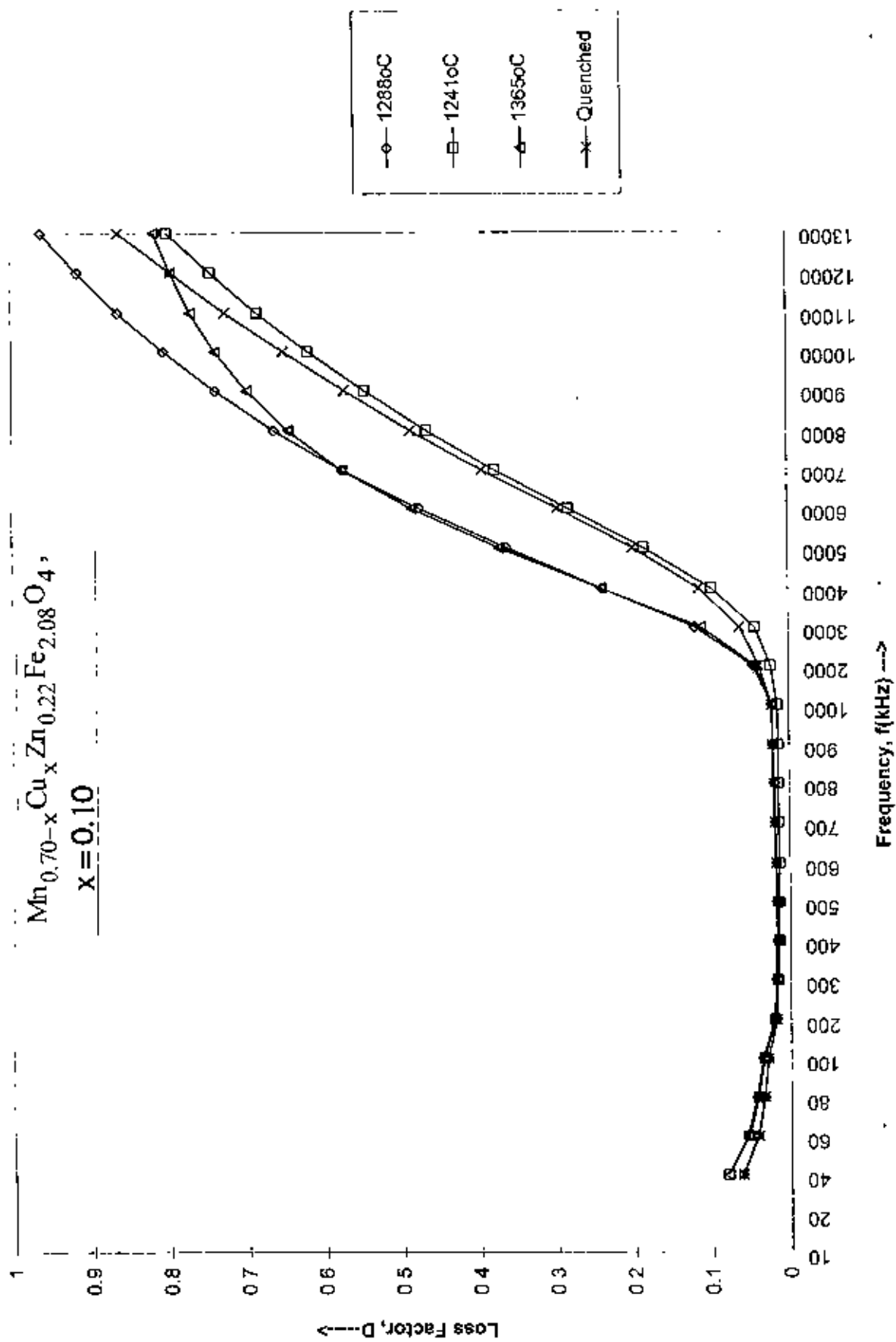


Fig 5.64: The variation of $\tan \delta$ or D with frequency for the samples $\text{Mn}_{0.7-x}\text{Cu}_x\text{Zn}_{0.22}\text{Fe}_{2.08}\text{O}_4$ with $x = 0.10$ sintered at different temperatures.

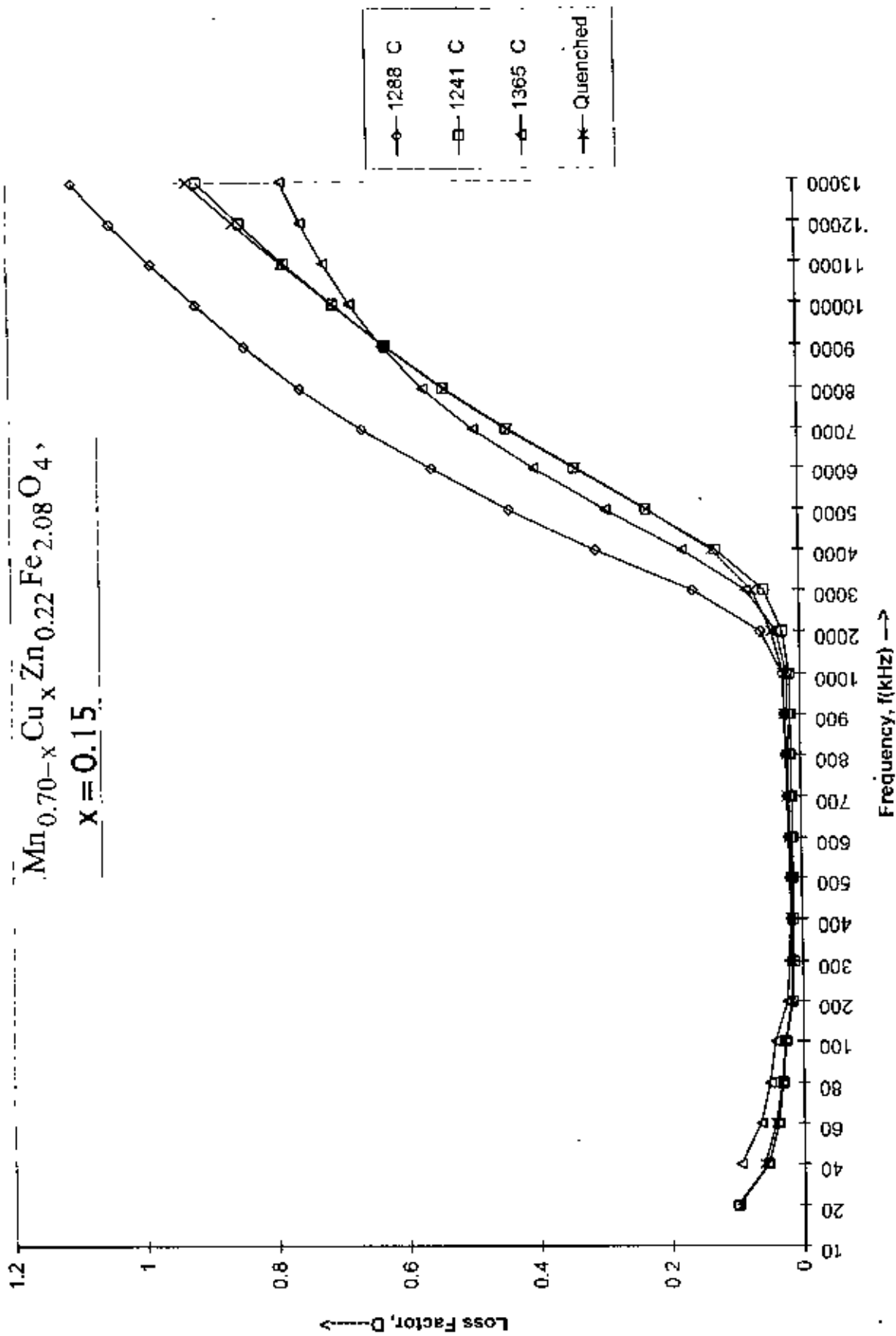


Fig. 5.65: The variation of $\tan\delta$ or D with frequency for the samples $\text{Mn}_{0.7-x}\text{Cu}_x\text{Zn}_{0.22}\text{Fe}_{2.08}\text{O}_4$ with $x = 0.15$ sintered at different temperatures.

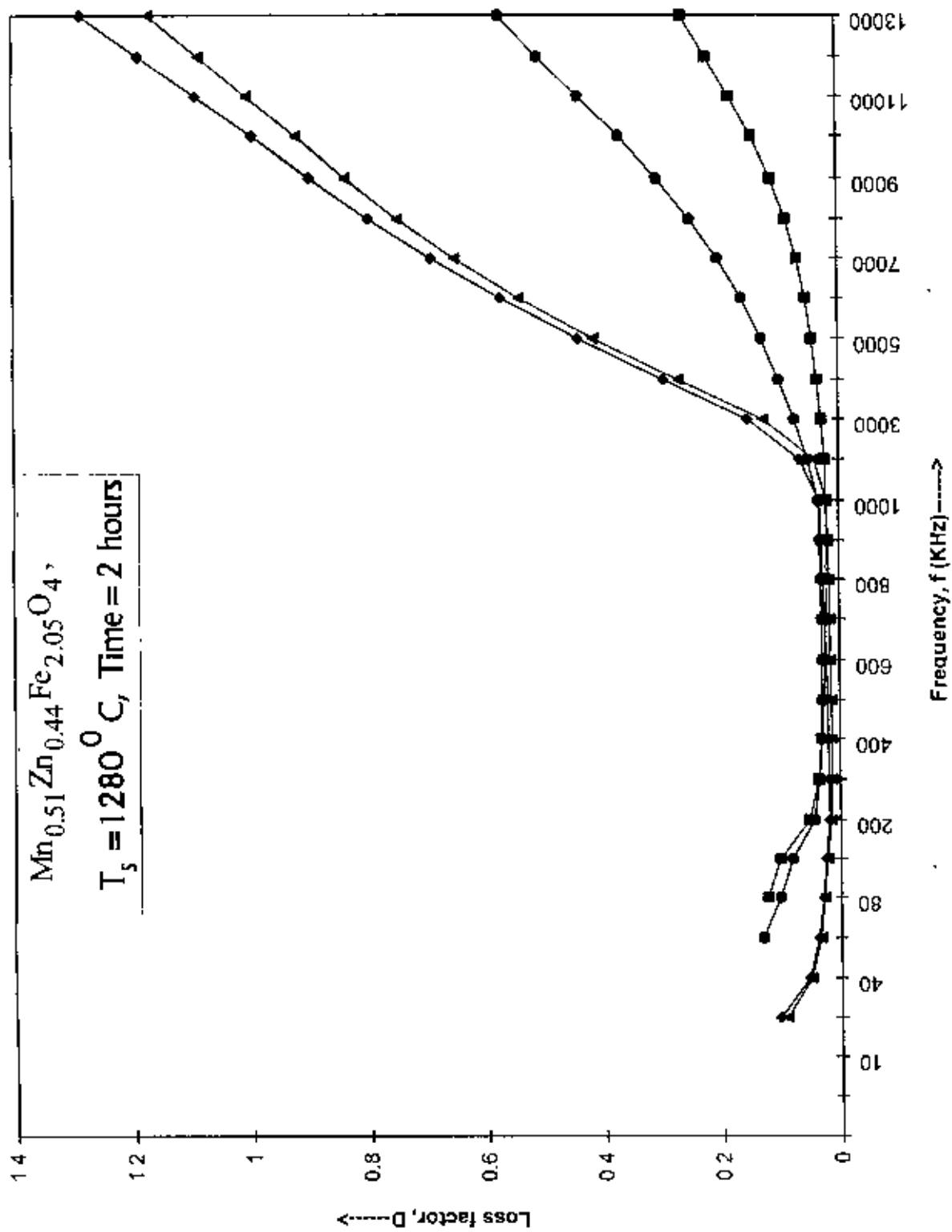
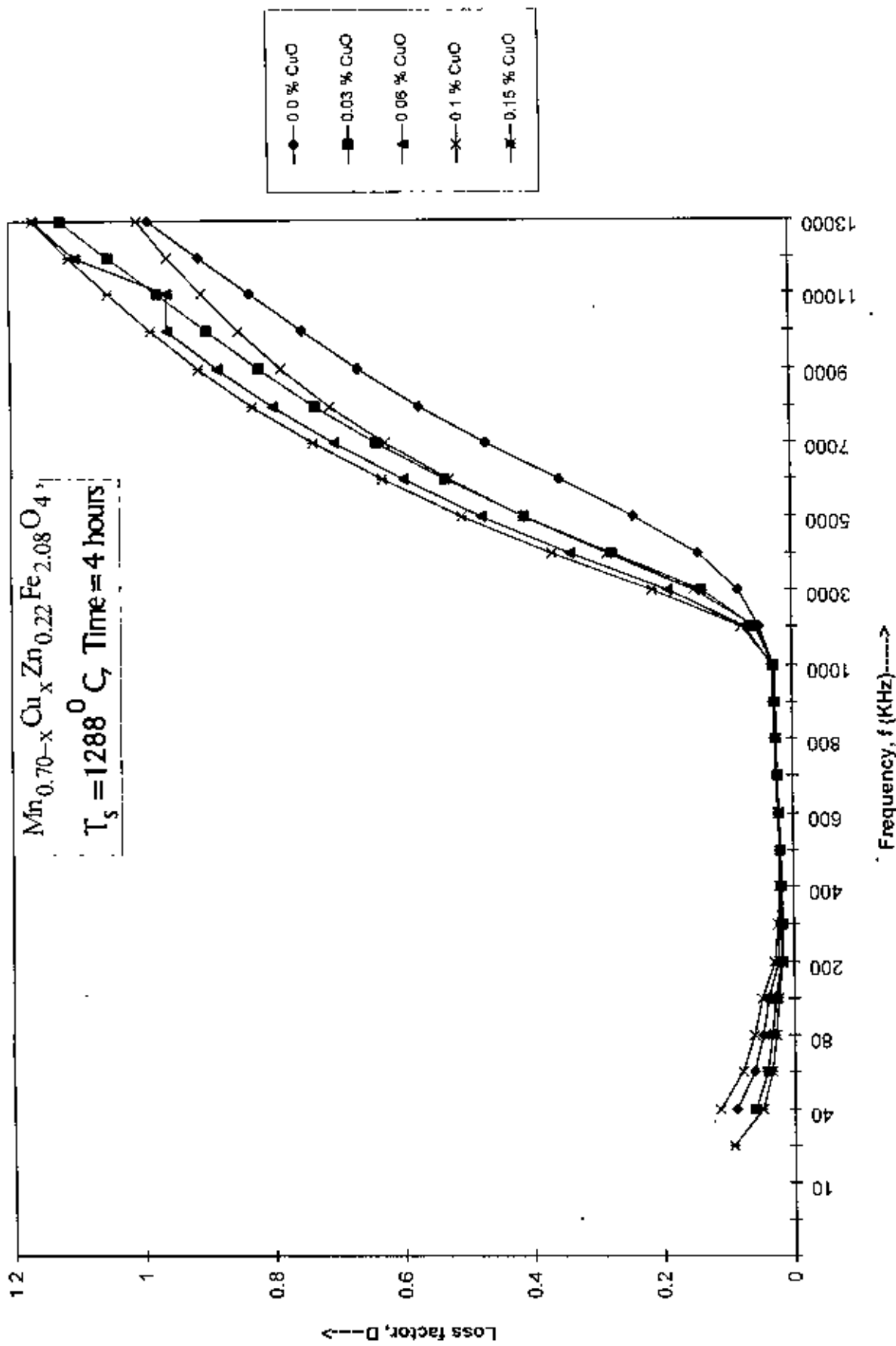


Fig.5.66: The variation of $\tan\delta$ or D with frequency for the samples $\text{Mn}_{0.51}\text{Zn}_{0.44}\text{Fe}_{2.05}\text{O}_4$ without and with 1 mole % additives of V_2O_5 , TiO_2 and CoO sintered at 1280°C .



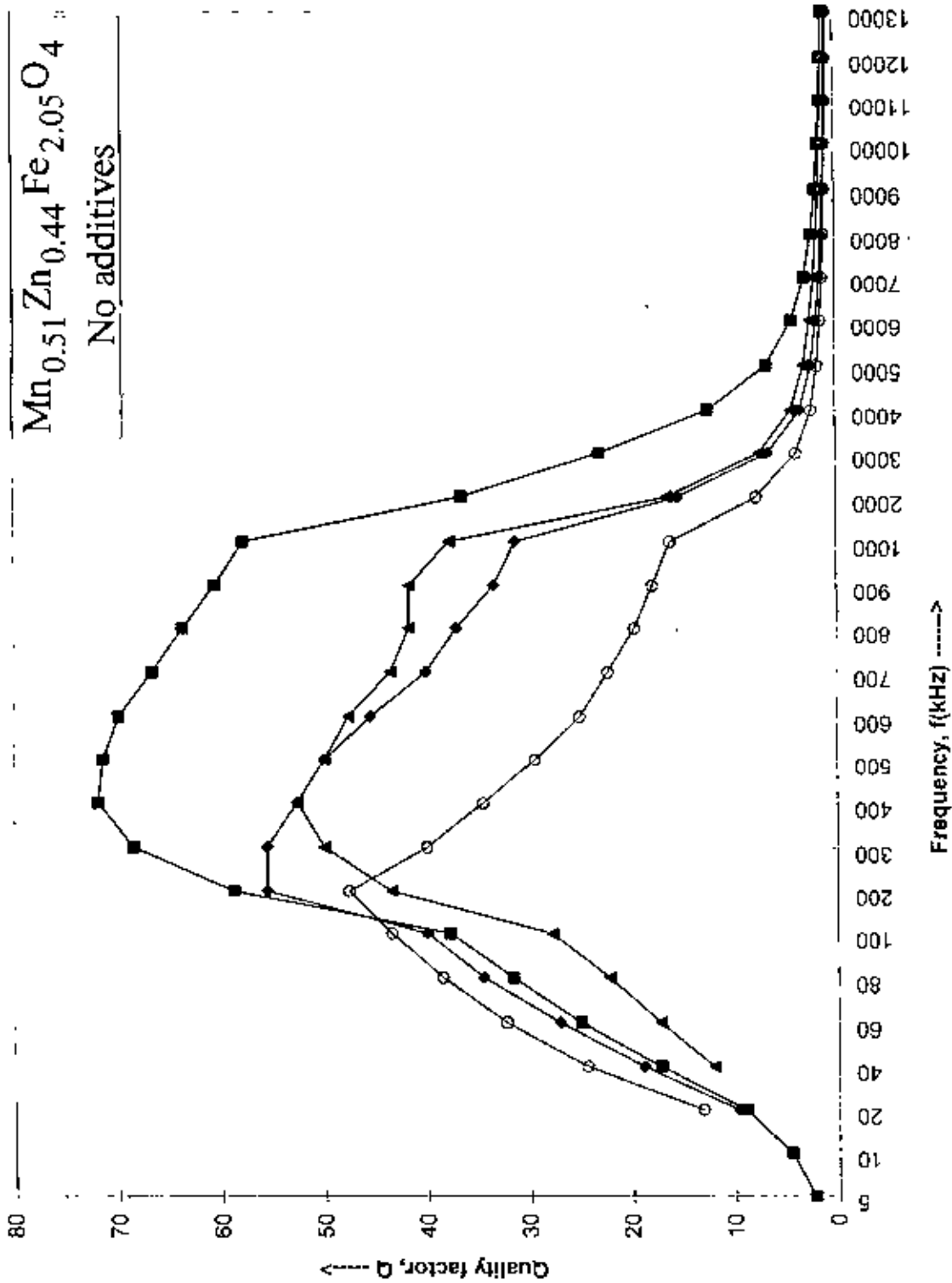


Fig. 5.68: The variation of Q with frequency for the samples $Mn_{0.51}Zn_{0.44}Fe_{2.05}O_4$ sintered at different temperatures.

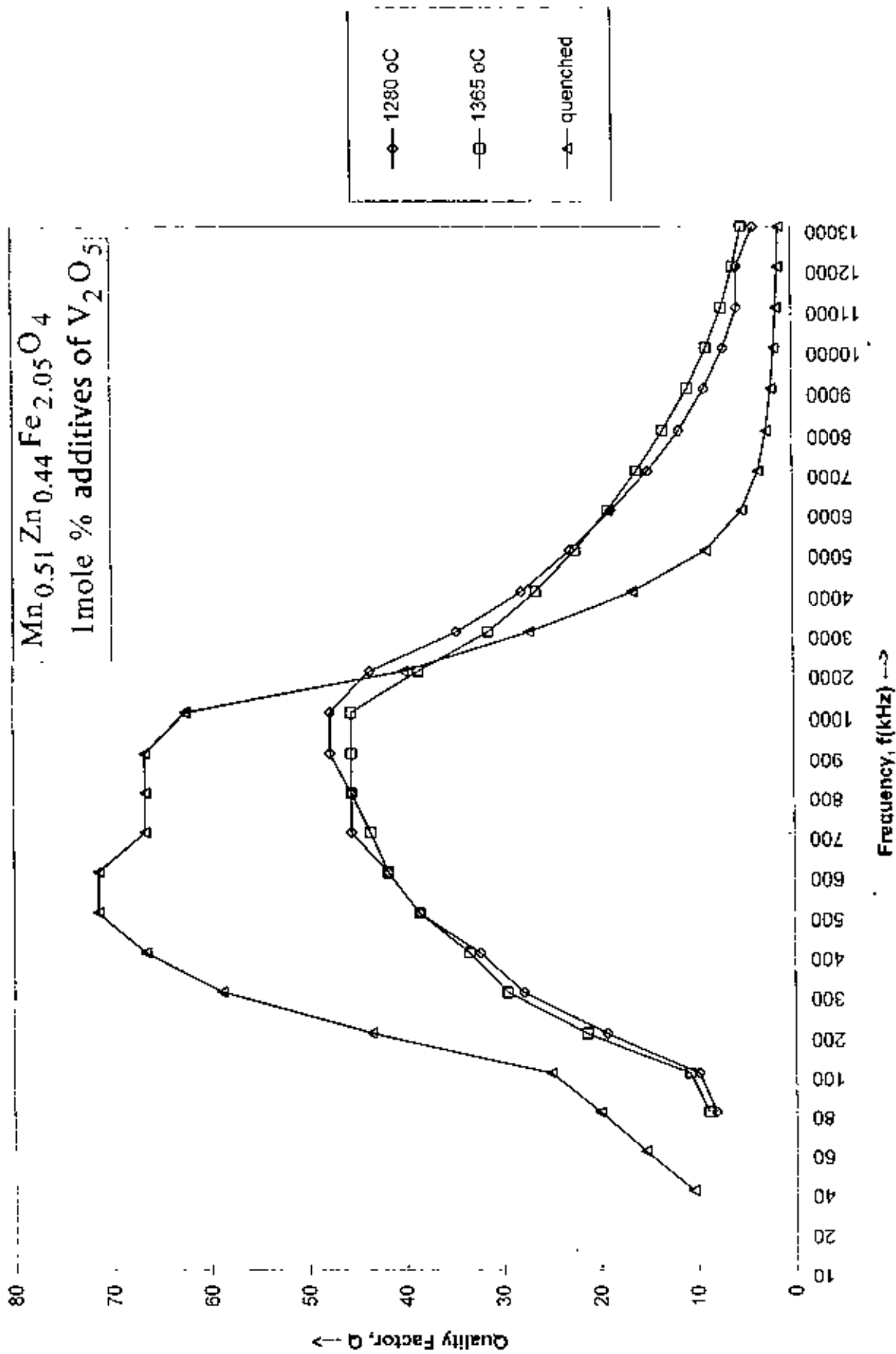


Fig 5.69: The variation of Q with frequency for the samples $\text{Mn}_{0.51}\text{Zn}_{0.44}\text{Fe}_{2.05}\text{O}_4$ with 1 mole % additives of V_2O_5 sintered at different temperatures.

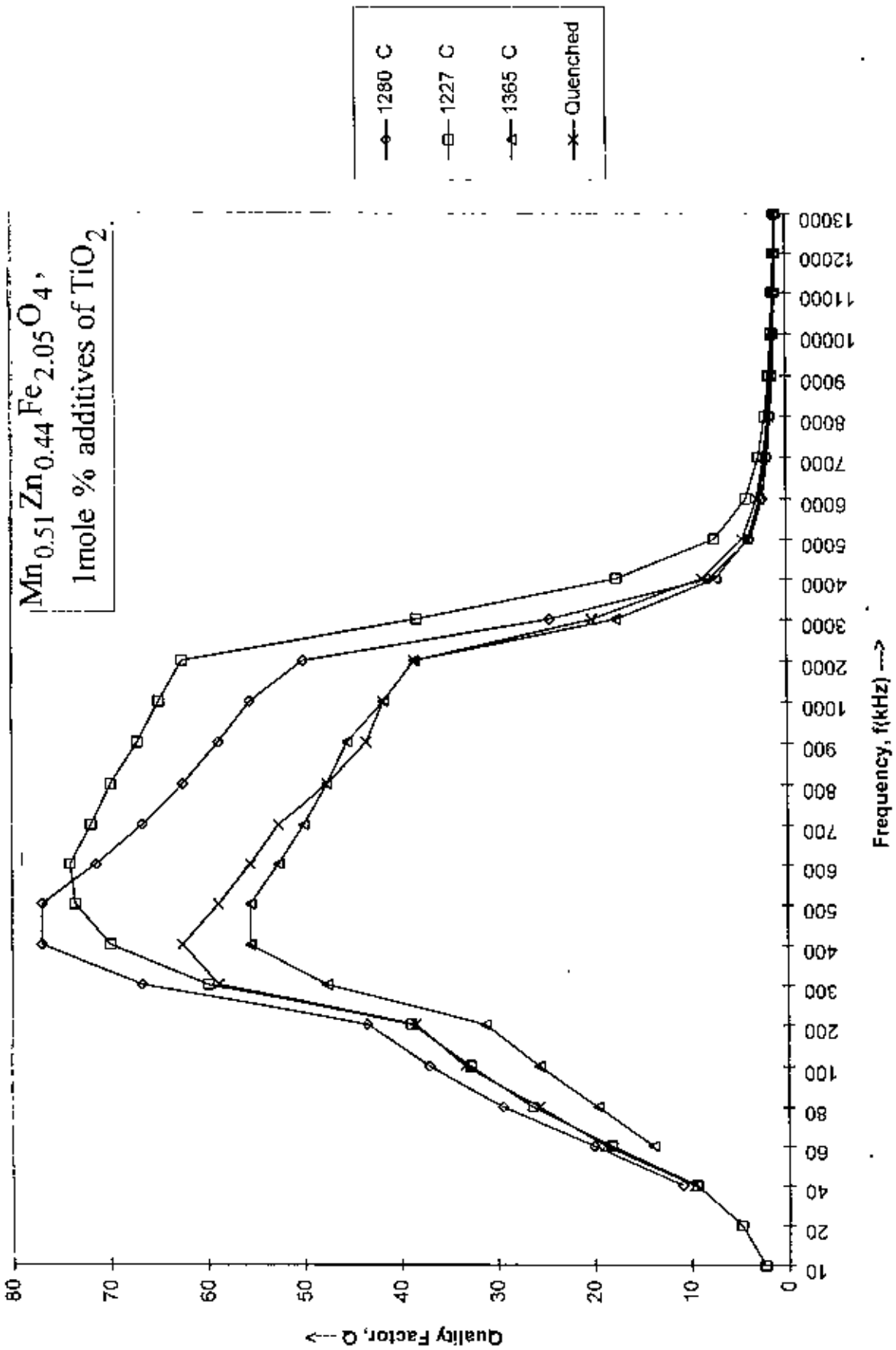


Fig. 70: The variation of Q with frequency for the samples $\text{Mn}_{0.51}\text{Zn}_{0.44}\text{Fe}_{2.05}\text{O}_4$ with 1 mole % additives of TiO_2 sintered at different temperatures.

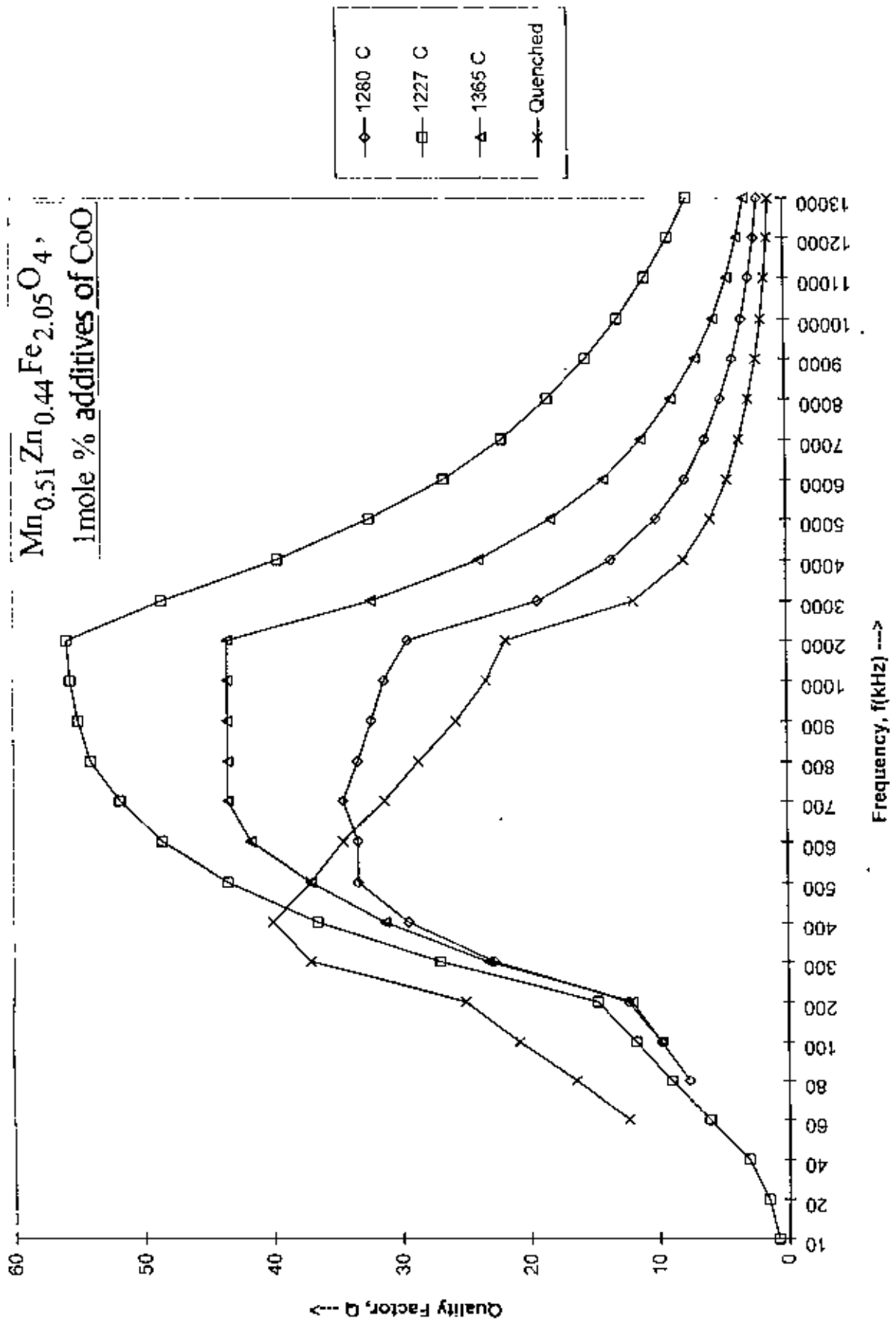


Fig 5.71: The variation of Q with frequency for the samples $\text{Mn}_{0.51}\text{Zn}_{0.44}\text{Fe}_{2.05}\text{O}_4$ with 1 mole % additives of CoO sintered at different temperatures.

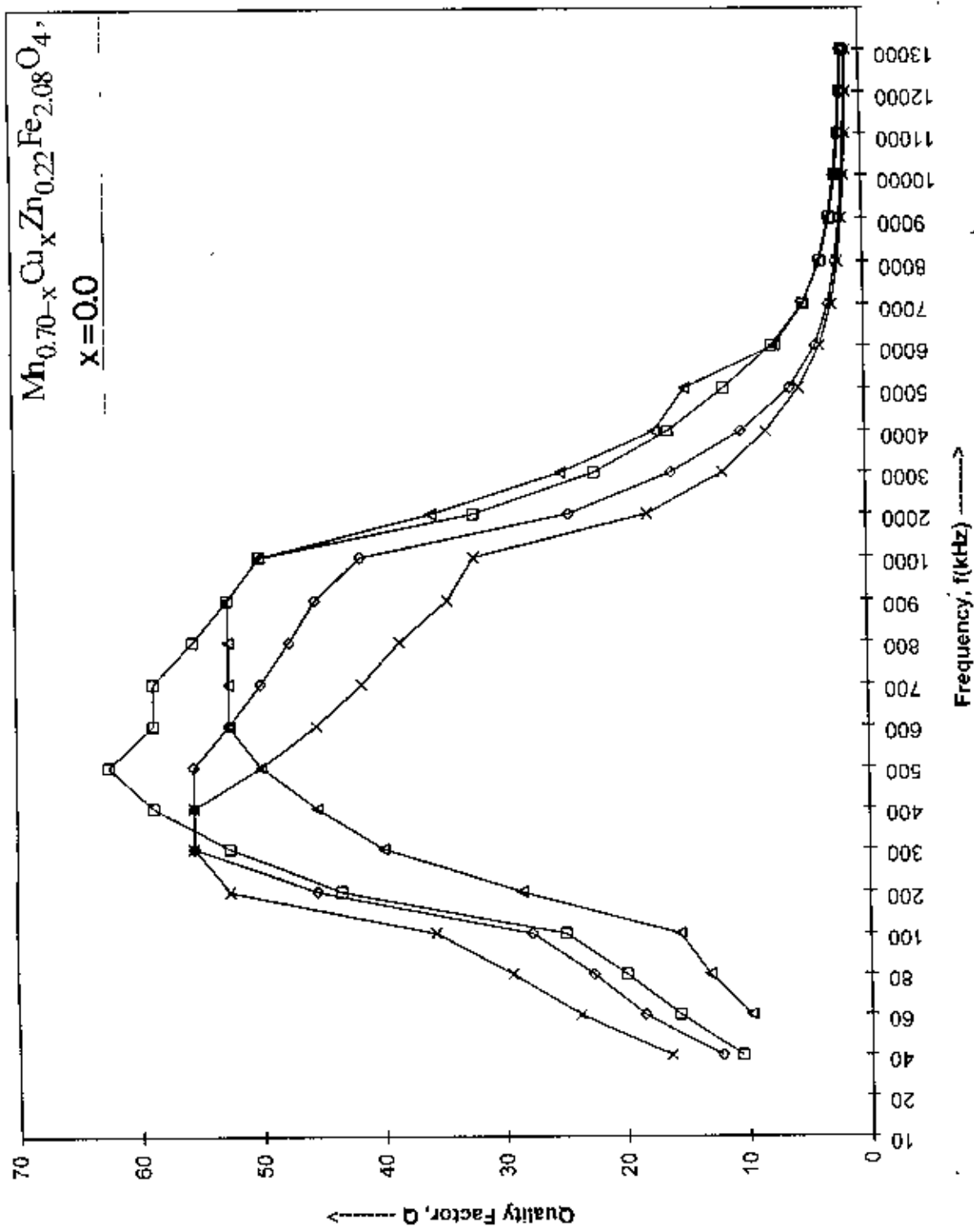


Fig5.72: The variation of Q with frequency for the samples $Mn_{0.70-x}Zn_{0.22}Fe_{2.08}O_4$ with $x=0.0$ sintered at different temperatures.

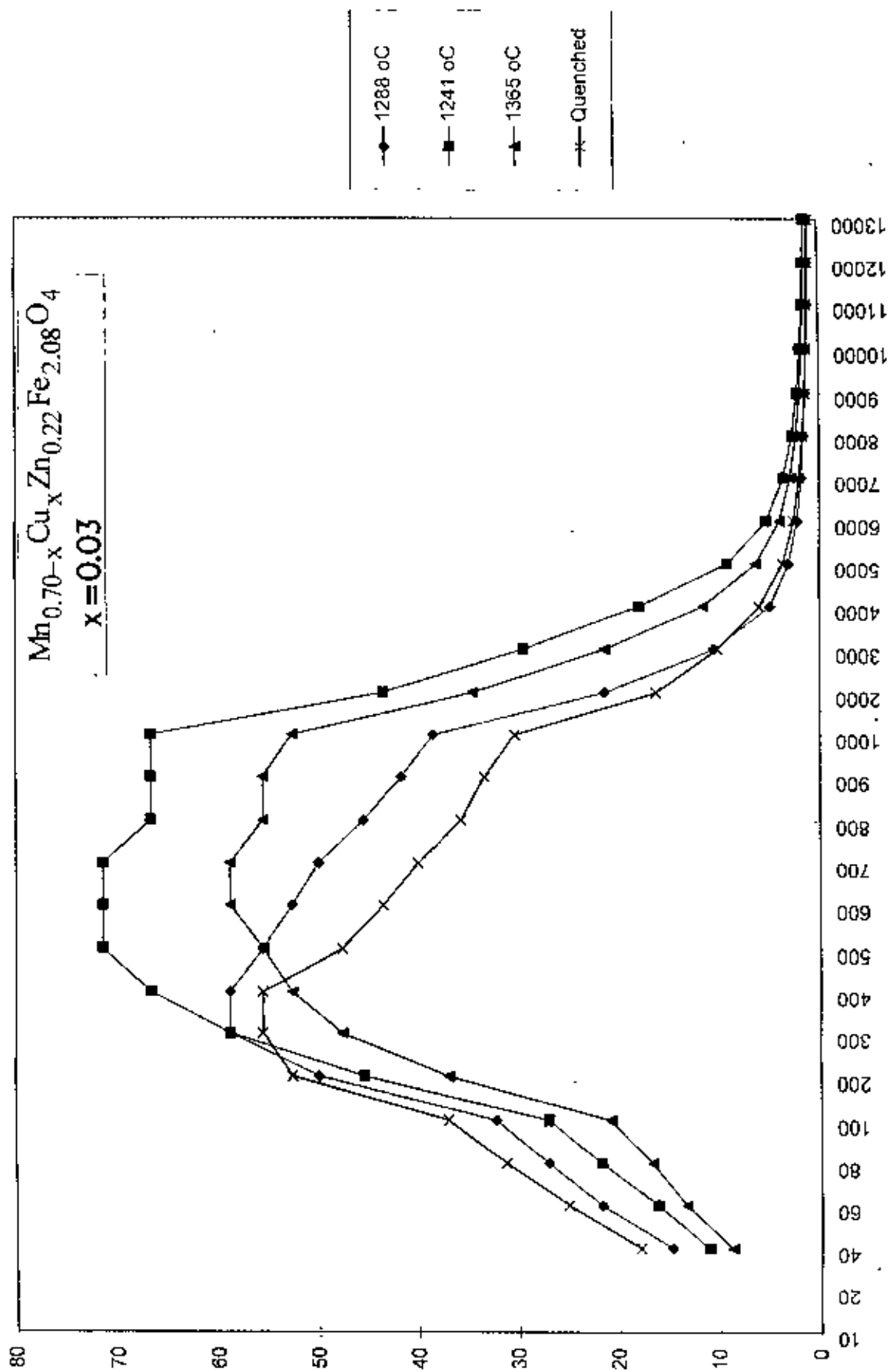


Fig 5.73: The variation of Q with frequency for the samples $\text{Mn}_{0.51}\text{Zn}_{0.4}\text{Fe}_{1.09}\text{O}_4$ with $x=0.03$ sintered at different temperatures.

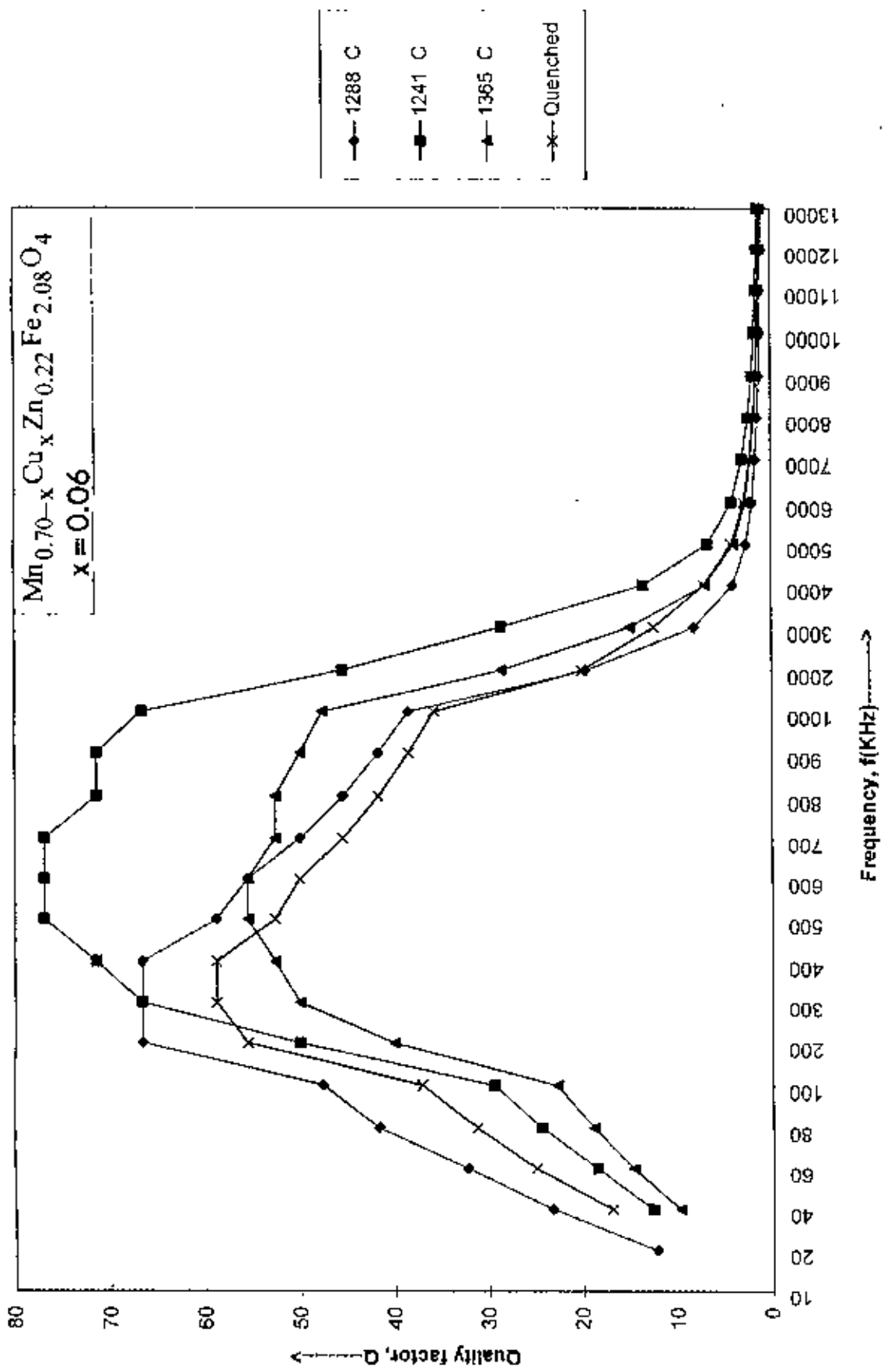


Fig 5.74: The variation of Q with frequency for the samples $\text{Mn}_{0.51}\text{Zn}_{0.44}\text{Fe}_{2.05}\text{O}_4$ with $x=0.06$ sintered at different temperatures.

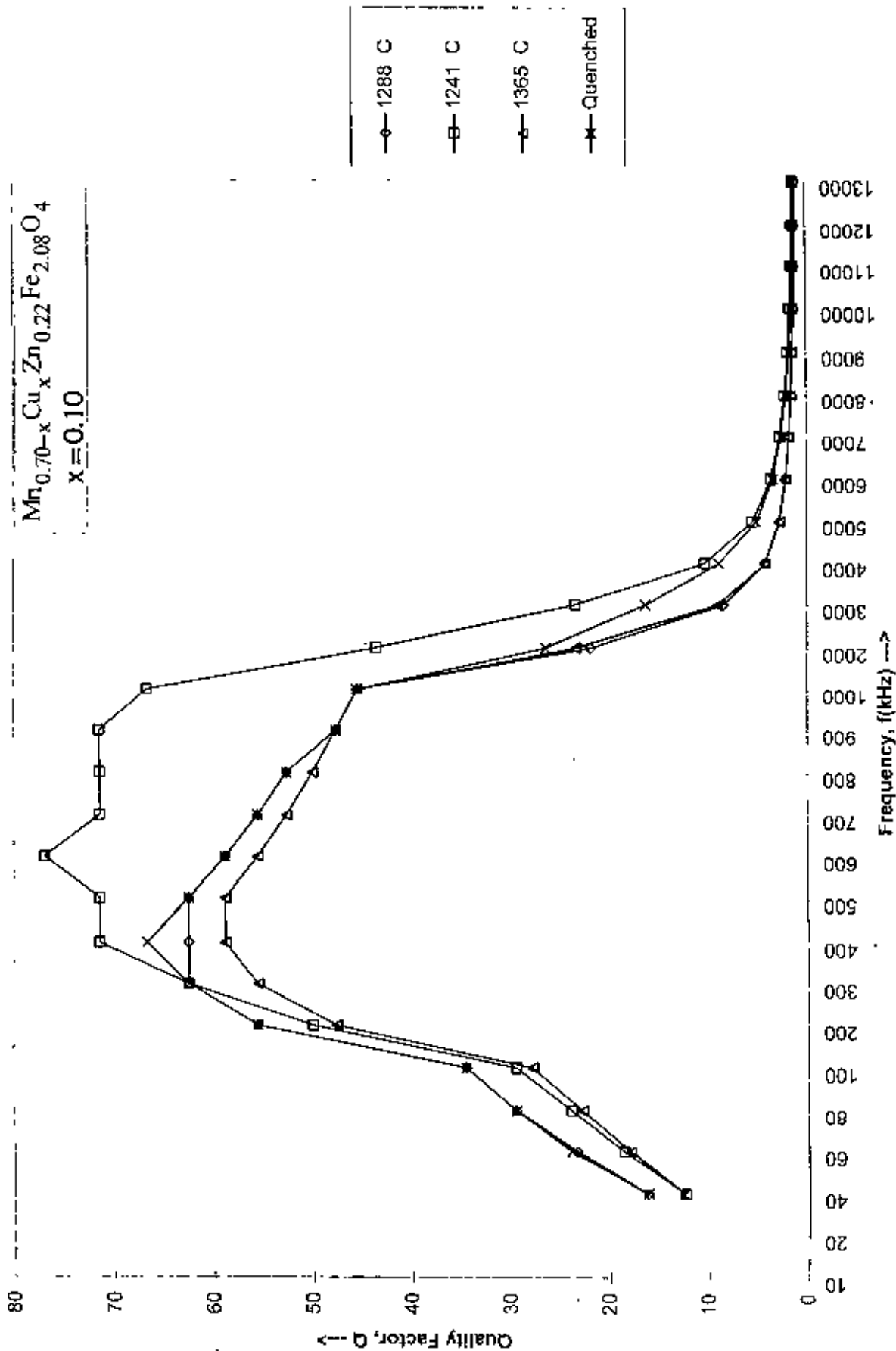


Fig5.75: The variation of Q with frequency for the samples $Mn_{0.51}Zn_{0.44}Fe_{2.03}O_4$ with $x=0.10$ sintered at different temperatures.

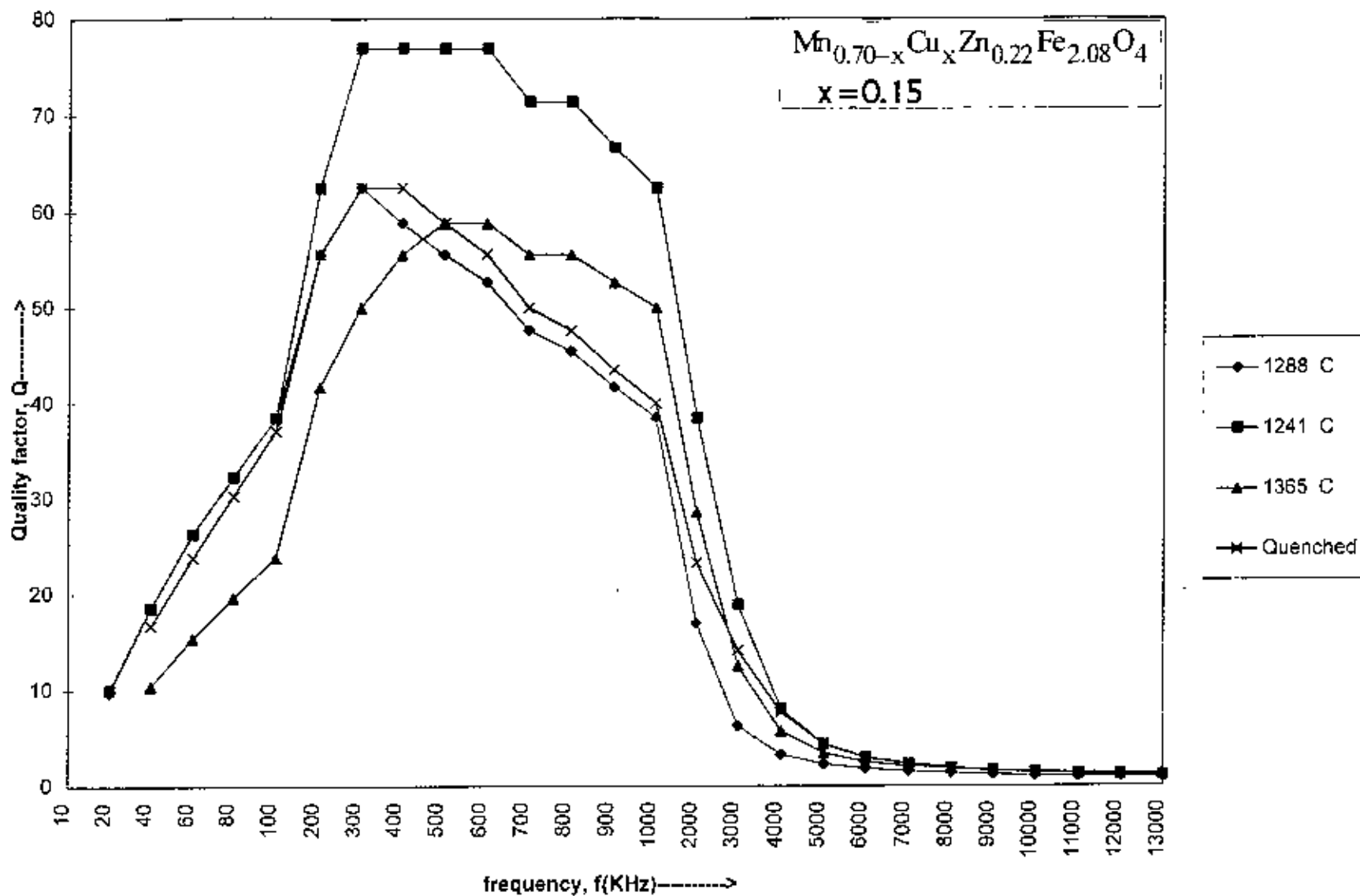


Fig 5.76: The variation of Q with frequency for the samples $\text{Mn}_{0.51}\text{Zn}_{0.44}\text{Fe}_{1.05}\text{O}_4$ with $x=0.15$ sintered at different temperatures.

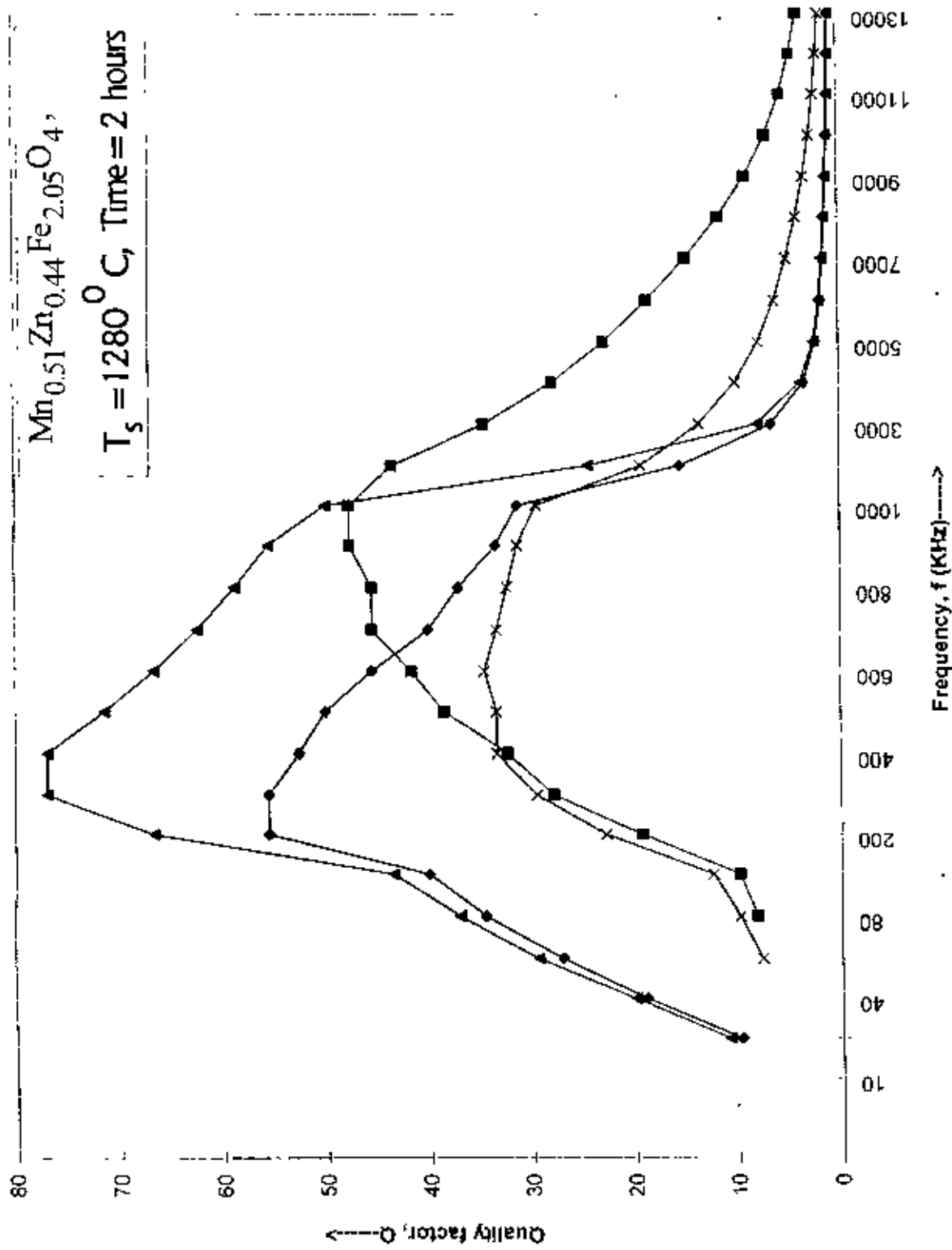


Fig. 77: The variation of Q with frequency for the samples $Mn_{0.51}Zn_{0.44}Fe_{2.05}O_4$ without and with 1 mole % additives of V_2O_5 , TiO_2 and CoO sintered at $1280^\circ C$.

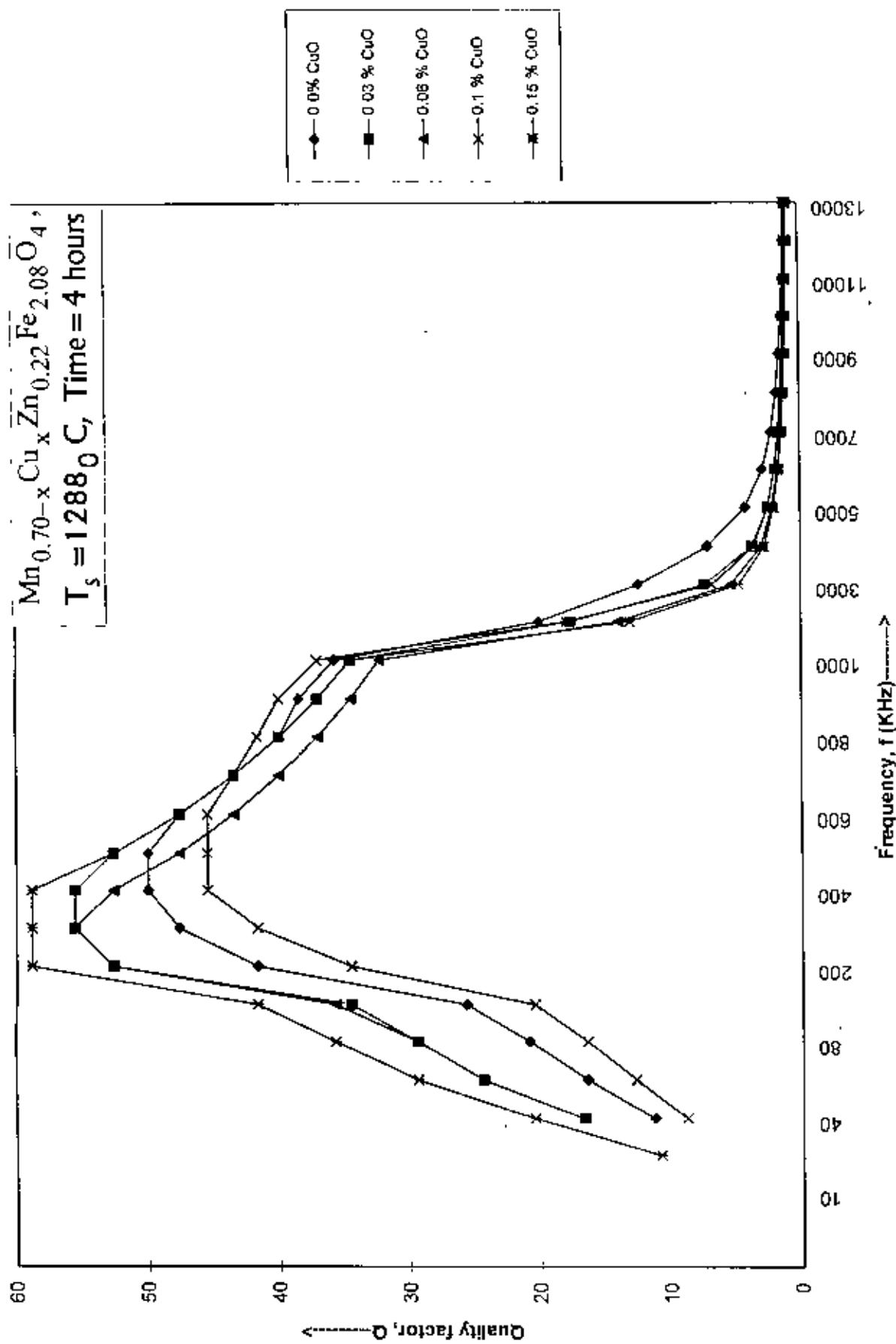


Fig 5.78: The variation of Q with frequency for the samples $\text{Mn}_{0.7-x}\text{Cu}_x\text{Zn}_{0.22}\text{Fe}_{2.08}\text{O}_4$, with $x=0, 0.03, 0.06, 0.10, 0.15$ sintered at 1288°C

- The samples sintered at low temperature and small duration of time (from fig, it is 1241°C, 2 hours) is of highest Q-value. This is probably due to the growth of less imperfections and defects in them than the samples sintered at higher T_s.
- The samples sintered at higher temperature 1288°C show a low Q value consistently. These samples are sintered for relatively longer times (4 hours) than others. So, the number of imperfection may increase in them relative to others, which may be yielding the phenomenon.
- Smaller grain size is competent for larger Q-values. Both the samples sintered at 1241°C and the quenched ones have smaller grain size (as is evident from our microstructural studies). These two are the owner of the higher Q-values.

Figs 5.68 to 5.71 are the samples of addition of 1 mole% additives of V₂O₅, TiO₂ and CoO. Again we observed that samples sintered at lowest temperature i.e., 1227°C are the candidate for higher Q-values. Samples sintered at higher temperatures 1365°C are the ones having lowest Q-values.

Another interesting thing that can be figured out from figs 5.68 to 5.76 i.e., both the composition is that, roughly 100KHz to 2 MHz is the frequency region over which Q-values is highest and shows almost identical behaviour.

REFERENCES

1. J. Smit, H.P.J. Wijn, Ferrites (Wiley, New York) 1959.
2. K. Standley, In Oxide magnetic material, 97, 1947, Oxford, Clarendon.
3. N. Reslescu, E. reslescu, P.D. Popa, M. L.Craus, L. Reslescu, JMMM 182 (1998) 199-206.
4. J.J. Piekoszewski, Suwalski and L. Dabrowski, Acta. Phys. Pol A51. 179. 1977.
5. H. Forestier, Ann. de Chem. 10e ser. 9. 316,1951.
6. U. König, J. Appl. Phys. 4, 237, 1974.
7. R.K. Puri, Vijoy K. Babbar and R.G. Mendiratta, Proc. ICF-5, 1989.
8. Y. Yafet and C. Kittel, C. Phys. Rev , 87(2), 290-294, 1952.
9. A.G. Sawatzky et.al., Phys. Rev. 187(2), 747-757, 1969.
10. U.V. König, J. Appl. Cryst. 1 (1968) 124-126
11. M.A. Gilleo, J. Phys. Chem. Solids 13 (1960) 33.
12. I.Nowik, Phys.Rev. 171(1968)550.
13. A. Globus, Proc. 2nd EFS Conf. On Soft Magnetic Materials (Wolfson center for Magnetic Technology, Cardiff, Wales), 1975.
14. J. Pankert, JMMM,138, 45-51, 1994.
15. C. Guillaud, 1957, Proc. IEE, 104B, 165.
16. E.G. Visser, JMMM, 42, 286-290, 1984.

17. T. Kimura, Y. Shiroishi, H. Fujiwara, M.Kudo, IEEE Trans. On Magn. MAG-15(1979)1640.
18. M I.Johnson, Proc. ICF-5, 1989, 401.
19. A. Globus et.al., IEEE Trans. On Mag., Mag-7,617, 1971.
20. Pyun, Su-II, Am. Ceram. Soc. Bull., 64(4), 585-588, 1985.
21. A.D. Giles, F.F. Westendorp, J. Phys. D: Appl. Phys. 9: 2117-2122, 1976.
22. A. Globus, Phys. (Paris) (Sppl.ci) Proc. ICF-3 , 1977.
23. J. E. Burke, J. Am. Ceram. Soc. 40(1957)80.
24. F.G Brockman, P.H Dowling and W.G. Stenceck, Phys.Rev.77, 85, 1950.

Conclusions

6.1 Conclusions

Mn-Zn ferrites samples were subjected to various investigations. The analysis of our experimental measurements indicate the following results:

From the XRD patterns, it can be concluded that Mn-Zn ferrite samples are in good crystalline form and the material formed is of single phase. Density calculation shows that copper substitution helped in the densification of the materials of the composition $Mn_{0.7-x}Cu_xZn_{0.22}Fe_{2.04}O_4$ whereas the density rather decreased for the sample $Mn_{0.51}Zn_{0.44}Fe_{2.05}O_4$ with additives like CoO, V_2O_5 and TiO_2 .

From Curie temperature measurements, a decreasing trend in the Curie temperature is observed for the substitution of Cu^{2+} for Mn^{2+} . The Curie temperature is found to be very sensitive for the additives like TiO_2 and CoO, V_2O_5 in $Mn_{0.51}Zn_{0.44}Fe_{2.05}O_4$. In the case of 1 mole % TiO_2 added sample Curie temperature decreased by $8^\circ C$, and in the case of CoO, T_c increased by $40^\circ C$. In the case of V_2O_5 added sample, T_c could not be measured.

The results from the magnetization measurements reveal that crystal site preference of cations, sintering conditions, preparation procedure etc can significantly affect the saturation magnetization, M_s value. The saturation magnetization increases for $x=0.03$ in $Mn_{0.7-x}Cu_xZn_{0.22}Fe_{2.08}O_4$ and then decreases for further increases of Cu^{2+} . Saturation magnetization significantly increases by the addition of 1 mole% CoO in $Mn_{0.51}Zn_{0.44}Fe_{2.05}O_4$. But it decreases for the addition of TiO_2 and V_2O_5 , and the effect is drastic for V_2O_5 doped sample than for TiO_2 ones.

From permeability spectra, it is noticed that sintering condition and additives substantially affect the permeability value. Quenched samples are found to possess higher permeability. From 10KHz to 1 MHz, for all the samples the permeability was found to remain almost frequency independent. The loss factor and quality factors are

also calculated and this study revealed that sintering condition is a determining factor for high quality Mn-Zn ferrites. They also show a slight compositional dependence.

The microstructure study show that grain size increases with sintering temperature. The quenched samples have smaller grain size but almost uniform in size.

In a nutshell, from the investigation carried out in this work we may aptly draw the following inferences:

- a) quenching is the best sintering condition for obtaining materials of higher permeability.
- b) the highest permeability can be obtained by choosing the proper composition and maintaining the best sintering condition. The sample $Mn_{(1-x)}Cu_xZn_{(1-2x)}Fe_{2.0x}O_4$ with $x=0.15$ sintered at 1280°C exhibited the best composition of high permeability.
- c) Pores have profound effect on various aspects of Mn-Zn ferrite. Control of microstructure is therefore essential for producing technologically useful materials.

6.2 Further Suggestions

Some of our results are interpreted in terms of changed anisotropy and magnetostriction with composition and sintering. However, experimental values of these parameters are not known. Measurements of magnetostriction and anisotropy for these materials are therefore essential.

Since large number of parameters are involved in determining the optimum composition and sintering condition, further work in this field is needed. For anisotropy measurements, single crystals of these ferrites are needed. Growing of single crystal of these ferrites is another proposed research work for the future.

Appendix

Table-1.1: Name of the Mn-Zn ferrite samples and their chemical formula

Series	Name of the samples	Chemical formulae
A-Series	A-1	$Mn_{0.51}Zn_{0.44}Fe_{2.05}O_4$
	A-2	$Mn_{0.51}Zn_{0.44}Fe_{2.05}O_4$, 1 mole % additives of V_2O_5
	A-3	$Mn_{0.51}Zn_{0.44}Fe_{2.05}O_4$, 1 mole % additives of TiO_2
	A-4	$Mn_{0.51}Zn_{0.44}Fe_{2.05}O_4$, 1 mole % additives of CoO
B-Series	B-1	$Mn_{0.70-x}Cu_xZn_{0.22}Fe_{2.08}O_4$, $x=0.00$
	B-2	$Mn_{0.70-x}Cu_xZn_{0.22}Fe_{2.08}O_4$, $x=0.03$
	B-3	$Mn_{0.70-x}Cu_xZn_{0.22}Fe_{2.08}O_4$, $x=0.06$
	B-4	$Mn_{0.70-x}Cu_xZn_{0.22}Fe_{2.08}O_4$, $x=0.10$
	B-5	$Mn_{0.70-x}Cu_xZn_{0.22}Fe_{2.08}O_4$, $x=0.15$

Table1.2: Specifications for toroidal samples of A-series sintered at $1300^\circ C$.

General formula $Mn_{0.51}Zn_{0.44}Fe_{2.05}O_4$					
Additives	Mean height h (in cm)	Mean outer dia. d_1 (in cm)	Mean inner dia. d_2 (in cm)	$d=d_1+d_2/2$ (in cm)	$d=d_1-d_2/2$ (in cm)
No additives	0.480	1.005	0.535	0.770	0.235
1 mole % V_2O_5	0.341	1.044	0.560	0.802	0.242
1 mole % TiO_2	0.466	1.026	0.548	0.787	0.238
1 mole % CoO	0.390	1.028	0.550	0.789	0.239

Table-1.3: Specifications for toroidal samples of B-series sintered at 1300°C

General formula $Mn_{0.70-x}Cu_xZn_{0.22}Fe_{2.08}O_4$					
Values of x	Mean height h(in cm)	Mean outer dia. d_1 (in cm)	Mean inner dia. d_2 (in cm)	$d=(d_1+d_2)/2$ (in cm)	$d=(d_1-d_2)/2$ (in cm)
0.00	0.4987	1.0025	0.5325	0.7675	0.2350
0.03	0.4850	1.0212	0.5425	0.7818	0.2394
0.06	0.4733	1.0337	0.5512	0.7925	0.2412
0.10	0.4800	1.0450	0.5537	0.7994	0.2456
0.15	0.4812	1.0225	0.5450	0.7837	0.2387

Table 1.4: Specifications for rod shaped samples

Samples	Mean diameter (in cm)	Mean height (in cm)	Mass (in gm)	Density (in gm/cm ³)
A-1	1.3433	1.2475	8.30	4.6945
A-2	1.3616	1.1087	7.14	4.4222
A-3	1.3608	1.0125	6.61	4.4885
A-4	1.3286	1.0987	7.42	4.8706
B-1	1.3250	1.0650	6.88	4.6858
B-2	1.3250	0.9987	6.60	4.7925
B-3	1.3391	1.1287	7.61	4.7866
B-4	1.3270	1.1412	7.58	4.8024
B-5	1.3233	1.2787	8.40	4.7761

Table-2.1: Summary of the XRD results

Major 2θ values (in deg.) observed in XRD pattern					
A-1	29.90	35.16	42.58	56.36	61.80
A-2	29.56	34.90		56.10	61.64
A-3	29.59	35.04	42.54	56.18	61.78
A-4	29.48	34.80	42.38	56.10	61.76
B-1	29.68	34.88	42.34	56.00	61.50
B-2	29.56	34.94	42.30	55.98	61.50
B-3	29.52	34.92	42.48	56.26	61.78
B-4	29.56	34.88	42.48	56.00	61.58
B-5	29.60	34.90	42.44	56.20	61.72
(hkl)	(220)	(311)	(400)	(511)	(440)

Table-2.2: XRD results for a-series samples

Samples	a (in Å)	ρ_x (in gm/cm ³)	Calculated density ρ_n (in gm/cm ³)	Porosity %
A-1	8.470	5.143	4.694	8.730
A-2	8.520	5.069	4.422	12.764
A-3	8.500	5.096	4.488	11.926
A-4	8.520	5.048	4.871	3.522

Table-2.3: XRD results for B-series samples

Samples	a (in Å)	ρ_x (in gm/cm ³)	Calculated density ρ_B (in gm/cm ³)	Porosity %
B-1	8.528	4.992	4.686	6.129
B-2	8.530	4.994	4.792	4.045
B-3	8.510	5.035	4.786	4.945
B-4	8.526	5.012	4.802	4.189
B-5	8.514	5.042	4.776	5.275

Table-3.1 Curie temperature for the samples

Samples	Curie temperature (in °C)
$Mn_{0.51}Zn_{0.44}Fe_{2.05}O_4$	190
$Mn_{0.51}Zn_{0.44}Fe_{2.05}O_4$, 1 mole% additives of V_2O_5	not found
$Mn_{0.51}Zn_{0.44}Fe_{2.05}O_4$, 1 mole% additives of TiO_2	182
$Mn_{0.51}Zn_{0.44}Fe_{2.05}O_4$, 1 mole% additives of CoO	230
$Mn_{0.7-x}Cu_xZn_{0.22}Fe_{2.08}O_4$ with $x=0.0$	297
$Mn_{0.7-x}Cu_xZn_{0.22}Fe_{2.08}O_4$ with $x=0.03$	270
$Mn_{0.7-x}Cu_xZn_{0.22}Fe_{2.08}O_4$ with $x=0.06$	255
$Mn_{0.7-x}Cu_xZn_{0.22}Fe_{2.08}O_4$ with $x=0.10$	237
$Mn_{0.7-x}Cu_xZn_{0.22}Fe_{2.08}O_4$ with $x=0.15$	242

Table-4.1: Magnetization values for A-series samples

Samples	Field intensity (in Oe)									Magnetization values in (emu/g)
	300	600	800	1000	1600	2000	2600	2800	3000	
A-1	52.98	64.67	66.75	67.59	68.84	69.26	69.67	69.67	70.09	
A-2	23.62	27.89	29.02	29.47	30.59	30.82	31.27	31.27	31.27	
A-3	54.39	64.94	66.92	68.23	67.90	67.90	68.23	68.56	68.56	
A-4	54.79	73.68	74.88	76.10	76.71	77.32	77.32	77.93	78.54	

Table-4.2: Magnetization values for B-series samples

Samples	Field intensity (in Oe)									Magnetization values in (emu/gm)
	300	600	800	1000	1600	2000	2600	2800	3000	
B-1	52.01	71.27	74.16	77.05	78.98	78.50	78.98	78.98	78.98	
B-2	73.20	96.32	98.24	100.2	102.6	102.6	103.5	103.5	103.5	
B-3	54.39	64.94	66.92	68.23	67.90	67.90	68.23	68.56	68.56	
B-4	54.79	73.68	74.88	76.10	76.71	77.32	77.32	77.93	78.54	
B-5	49.41	69.18	72.14	73.62	75.11	75.60	76.09	76.09	76.09	

Table-5.1: Data for Permeability measurement of sample A-1 sintered at 1280^oC

f(KHz)	L (in Henry) $\times 10^{-6}$	L_0 ($\times 10^{-8}$)	$\tan\delta$ or D	Q=1/D	μ'	μ''
5	5.00	1.5278	-----	-----	327.27	-----
20	4.90		0.103	9.708	320.72	33.03
80	4.84		0.029	34.482	316.79	9.18
100	4.84		0.025	40.000	316.79	7.92
200	4.83		0.018	55.555	316.14	5.69
400	4.83		0.019	52.631	316.14	6.01
800	4.84		0.027	37.037	316.79	8.55
1000	4.86		0.032	31.250	318.10	10.18
2000	5.05		0.065	15.384	330.54	21.48
4000	5.30		0.295	3.389	346.90	102.33
6000	4.40		0.572	1.748	287.99	164.73
8000	3.35		0.797	1.254	231.05	184.15
10000	2.86		0.994	1.006	187.19	186.63
11000	2.58		1.090	0.917	168.87	184.07
12000	2.34		1.186	0.843	153.16	181.65
13000	2.12	1.283	0.779	138.76	178.03	

Table-5.2: Data for Permeability measurement of sample A-1 sintered at 1300^oC

f(KHz)	L (in Henry) $\times 10^{-6}$	L_0 ($\times 10^{-8}$)	$\tan\delta$ or D	Q=1/D	μ'	μ''
5	6.00	1.4649	-----	-----	409.58	-----
20	5.90		0.076	13.158	402.76	30.61
80	5.83		0.026	38.461	397.98	10.35
100	5.83		0.023	43.478	397.98	9.15
200	5.82		0.021	47.619	397.29	8.34
400	5.80		0.029	34.482	395.93	11.48
800	5.83		0.051	19.608	397.98	20.29
1000	5.84		0.062	16.129	398.66	24.72
2000	6.00		0.130	7.692	409.58	53.24
4000	5.60		0.428	2.336	382.28	163.61
6000	4.40		0.719	1.391	300.36	215.96
8000	3.37		0.946	1.057	230.05	217.63
10000	2.56		1.136	0.880	174.75	198.52
11000	2.43		1.224	0.817	165.88	203.04
12000	2.21		1.310	0.763	150.86	197.63
13000	2.01	1.395	0.717	137.21	191.41	

Table-5.3: Data for Permeability measurement of sample A-2 sintered at 1280^oC

f(KHz)	L (in Henry) $\times 10^{-6}$	L_0 ($\times 10^{-8}$)	$\tan\delta$ or D	Q=1/D	μ'	μ''
5	1.00	1.4925	-----	-----	67.00	-----
20	1.30		-----	-----	87.10	-----
80	1.27		0.123	8.130	85.09	10.46
100	1.27		0.102	9.804	85.09	8.68
200	1.27		0.052	19.230	85.09	4.42
400	1.27		0.031	32.258	85.09	2.64
600	1.27		0.024	41.666	85.09	2.04
800	1.268		0.022	45.454	84.96	1.87
1000	1.267		0.021	47.619	84.89	1.78
2000	1.27		0.023	43.478	85.09	1.95
4000	1.28		0.036	27.777	85.76	3.09
6000	1.30		0.054	18.518	87.10	4.70
8000	1.346		0.087	11.494	90.18	7.84
10000	1.381		0.144	6.944	92.53	13.32
11000	1.386		0.181	5.525	92.86	16.81
12000	1.383		0.220	4.545	92.66	20.38
13000	1.370	0.261	3.831	91.79	23.96	

Table-5.4: Data for Permeability measurement of sample A-2 sintered at 1300^oC

f(KHz)	L (in Henry) $\times 10^{-6}$	L_0 ($\times 10^{-8}$)	$\tan\delta$ or D	Q=1/D	μ'	μ''
5	2.00	1.0293	-----	-----	194.31	-----
20	2.00		-----	-----	213.74	-----
80	2.21		0.050	20.00	214.71	10.73
100	2.21		0.040	25.00	214.71	8.59
200	2.20		0.023	43.478	213.74	4.91
400	2.20		0.015	66.666	213.74	3.21
800	2.21		0.015	66.666	214.71	3.22
1000	2.21		0.016	62.500	214.71	3.43
2000	2.23		0.025	40.000	216.65	5.41
4000	2.38		0.061	16.393	231.22	14.10
6000	2.55		0.193	5.181	247.74	47.81
8000	2.43		0.382	2.617	236.08	90.18
10000	2.15		0.561	1.782	208.88	117.18
11000	2.01		0.641	1.560	195.28	125.17
12000	1.87		0.717	1.384	181.67	130.26
13000	1.74		0.790	1.266	169.05	133.55

Table-5.5: Data for Permeability measurement of sample A-3 sintered at 1280°C

f(KHz)	L (in Henry) $\times 10^{-6}$	L_0 ($\times 10^{-8}$)	$\tan\delta$ or D	Q=1/D	μ'	μ''
5	5.00	1.5711	-----	-----	318.25	-----
20	4.80		0.092	10.969	305.52	28.11
80	4.76		0.027	37.037	302.97	8.18
100	4.76		0.023	43.478	302.97	6.97
200	4.76		0.015	66.666	302.97	4.54
400	4.78		0.013	76.923	302.97	3.94
600	4.80		0.015	66.666	305.52	4.58
800	4.78		0.017	58.823	304.24	5.17
1000	4.80		0.020	50.000	305.52	6.11
2000	5.03		0.041	24.390	320.16	13.12
4000	5.40		0.270	3.703	343.71	92.80
6000	4.50		0.541	1.848	286.42	154.95
8000	3.66		0.747	1.338	232.96	174.02
10000	3.01		0.920	1.087	191.58	176.26
11000	2.75		1.003	0.997	175.04	175.56
12000	2.52		1.085	0.921	160.39	174.03
13000	2.31	1.168	0.856	147.03	171.73	

Table-5.6: Data for Permeability measurement of sample A-3 sintered at 1300°C

f(KHz)	L (in Henry) $\times 10^{-6}$	L_0 ($\times 10^{-8}$)	$\tan\delta$ or D	Q=1/D	μ'	μ''
5	4.00	1.4135	-----	-----	282.98	-----
20	4.10		0.103	9.708	290.06	29.87
80	4.07		0.030	33.333	287.94	8.67
100	4.07		0.026	38.461	287.94	7.48
200	4.06		0.017	58.823	287.23	4.88
400	4.06		0.017	58.823	287.23	4.88
600	4.10		0.019	52.631	290.06	5.51
800	4.07		0.023	43.478	287.23	6.62
1000	4.08		0.026	38.461	288.64	7.50
2000	4.21		0.050	20.000	297.84	14.89
4000	4.50		0.223	4.484	318.36	70.99
6000	4.00		0.447	2.237	282.98	126.49
8000	3.41		0.643	1.555	241.24	155.12
10000	2.87		0.811	1.233	203.04	164.68
11000	2.65		0.891	1.122	187.48	167.04
12000	2.45		0.969	1.032	173.33	167.95
13000	2.26	1.048	1.048	159.88	167.56	

Table-5.7: Data for Permeability measurement of sample A-4 sintered at 1280°C

f(KHz)	L (in Henry) $\times 10^{-6}$	L_0 ($\times 10^{-8}$)	$\tan\delta$ or D	Q=1/D	μ'	μ''
5	1.00	1.4659	-----	-----	68.23	-----
20	1.40		-----	-----	95.50	-----
80	1.34		0.102	9.804	91.41	9.32
100	1.34		0.081	12.345	91.41	7.40
200	1.34		0.044	22.727	91.41	4.02
400	1.34		0.030	33.333	91.41	2.74
600	1.34		0.029	34.482	91.41	2.65
800	1.339		0.031	32.258	91.34	2.83
1000	1.338		0.034	29.411	91.27	3.10
2000	1.34		0.052	19.231	91.41	4.75
4000	1.35		0.100	10.000	92.09	9.20
6000	1.36		0.162	6.173	92.77	15.03
8000	1.368		0.249	4.016	93.32	23.24
10000	1.323		0.369	2.710	90.25	33.30
11000	1.273		0.438	2.283	86.84	38.03
12000	1.209		0.507	1.972	82.47	41.81
13000	1.138	0.572	1.748	77.63	44.40	

Table-5.8: Data for Permeability measurement of sample A-4 sintered at 1300°C

f(KHz)	L (in Henry) $\times 10^{-6}$	L_0 ($\times 10^{-8}$)	$\tan\delta$ or D	Q=1/D	μ'	μ''
5	3.00	1.1826	-----	-----	253.68	-----
20	2.80		-----	-----	236.76	-----
80	2.83		0.048	20.833	239.30	11.48
100	2.83		0.040	25.000	239.30	9.57
200	2.83		0.027	37.037	239.30	6.98
400	2.83		0.027	37.037	239.30	6.46
600	2.82		0.039	31.250	238.46	7.63
800	2.82		0.032	25.641	238.46	9.30
1000	2.82		0.046	21.739	238.46	10.97
2000	2.82		0.085	11.764	238.46	20.27
4000	2.83		0.172	5.813	239.30	41.16
6000	2.84		0.282	3.546	240.15	67.72
8000	2.73		0.452	2.212	230.85	104.34
10000	2.38		0.676	1.479	201.25	136.05
11000	2.16		0.789	1.267	182.65	144.11
12000	1.96		0.898	1.113	165.74	148.83
13000	1.77	1.004	0.996	149.67	150.27	

Table-5.9: Data for Permeability measurement of sample B-1 sintered at 1288^oC

f(KHz)	L (in Henry) x 10 ⁻⁶	L ₀ (x10 ⁻⁸)	tanδ or D	Q=1/D	μ'	μ''
5	3.00	1.3352	-----	-----	224.68	-----
20	2.60		-----	-----	194.73	-----
80	2.60		0.048	20.833	194.73	9.34
100	2.60		0.039	25.641	194.73	7.59
200	2.60		0.024	41.666	194.73	4.67
400	2.60		0.020	50.000	194.73	3.89
600	2.60		0.021	47.619	194.73	4.09
800	2.60		0.025	40.000	194.73	4.87
1000	2.61		0.028	35.714	195.47	5.47
2000	2.65		0.050	20.000	198.47	9.92
4000	2.84		0.142	7.042	212.70	30.20
6000	2.77		0.355	2.817	207.46	73.64
8000	2.38		0.571	1.751	178.25	101.78
10000	2.00		0.751	1.331	149.79	112.49
11000	1.38		0.832	1.202	137.06	114.03
12000	1.68		0.910	1.099	125.82	114.50
13000	1.55	0.987	1.013	116.09	114.58	

Table-5.10: Data for permeability measurement of sample B-1 sintered at 1300^oC

f(KHz)	L (in Henry) x 10 ⁻⁶	L ₀ (x10 ⁻⁸)	tanδ or D	Q=1/D	μ'	μ''
5	4.00	1.5271	-----	-----	261.93	-----
20	3.50		-----	-----	229.19	-----
80	3.50		0.034	29.412	229.19	7.79
100	3.50		0.028	35.714	229.19	6.42
200	3.50		0.019	52.631	229.19	4.35
400	3.50		0.018	55.555	229.19	4.57
600	3.50		0.022	45.454	229.19	5.04
800	3.50		0.026	38.461	229.19	5.96
1000	3.50		0.031	32.258	229.19	7.10
2000	3.52		0.056	17.857	230.50	12.91
4000	3.69		0.124	8.064	241.63	29.96
6000	3.80		0.281	3.558	248.84	69.92
8000	3.48		0.495	2.020	227.88	112.80
10000	2.96		0.700	1.428	193.83	135.68
11000	2.71		0.796	1.256	177.46	141.26
12000	1.48		0.889	1.125	162.40	144.37
13000	2.27	0.980	1.020	148.65	145.67	

Table-5.11: Data for Permeability measurement of sample B-2 sintered at 1288^oC

f(KHz)	L (in Henry) x 10 ⁻⁶	L ₀ (x10 ⁻⁸)	tanδ or D	Q=1/D	μ'	μ''
5	3.00	1.4368	-----	-----	208.80	-----
20	3.30		-----	-----	229.68	-----
80	3.22		0.034	29.411	224.11	7.62
100	3.22		0.029	34.483	224.11	6.50
200	3.21		0.019	52.631	223.41	4.24
400	3.21		0.018	55.555	223.41	4.02
600	3.21		0.021	47.619	223.41	4.69
800	3.21		0.025	40.000	223.41	5.58
1000	3.22		0.029	34.482	224.11	6.50
2000	3.34		0.057	17.544	232.46	13.25
4000	3.49		0.274	3.649	242.90	66.55
6000	2.96		0.532	1.879	206.01	109.60
8000	2.41		0.732	1.366	167.73	122.78
10000	2.00		0.898	1.113	139.20	125.00
11000	1.83		0.974	1.026	127.37	124.05
12000	1.68		1.048	0.954	116.92	122.54
13000	1.55	1.121	0.892	107.88	120.93	

Table-5.12: Data for Permeability measurement of sample B-2 sintered at 1300^oC

f(KHz)	L (in Henry) x 10 ⁻⁶	L ₀ (x10 ⁻⁸)	tanδ or D	Q=1/D	μ'	μ''
5	4.00	1.4847	-----	-----	269.41	-----
20	3.90		-----	-----	262.68	-----
80	3.92		0.032	31.250	264.03	8.45
100	3.92		0.027	37.037	264.03	7.13
200	3.91		0.019	52.631	263.35	5.00
400	3.91		0.018	55.555	263.35	4.74
600	3.90		0.027	43.478	262.68	6.04
800	3.91		0.028	35.714	263.35	7.37
1000	3.92		0.033	30.303	264.03	8.71
2000	3.97		0.062	16.129	267.39	16.58
4000	4.25		0.169	5.917	286.25	48.38
6000	4.00		0.398	2.512	269.41	107.23
8000	3.43		0.613	1.631	231.02	141.62
10000	2.86		0.799	1.252	192.63	153.91
11000	2.61		0.885	1.129	175.79	155.58
12000	2.40		0.967	1.034	161.65	156.31
13000	2.20	1.047	0.955	148.18	155.14	

Table-5.13: Data for Permeability measurement of sample B-3 sintered at 1288^oC

f(KHz)	L (in Henry) x 10 ⁻⁶	L ₀ (x10 ⁻⁸)	tanδ or D	Q=1/D	μ'	μ''
5	4.00	1.4569	-----	-----	274.55	-----
20	3.90		-----	-----	267.69	-----
80	3.86		0.034	29.411	264.64	9.01
100	3.85		0.028	35.714	264.26	7.40
200	3.85		0.019	52.632	264.26	5.02
400	3.84		0.019	52.632	263.57	5.01
600	3.90		0.023	43.478	267.69	6.16
800	3.86		0.027	37.037	264.94	7.15
1000	3.88		0.031	32.258	266.32	8.25
2000	4.07		0.072	13.888	279.36	20.11
4000	4.03		0.339	2.949	276.61	93.77
6000	3.30		0.596	1.678	226.51	135.00
8000	2.64		0.797	1.255	181.21	144.42
10000	2.15		0.959	1.043	147.57	141.52
11000	2.15		0.959	1.043	147.57	141.52
12000	1.80		1.098	0.911	123.55	135.66
13000	1.66	1.163	0.859	113.94	113.51	

Table-5.14: Data for Permeability measurement of sample B-3 sintered at 1300^oC

f(KHz)	L (in Henry) x 10 ⁻⁶	L ₀ (x10 ⁻⁸)	tanδ or D	Q=1/D	μ'	μ''
5	4.00	1.4408	-----	-----	277.62	-----
20	3.80		-----	-----	263.74	-----
80	3.77		0.032	31.250	261.66	8.37
100	3.76		0.027	37.037	260.96	7.04
200	3.76		0.018	55.555	260.96	4.69
400	3.75		0.017	58.823	260.27	4.42
600	3.80		0.020	50.000	263.74	5.27
800	3.76		0.024	41.666	260.96	6.26
1000	3.76		0.028	35.714	260.96	7.31
2000	3.82		0.050	20.000	265.13	13.25
4000	4.10		0.142	7.042	284.56	40.41
6000	4.00		0.349	2.865	277.62	96.89
8000	3.49		0.557	1.795	242.22	134.92
10000	2.93		0.740	1.351	203.36	150.48
11000	2.70		0.824	1.213	187.39	154.41
12000	2.49		0.903	1.107	172.82	156.06
13000	2.29	0.981	1.019	158.94	155.92	

Table-5.15: Data for Permeability measurement of sample B-4 sintered at 1288^oC

f(KHz)	L (in Henry) $\times 10^{-6}$	L_0 ($\times 10^{-8}$)	$\tan\delta$ or D	Q=1/D	μ'	μ''
5	4.00	1.5810	-----	-----	253.00	-----
20	3.80		-----	-----	240.35	-----
80	3.76		0.061	16.393	237.82	14.51
100	3.76		0.049	20.408	237.82	11.65
200	3.75		0.029	34.482	237.19	6.88
400	3.75		0.022	45.454	237.19	5.22
600	3.80		0.022	45.454	240.35	5.28
800	3.76		0.024	41.666	237.82	5.71
1000	3.77		0.027	37.037	238.90	6.45
2000	3.94		0.056	17.857	249.21	13.95
4000	4.04		0.282	3.546	255.53	72.06
6000	3.40		0.525	1.904	215.05	112.90
8000	2.79		0.709	1.410	176.47	125.11
10000	2.32		0.849	1.178	146.74	124.58
11000	2.14		0.906	1.104	135.36	122.63
12000	1.98	0.958	1.044	125.24	119.97	
13000	1.85	1.004	0.996	117.01	117.48	

Table-5.16: Data for Permeability measurement of sample B-4 sintered at 1300^oC

f(KHz)	L (in Henry) $\times 10^{-6}$	L_0 ($\times 10^{-8}$)	$\tan\delta$ or D	Q=1/D	μ'	μ''
5	4.00	1.4853	-----	-----	269.31	-----
20	3.80		-----	-----	255.84	-----
80	3.79		0.034	29.411	255.17	8.67
100	3.79		0.029	34.482	255.17	7.40
200	3.79		0.018	55.555	255.17	4.59
400	3.78		0.015	66.666	254.49	3.82
600	3.80		0.017	58.823	255.84	4.35
800	3.78		0.019	52.631	254.49	4.83
1000	3.79		0.022	45.454	255.16	5.61
2000	3.85		0.038	26.316	259.21	8.85
4000	4.13		0.114	8.771	278.06	31.70
6000	4.10		0.296	3.378	276.04	81.71
8000	3.70		0.486	2.057	249.11	121.06
10000	3.20		0.650	1.538	215.44	140.04
11000	2.96		0.725	1.379	199.28	144.48
12000	2.75	0.795	1.258	185.15	147.19	
13000	2.56	0.861	1.161	172.35	148.40	

Table-5.17: Data for Permeability measurement of sample B-5 sintered at 1288^oC

f(KHz)	L (in Henry) x 10 ⁻⁶	L ₀ (x10 ⁻⁸)	tanδ or D	Q=1/D	μ'	μ''
5	5.00	1.4931	-----	-----	334.87	-----
20	4.70		0.093	10.752	314.78	29.25
80	4.63		0.028	35.714	310.09	8.68
100	4.63		0.024	41.666	310.09	7.44
200	4.62		0.017	58.823	309.42	5.26
400	4.61		0.017	58.823	308.75	5.25
600	4.60		0.021	47.619	308.08	6.45
800	4.63		0.025	40.000	310.09	7.75
1000	4.65		0.029	34.482	311.43	9.03
2000	4.93		0.077	12.987	330.18	25.42
4000	4.75		0.367	2.724	318.13	116.75
6000	3.80		0.628	1.592	254.50	159.83
8000	3.01		0.829	1.206	201.59	167.12
10000	2.45		0.984	1.016	164.09	161.46
11000	2.24		1.049	0.953	150.02	157.37
12000	2.06		1.108	0.902	137.97	152.87
13000	1.90	1.163	0.859	127.25	147.99	

Table-5.18: Data for Permeability measurement of sample B-5 sintered at 1300^oC

f(KHz)	L (in Henry) x 10 ⁻⁶	L ₀ (x10 ⁻⁸)	tanδ or D	Q=1/D	μ'	μ''
5	4.00	1.4659	-----	-----	272.28	-----
20	3.80		-----	-----	259.22	-----
80	3.79		0.033	23.809	258.54	8.53
100	3.79		0.027	37.037	258.54	6.98
200	3.78		0.018	55.555	257.86	4.64
400	3.78		0.016	62.500	257.86	4.12
600	3.80		0.018	55.555	259.22	4.66
800	3.78		0.021	47.619	257.86	5.41
1000	3.78		0.025	40.000	257.86	6.45
2000	3.84		0.043	23.256	261.95	11.26
4000	4.16		0.131	7.633	283.78	37.17
6000	4.10		0.336	2.976	279.69	93.97
8000	3.56		0.536	1.865	242.85	130.17
10000	3.03		0.707	1.414	206.70	146.13
11000	2.79		0.784	1.275	190.32	149.21
12000	2.58		0.857	1.167	176.00	150.83
13000	2.39	0.927	1.078	163.40	-----	

